RE-EVALUATION OF EARTHQUAKE PERFORMANCE AND STRENGTHENING ALTERNATIVES OF HAGIA SOPHIA

by

Ahmet Serhan Kırlangıç

B.S., Civil Engineering, Istanbul Technical University, 2004

Submitted to the Kandilli Observatory and Earthquake
Research Institute in partial fulfillment of
the requirements for the degree of
Master of Science

Graduate Program in Earthquake Engineering
Boğaziçi University
2008

RE-EVALUATION OF EARTHQUAKE PERFORMANCE AND STRENGTHENING ALTERNATIVES OF HAGIA SOPHIA

APPROVED BY:

Assoc. Prof. Dr. Eser Durukal . . . . . .
(Thesis Supervisor)

Prof. Dr. Mustafa Erdik . . . . . .

Assoc. Prof. Dr. Oğuz Özel . . . . . .

DATE OF APPROVAL: 22.January.2008

ACKNOWLEDGEMENTS

I would like to thank my supervisor Assoc. Prof. Dr. Eser Durukal for providing me such a challenging subject and for the guidance during the study.

Next, I would like to express my gratitude to Prof. Dr. Mustafa Erdik for his valuable suggestions.

And finally, I thank my family for all their support and patience during my study.

ABSTRACT

RE-EVALUATION OF EARTHQUAKE PERFORMANCE AND STRENGTHENING ALTERNATIVES OF HAGIA SOPHIA

Static and dynamic linear analyses were carried out to evaluate the structural behaviour of and to propose strengthening strategies for Hagia Sophia. A Finite Element model of the structure was used for this purpose. While linear static self-weight and eigenvalue analyses were performed to ensure that the finite element model represents the structure, response spectrum analysis was used to obtain the deformation and stress distributions for determining the regions where intervention is needed. Response spectrum analysis revealed that main arches, semidomes and domebase exhibit high stress concentrations. These particular elements were the target zones for intervention. Two main strengthening strategies were considered: i) Retrofitting the main arches with post-tensioned bars, ii) Wrapping the structural elements with fiber reinforced polymers – FRPs. These two strategies were modelled and changes in the structural behaviour were observed. The analyses revealed post-tensioning as a more effective approach as compared to wrapping the structural elements with FRP laminates.

ÖZET

AYA SOFYA'NIN DEPREM PERFORMANSININ TAYİNİ VE GÜÇLENDİRME ALTERNATİFLERİ

Söz konusu çalışma ile Aya Sofya'nın yapısal davranışının incelenmesi ve muhtemel güçlendirme stratejilerinin belirlenebilmesi amaçlanmaktadır. Bu amaçla, yapının sonlu elemanlar modeli kullanılarak statik ve özdeğer analizleri gerçekleştirilmiş ve kullanılan modelin gerçek yapıyı temsil ettiği gösterilmiştir. Dinamik tepki analizi ile gerilme dağılımları belirlenmiş ve güçlendirme ihtiyacı olabilecek yapısal elemanlar tesbit edilmiştir. Ana kemerler, yarı kubbeler ve kubbe tabanı güçlendirme için öne çıkan yapı elemanlarıdır. Güçlendirme içi iki strateji geliştirilmiştir: i) Ana kemerlerin ard-gerilmiş tendonlarla güçlendirilmesi ve ii) Yapısal elemanların fiber takviyeli polimer ile sarılması. Her iki metot da modellenerek yapısal davranıştaki değişiklikler incelenmiştir. Ard-gerilmiş tendon kullanmanın FRP ile güçlendirmekten daha etkili olduğu analizler sonuçunda ortaya konulmuştur.

TABLE OF CONTENTS

LIST OF FIGURES

LIST OF TABLES

1. INTRODUCTION

1.1. Overview of Hagia Sophia

Architecture of Hagia Sophia represents a combination of a centrally-planned church with a traditional basilica. Its layout is longitudinally oriented. Entrance to the nave of the structure is provided by through a narthex from west. The nave is shaped by a procession of piers and colonnades that separates it from aisles at the ground level and from the galleries above. The nave ends with an apse on the east side, covered by a barrel vault and semidome. At the corners of the nave, the colonnades become exedra, covered with semidomes above the gallery level. Four main piers, forming a square at the centre of the structure, support arches above them. Four buttress piers are connected to the main piers by barrel vaults and arches passing transversely the aisles at ground and gallery levels. Four great arches span 30 meter between the main piers. The north and south ones are actually two arches which are supported by tympana walls and the gallery and aisle colonnades under them. The east and west arches are abutted by semidomes. These two huge semidomes are supported by both secondary piers and exedra semidomes. A square formed by surcharge over the arches is transformed to a circle by four pendentives. Main dome, supported by ribs resting on this circle, reaches 55 meter height above floor (Hill, 1991). The general view of Hagia Sophia can be seen in Figure 1.1.

Construction of Hagia Sophia had started in 532 and been completed in 537. During its lifetime Hagia Sophia suffered from many incidents. Even before the construction of the main dome began, remarkable deformations had occurred in the piers and arches. In 558, following the earthquakes of 553 and 557, the eastern arch, bringing with it the eastern semidome and a portion of the main dome collapsed. As a consequence of this, the main dome was replaced with a new one which is six meters higher then the original dome. By this way the outward thrusts applied by the main dome were believed to be reduced. In 989 another earthquake caused the west main arch, semidome and a portion of the dome to fall. This time the arch was rebuilt wider and thicker than before, and the ribs in the western portion of the dome were strengthened. The last major collapse occurred due to a third earthquake in 1346. The east structural elements - arch, semidome and a portion of

main dome – fell down. These damaged elements were rebuilt in their original dimensions unlike the west structural elements strengthened in the tenth century (Hill, 1991). A chronology of the historical damages due to earthquakes is given in Appendix A.

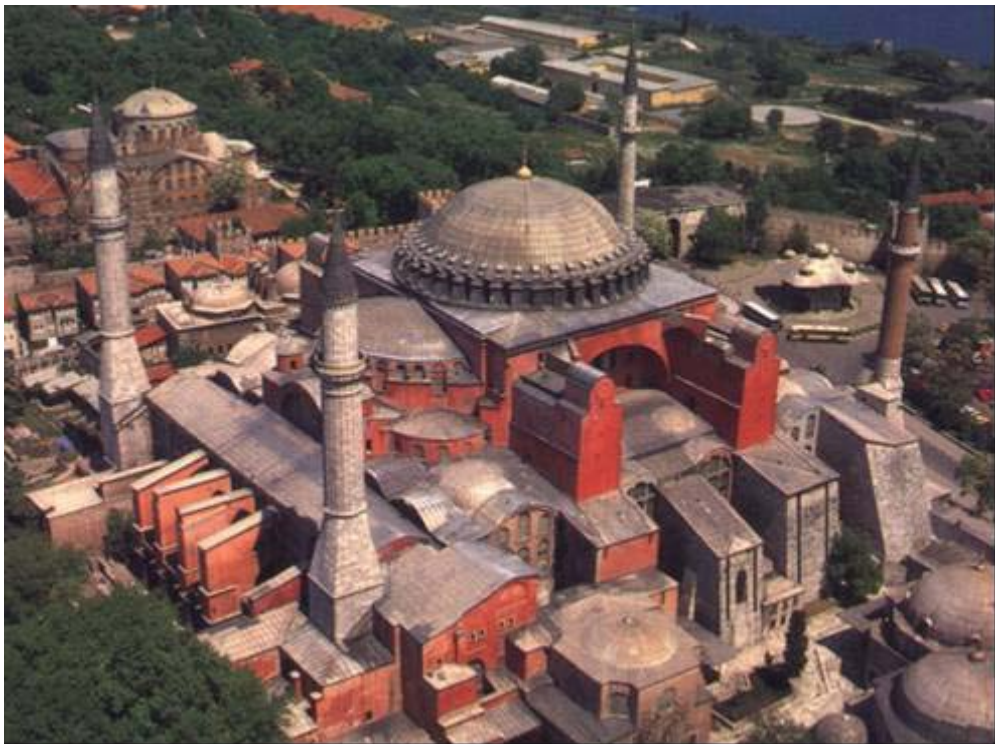

Figure 1.1. General view of Hagia Sophia (Erdik, *et al.* 2003)

1.2. Structural System

The primary structural support system of Hagia Sophia consists of four main piers, four main arches, surcharge, pendentives, main dome and its ribs. A square, set out by the main piers, forms the center of the structure. Four main arches that spring from the tops of the main piers connect one pier to next. The north and south arches are doubled, with a layer of fill separating one from the other one. Space above the main arches is filled by surcharge for the purpose of generating a square platform. This platform is converted into a circle shaped domebase by four pendentives which have a form of equilateral triangles. Forty ribs rise on this domebase to support a dome with a 30 meter diameter whose thickness is about 0.7 meter.

Two semidomes with a thickness of 0.8 meter flank the main dome at the east and west. Each one connects to a main arch at the top and rests on a barrel vault supported by two secondary piers at the bottom. Each semidome is also supported by two exedra domes and colonnades under them. The exedra domes connect also the secondary and the main piers. Thickness of the exedra domes is about 0.375 m. In the west the secondary piers covered by barrel vault provide the main entrance into the nave of the structure, while in the east, the secondary piers support another barrel vault which ends up with an apse.

In addition to the primary structure, four buttress piers provide lateral support to the main piers in N-S direction. The buttress piers are connected to the main piers by barrel vaults and arches at ground and gallery levels creating aisles along the length of the nave. Colonnades separate the aisles from the nave at both levels.

Although some irregularities exist, the plan of Hagia Sophia can be assumed symmetrical in both axes. The structure's nave has an uninterrupted free internal space of 30 m wide, 80 m long and 55 m high. For a more detailed treatment of the structural, architectural and historical particularities of Hagia Sophia, the reader is referred to Mainstone (1988) and Van Nice (1986). Described elements can be seen in the longitudinal section of Hagia Sophia as shown in Figure 1.2.

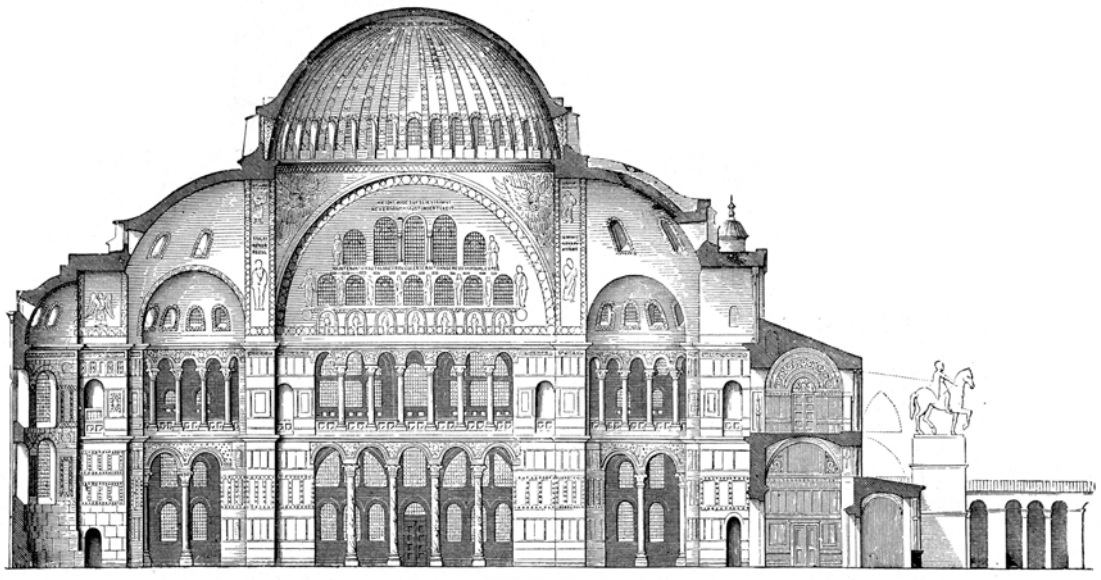

Figure 1.2. Structural elements of Hagia Sophia (Wikipedia)

1.3. Material Properties

The main building materials used in the Hagia Sophia are stone, brick, and mortar. The majority of the structure is built with brick masonry, while the main piers and the lower parts of the external buttresses are made of stone block masonry.

The block stones used in the piers are tender limestone or green granites. Colonnades are made of marble (Şahin, 2002). Stones used in the piers have a dimension of 45 cm in horizontal and length of 1 meter in vertical directions (Davidson, 1993). On the other hand bricks are square shaped with a dimension of 35-40 cm and a thickness of 4-5 cm. Mortar, as the conjunction material of bricks and stones, has a typical thickness of 5-6 cm which has almost an equal volume with brick (Şahin, 2002).

According to Livingston *et al.* (1992) the mortar used in Hagia Sophia is a pozzolanic one rather than a pure lime one. The ingredients used in the mortar provide it some sort of concrete behaviour which enables a higher tension capacity than the usual mortar. He proposes 3.5 MPa for the tensile strength of mortar. The tests implemented during this study also showed that mortar needs approximately a curing period of one year to gain its full strength which is important in understanding the nonlinearity of the structure. However, the samples taken from Hagia Sophia tested at National Technical University of Athens exhibited strength varying between 0.5 to 1.2 MPa for brick masonry (Çakmak *et al*., 1994). In another research implemented by Yüzügüllü *et al.* (1997), the ultrasonic test results suggest the following values for the elasticity of the masonry; $E_{brick}=4200$ MPa, $E_{mortar}=900$ MPa, and $E_{masonry}=2xE_bxE_m/(E_b+E_m)=1500$ MPa. The material properties assumed in this thesis are given in Chapter 2.2.

1.4. Observed Structural Deformation

Along the north-south direction, main piers have an approximately 85 cm outward inclination from ground level to top of the piers. In the east-west direction the piers exhibit a 16 cm outward inclination. The same outward tendency in the east-west direction can be observed especially for the secondary piers. On the main arches, vertical drops are obvious at the crowns. The crowns of north, south, east and west arches have vertical displacements

of 9, 18, 26, 13 cm in the direction of gravity respectively. The east and west arches tilt inward 14 and 15 cm respectively due to the semidomes attached to them. The north and south arches' crowns also lean outward 60 and 57 cm respectively. The lower cornices on the north and south sides bow inward in contrast to the outward bowing of arches. This deformation can be explained by the tilt of piers. The columns at southeast and southwest corners incline outward diagonally. The arches connecting the main and buttress piers are deformed due to shear stress they deal with (Davidson, 1993).

The high values of displacements should be the result of short construction period and long curing time of mortar. It is believed that the current deformation seen today occurred mostly while the construction was going on. The strengthened north and south arches (doubled ones) and addition at the tops of the buttress piers can be thought as the proof of this idea (Davidson, 1993).

1.5. Literature Review

In this section a summary of previous studies carried out with the purpose of assessment of the earthquake behaviour of Hagia Sophia is given. The first efforts towards this aim started in 1991 within the framework of a joint project of Princeton and Boğaziçi Universities. The completed studies in this Project can be listed as follows (Erdik *et al*., 2003):

- The structural system properties and dimensions were determined.
- A three-dimensional linear finite and non-linear element models were created.
- The modal frequencies were identified through ambient vibration tests.
- To record the earthquake response of the structure ten inter-connected three-component accelerometers were installed at the critical locations.
- The properties of the construction material were assessed through in-situ non-destructive and shear testing. Chemical and physical properties of mortar were determined.
- Expected earthquake ground motions for different return periods were simulated for the determination of the earthquake performance.

- Soil and foundation properties and the underground structure were assessed by means of seismic refraction, tomography and micro-gravimetry methods.
- The location of embedded iron ties and rings were analyzed through magnetometric procedures.
- The forces on the tie bars of secondary arches were determined.
- The possible damage and collapse patterns during a strong earthquake were determined.

Below in separate subsections the efforts of several researchers that contributed to the earthquake safety assessment of Hagia Sophia are summarized.

Hagia Sophia; Static Analysis of A Finite Element Model by Hill, 1991: This study was the preliminary one of a series of studies done at Princeton University. Creating a finite element model representing the structural system and static behaviour of Hagia Sophia was the main goal. The scope included generation, refinement and cracking of the model. Also construction sequence of Hagia Sophia was simulated.

Hill's modelling strategy was adding structural elements one by one and to display the effect of that structural component on the whole structure. The main objective of this analysis was to obtain the observed deformation of Hagia Sophia. Therefore a FE model was created without some structural components like as; buttress piers, exedra domes, and tympanum walls. The physical constants were regarded as; 10000 MPa for young's modulus, 1/6 for Poisson ratio and 1700 kg/m^3 for density of masonry. The model was analysed under its self-weight. The result obtained from the static linear analysis was sufficient enough to resemble the current deformation shape. Besides the order of displacement values were matching with the real ones. But to get close to the real deformation values, cracking was taken into account. The regions under tensile stress were assumed to be cracked. To achieve this a subsequence of static self-weight analysis were carried out; by this way the tensile regions were identified and cracked until no tensile were observed. Cracking was simulated by defining a second node at the coordinate of the node where two elements' joints stressed under tensile. Only solid elements were introduced to cracking. The displacements obtained by this method were much closer to the real deformation of the structure.

Lastly, an unfinished model to display the construction sequence was started. This analysis did not completed in this study, but some general ideas were given. The main principle was to analyse the structure in the order of its real construction phases. So it would be possible to model the realistic deformation pattern occurred during the construction of Hagia Sophia.

A Study on Structural Identification and Seismic Vulnerability Assessment of Aya Sofya by Durukal, 1992: The aim of the study was to determine the seismic behaviour of Hagia Sophia. The FE model used in the study depends on the model created by K. E. Hill. The model was developed by adding the structural parts such as, exedra domes, apse, and tympanum walls. It was calibrated with modal frequencies obtained from ambient vibration surveys. Static self-weight analysis, modal-eigenvalue analysis, response spectrum of a simulated earthquake and time history analysis with real earthquake records obtained from accelerometers on Hagia Sophia were carried out. All of these analyses were performed according to linear assumptions. The self-weight analysis resulted with much less deformations than the measured deformations, but general deformation form matched with the real one. To obtain the same frequencies with the ambient vibration results, many eigenvalue analyses were carried with different elasticity modulus. The best fitted frequencies were achieved with E=10000 MPa, which are 1.9, 2.3 and 2.4 Hz respectively for the first three natural frequencies. Also a set of earthquake records were used to perform time history analysis. By this way, it became possible to compare the displacement-time responses of the FE model with the real responses. Lastly, a response spectrum analysis carried out acting in three global directions; X, Y and Z, with a simulated earthquake equivalent to a magnitude of 5 at an epicentral distance of 20 km. Results of this analysis exhibited that top of the main arches, semidomes and springing points of the arches would be subjected to stress concentrations.

The Mother of All Churches: A Static and Dynamic Structural Analysis of Hagia Sophia by Davidson, 1993: Within the study, a series of finite element analyses were carried out to determine the static and dynamic behaviours of Hagia Sophia. The models analysed by Davidson can be summarized as;

- Static linear elastic model of main structure and whole structure,
- Dynamic linear elastic model – eigenvalue analysis – of main structure and whole structure,
- Static nonlinear model - staged construction analysis,
- Dynamic nonlinear model – eigenvalue analysis,
- Time history analysis.

Linear static analysis resulted with correct deformation shape of the structure. Displacements displayed the same order with the measured ones on the structure, but the determined values could not get close to real ones. For this analysis, the material properties were selected as; E=10000 MPa for stone, E=182 MPa for brick masonry and E=100 MPa, Poisson ratio=1/6 and shear modulus=10 MPa for mortar layers.

Modal-eigenvalue analysis yielded 1.83, 1.99 and 2.23 Hz respectively as the frequencies of the first three modes. The FE model was same as the one used for the static linear analysis, but the material properties were set as; E=10000 MPa for stone, E=5000 MPa for brick masonry and mortar, and density=1700 kg/m^3 for all structure except pendentives; 1275 kg/m^3. Also a model named "whole" which includes all the surrounding structure such as; flying buttresses was analysed for modal analysis. Result showed that surrounding structures provide extra stiffness that frequencies could increase a little. But no remarkable change was observed for both static and dynamic behaviour of Hagia Sophia.

For static and dynamic analyses different elasticity modulus were employed to reach the measured values on the structure for both deformations and ambient vibration frequencies. This difference can be explained by the nonlinearity of the structure. To deal with nonlinearity, a pseudo-nonlinear static analysis simulating 7 construction phases was implemented. Two strategies were followed for the analysis. For the first one, three main collapses occurred in history were taken into account. The construction stages were modelled and analysed one by one in the order of chronology. The elasticity modulus of the previous static model was set for this run. The result revealed much higher displacements then the real ones, so the second strategy was followed. This time the hardening of the mortar was also taken into account. The same construction stages with the

material properties – representing the hardened mortar - taken from the dynamic model were used. This analysis yielded closer deformations to the measured ones. The results, expect the north and south arches, represent the current situation of the structure very well.

The cracking issue was also tried to be understood in this study. For cracking, the linear static model having an elasticity modulus of mortar of 182 MPa – was used. Unlike the previous ones, analysis run in one stage and the regions with a tensile stress of 1.4 MPa were obtained. For these regions elasticity modulus was decreased 1/10 times of the initial one. And procedure continued until no region with tensile stress higher than 1.4 MPa exists. This method allowed the possible crack pattern and stress distribution to be determined. This analysis indicated high stress concentration on the underside of the crowns of west and east arches and on the top of the surcharge of the same arches.

The next step of the study was a nonlinear dynamic model which could represent both the frequencies and the recorded responses of Hagia Sophia during Karacabey Earthquake. The target frequencies were the ones calculated through the transfer function analysis – 1.53, 1.85 and 2.15 Hz. It was problematic to catch both the target frequencies and the recorded responses at the same time. Setting material properties as, E=10000 MPa for stone, E=5000 MPa for masonry and density=2500 kg/m^3 for stone, resulted with the most proper frequencies and displacement-time history responses with the recorded ones.

Time history analysis was the last analysis to be investigated. Two simulated acceleograms corresponding to 6.5 and 7.5 magnitude earthquakes were employed for the nonlinear dynamic model. The stresses occurred on cross sections of east and west arches are examined. The stresses obtained from the self-weight analysis of the cracked model were added with the ones obtained from time history analysis. By this way, the maximum tensile and compression stresses were determined. The results showed 7.5 magnitude earthquake would cause damage on Hagia Sophia, if it is assumed 1.4 MPa for strength of mortar. Davidson advised post-tensioning for retrofitting the structure to decrease the tensile stress occurred on arches, especially in Y direction. For this reason a simulation was performed via setting point loads, ranging from 20 MN to 40 MN, on the solid elements. Davidson proposed this method to decrease the tensile stress lower then 1.4 MPa.

The Enigma of Hagia Sophia: A Dynamic Structural Analysis of Justinian's Great Church by Natsis, 1994: The goal was to develop an accurate finite element model of Hagia Sophia for its dynamic behaviour. This study was the successor of Davidson's study. Natsis took Davidson's nonlinear dynamic model as the starting model for her study. The model was calibrated according to two criteria; firstly the frequencies determined from the Karacabey Earthquake – 1.53, 1.85 and 2.15 Hz – and secondly time history traces of acceleration and displacement measured by accelerograms located on the structure. The parameters investigated in this study can be summarized as:

- Soil – structure interaction,
- Cracking in the arches,
- Using anisotropic properties in main piers.

Soil-structure interaction was incorporated by two methods; first the elasticity modulus obtained from two different seismic topography studies done by Gürbüz and KOERI were set into underground parts of the piers, second spring elements were employed for the same elements. A range of elasticity modulus was calculated according to P-wave velocity, soil density and depth of the piers. These values were used to calculate the stiffness of the springs. Introducing soil-structure interaction to the FE model revealed modal frequencies lower then the ambient vibration results and close to strong ground motion frequencies obtained form Karacabey Earthquake. Also time history response at ground level gave close results to the ones obtained from recorded responses during Karacabey Earthquake. But the responses at the arches did not match with the recorded ones. It was explained by the relatively less stiffness of the superstructure correspond to soil stiffness, while the FE model assumes a more stiff structure than the real one.

The next step of this study was modelling the cracking. The regions in tensile were introduced with lower stiffness and the nodes joining the elements doubled and released to move. The cracking method did not capture the expected results. Also anisotropic material properties were tried out for the piers to reach the recorded responses at the east and west arches, but did not end up with satisfactory results. Consequently, it would not be succeeded to develop an accurate dynamic model within the study.

Comprehensive nonlinear dynamic analysis of Ayasofya by Keypour, 2001: The aim of the study to investigate the nonlinear behaviour of Hagia Sophia against a strong ground motion. The FE model was generated using LUSAS software. The analyses performed were:

- Static linear analysis
- Modal eigenvalue analysis
- Spectral response analysis
- Linear time history analysis using real earthquakes
- Nonlinear dynamic analysis using artificial earthquakes

Nonlinear material types were assigned to main arches, semidomes and main dome. For the nonlinear constitutive model, Implicit Backward Euler Pressure Dependent Von Mises Material Model was chosen. Different properties in tension and compression were specified. An artificial input motion with 0.4 g maximum acceleration and 2 second duration was used for nonlinear dynamic analysis. The input motion was applied for each direction separately for the half symmetric model. The analysis performed in east-west direction revealed that the yielding occurs first at the semidomes bottom sections and then north-south arches followed by east-west arches. Also, top of the semi dome exhibited high tensile stresses which can cause detaching from the arch at the top point. On the other hand, analysis in north-south direction showed that yielding happens first at the top of east west arches and then spreads to the either side of the arch. The semidome failure occurs after the failure of the east arch. And then the outer sides of north-south arches begin to experience nonlinear action. The nonlinear dynamic analysis also let the main dome experience more deformation due to weakening of east-west arches during the excitation which causes yielding at the main dome.

Dynamic Response of Hagia Sophia Considering Cracks by Şahin, 2002: By this study, the effect of the cracks on response of the structure under both static and dynamic loading was investigated. For this purpose, analyses were set into two groups as static and dynamic ones. For the static analysis, load increment method was used to determine the cracking propagation under its self-weight. The dynamic analysis was performed in two stages; firstly the FE model was cracked under its self-weight, then response spectrum

analysis was carried out employing acceleration increment method. The crack propagation path was exhibited by running the analysis for each acceleration increment step, starting from 0.04g and finishing with 0.4g. Within the analyses, the cracking was simulated by either the smeared crack modelling or discrete crack modelling methods. The first method proposes to eliminate the elasticity modulus of the cracked elements in the stiffness tensor for the direction normal to the crack direction, and the second one is achieved by disconnecting the nodes of adjoining elements where the strength limit of whether tension or compression was exceeded. When a main structural element has a crack of one third of its surface, the collapse condition occurred.

The static analysis, which was carried out with the smeared cracking method, exhibited the collapsed of the west semidome and exedra domes caused probably because of the different thickness of these semidomes. Another static analysis, using discrete cracking method, revealed with the collapse of the main dome preliminarily. In this analysis, the FE model did not include the exedra domes due to investigate the main bearing structural elements primarily. The dynamic analysis resulted with a cracking propagation path starting from the exedra domes, and following the perimeter of semidomes and the crest of semidomes, and particularly the main dome. But no collapse was occurred. For dynamic analysis, the elasticity moduli of cracked elements were evaluated proportional to crack depth. This is the reason why no collapse occurred during dynamic analysis, while static analysis resulted in collapse of the domes. During the dynamic analysis, the reduction in stiffness caused by cracking lead more flexible behaviour with longer periods which means a better response under acceleration loading.

1.6. Objectives

This study is the last one in a series of studies carried out by many researches mentioned in Chapter 1.5. Each one tried to improve the predecessor's contribution. Static, dynamic, linear and nonlinear analyses were carried out to understand the seismic vulnerability of Hagia Sophia. Although previous studies have revealed the static and dynamic responses, efforts towards the retrofitting alternatives were limited. In this study, the author aims to investigate the efficiency of possible methods to strengthen the structure and to provide a comparative analysis of alternatives using a finite element model of Hagia

Sophia. For this purpose, the FEM used by Davidson is adopted. Preliminary analyses carried out included static, modal–eigenvalue and response spectrum investigations to declare an adequate FE model. They provided knowledge about the regions needing intervention to develop the strengthened models. Two main strategies are taken into account; one is retrofitting structural elements with post-tensioned bars, and the other one is using fiber reinforced polymers - FRPs. After performing a set of analyses, the most reasonable strengthened model will be suggested for each strategy. All analyses performed in this study are carried out assuming linear response. Although it is known from the previous studies and it is revealed by the deformation observed that Hagia Sophia behaves in a nonlinear manner, linear analyses can give useful information about the expected damage pattern.

2. FINITE ELEMENT OF HAGIA SOPHIA

2.1. Finite Element Model

The finite element model (FE model) used in this study was first generated in 1991, by K.E. Hill based on Mainstone's measurements and Van Nice's drawings. This model was further developed by Durukal in 1992. In 1994, Davidson modified Hill's model for her study. The model, named as HSDYNTC9, used here is taken from Davidson (1993). The original model was created in SAP90 software. This old version of the model is converted into SAP2000 Version 10.

The FE model consists of following structural elements; main dome and its ribs, four main arches, surcharge, four pendentives, four main piers, two semidomes, four secondary piers, four buttress piers, eight arches connecting main and buttress piers, four exedra semidomes and their arches, two tympanum walls, columns and beams under tympanum walls and exedra semidomes, two barrel vaults, apse semidome and two piers under the apse.

The FE model has an idealized geometry. The current deformations and irregularities of the structure are not taken into account in the model. Vertical structural elements like walls, piers and columns are modelled as perfectly vertical without any inclination. The domes are modelled considering a perfect shape. They are assumed as portions of spheres, while the arches have a perfect circular shape (Davidson, 1993).

The FE model's total length from the narthex in the west to the apse in the east is approximately 83 m. In the north-south direction, it has a length of 70 m. The top of the main piers is at 24 m from the ground level, while their total height reaches 29 m due to 5 m extension beneath the ground level. The rectangular domebase with dimensions of 38 m x 42 m has an elevation of 41 m. It reaches 41.8 m at the crown of the west arch. Top of the crowns of the arches reach a height of 40.5 m except the west arch. The main dome rise to 55 m from the ground. The radia of the main dome and semidomes are taken as 15.5 m.

Thickness of domes are 0.7 m, 0.8 m and 0.375 m for the main dome, semidomes and exedra domes respectively.

The origin of the model is at the ground level and corresponds to the center of the dome. X axis is selected as west-east direction; east being positive. Y axis corresponds to the north-south direction; north is taken as the positive Y direction. The structure's longitudinal axis corresponds roughly to the east-west direction; its transverse axis is roughly parallel to the north-south direction. For all structural elements at the entrance side of the building the word "west" is used; such as west semidome, west main arch and so on. The structural elements on the apse side are denoted with "east"; such as east semidome, east main arch and so on. The elements on the north and south sides are named accordingly.

The foundation is assumed fixed. To do so, solid elements representing the piers are restrained in their three translational degrees of freedom, while the frame elements representing the columns are restrained for six degrees of freedom including both translational and rotational ones. The finite element model of Hagia Sophia can be seen in Figures 2.1 and 2.2.

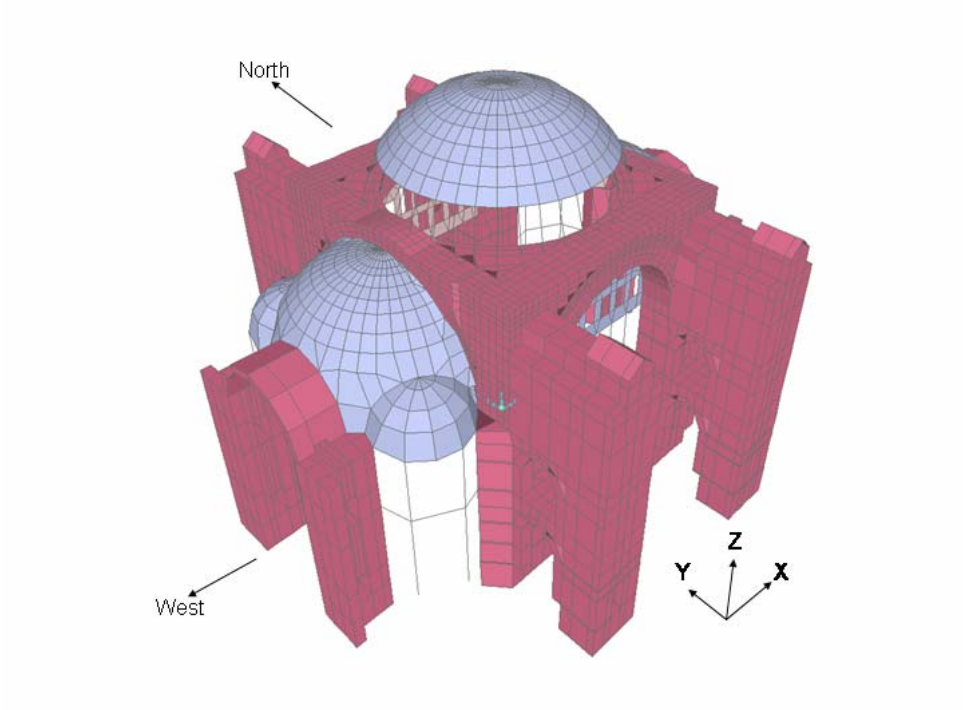

Figure 2.1. Finite element model of Hagia Sophia, 3D view

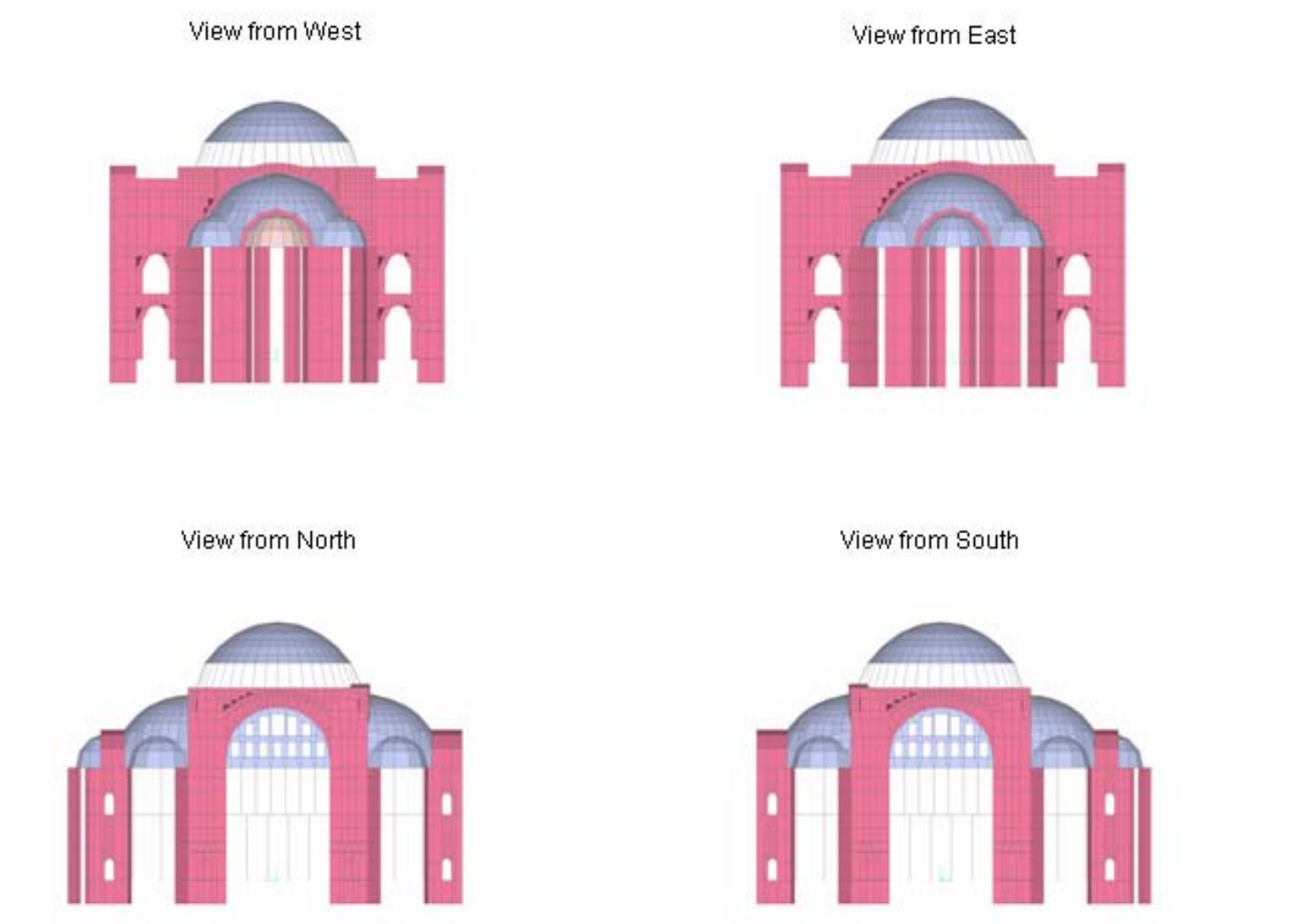

Figure 2.2. Finite element model of Hagia Sophia, side views

2.2. Material Properties Used in FE Model

Hagia Sophia is made of stone, brick and mortar. For the finite element model, the main piers up to the springing level of the arches and the lower part of buttress piers are modelled as stone masonry, while the upper part of these piers, pendentives, all arches and all domes are assumed as brick masonry. In the FE model, it is also assumed that mortar layers exist between the stone layers of the main piers and lower portions of the buttress piers as shown in Figure 2.3 (Davidson, 1993).

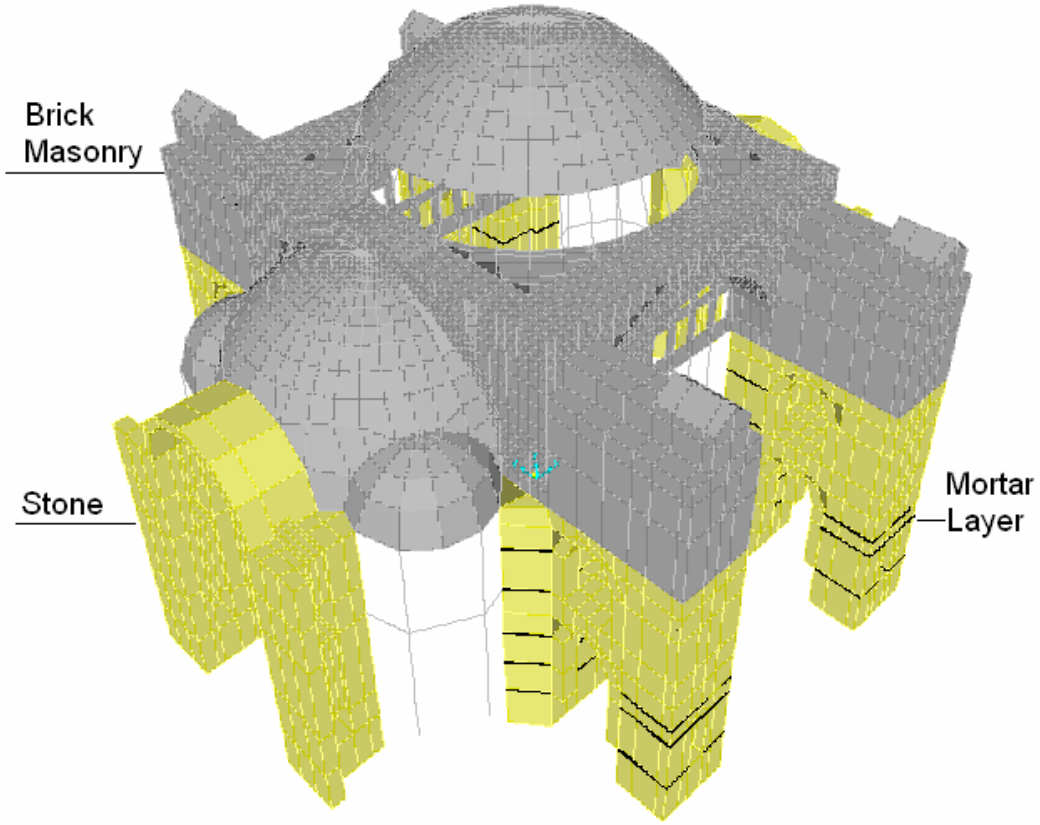

Figure 2.3. Building materials used in the finite element model of Hagia Sophia

The initial properties of the construction material of Hagia Sophia are obtained from Durukal (1992), Davidson (1993) and Şahin (2002). They are modified until the model's natural frequencies of vibration match those obtained by the ambient vibration surveys. The experimental low-amplitude natural vibration frequencies of Hagia Sophia, which were determined before 1999 Kocaeli Earthquake, are 1.85, 2.10 and 2.35 Hz for the first

three modes (Durukal, 1992). After 1999 Kocaeli Earthquake, a new ambient vibration survey obtain the frequencies as 1.75 and 2.01 Hz for the first two modes (Durukal *et al*., 2003). By observing the change of eigenvalue frequencies, the FE model's elasticity modulus is determined. Different input values of material properties are tried out and the values giving the best fitting modal frequencies with ambient vibration frequencies are selected. Mechanical properties of materials are assumed as anisometric, which means all mechanical behaviours are same for all directions and shearing behaviour is uncoupled from extensional behaviour (SAP2000, 2007). Table 2.1 gives the material properties used in this study.

Table 2.1. Material properties used in the finite element model of Hagia Sophia

Structural Element	Building Material	Elasticity Modulus (MPa)	Poisson Ratio	Mass (kN/m^3)	Thickness (m)
Piers	Stone	10000	1/6	2.0	-
Mortar layers	Mortar	5000	1/6	1.7	0.25
Main arches	Brick masonry	5000	1/6	1.7	-
Surcharge	Brick masonry	5000	1/6	1.7	-
Main dome	Brick masonry	5000	1/6	1.7	0.70
East-west semidomes	Brick masonry	5000	1/6	1.7	0.80
Exedrea domes	Brick masonry	5000	1/6	1.7	0.375
Apse dome	Brick masonry	5000	1/6	1.7	0.50
Pendentives	Brick masonry	5000	1/6	1.275	-
Tympanum Walls	Brick masonry	5000	1/6	1.7	0.87
Beams and columns	-	10000	1/5	2.0	-

A unique model which is capable of displaying both static i.e. current deformations of the structure and its dynamic behaviour – ambient vibration frequencies – could not be generated in previous studies. Ideally the model that would be the subject of dynamic analysis should reflect the current deformations on the structure, in terms of general characteristic and order of deformation. However as stated earlier all dynamic analyses carried out by previous researchers, as well as in this study, assume an ideal geometry. It turned out that creating a model reflecting the order of deformations seen in the actual structure, is a tedious and difficult task in the SAP2000 environment if not impossible. In this thesis, the same material properties are used for both static and dynamic analyses.

The nonlinearity of Hagia Sophia is a fact which can be proven by the transfer functions calculated from the records obtained from several earthquakes occurred since 1991. Those transfer functions exhibit lower natural frequencies than the ones obtained from ambient vibration surveys (Durukal, 1992, Durukal *et al*., 2003). But, in this thesis all the static and dynamic analyses are carried out assuming linear material behaviour i.e. the elasticity modulus is constant and the stress-strain behaviour is linear-elastic. The portions of the structure, where strengthening is needed, are decided as those parts where the strength limits for brick masonry (10 and 1 MPa respectively for compression and tension) are exceeded.

2.3. Element Types Used in FE Model

In the FE model of Hagia Sophia, frame, shell and solid elements are employed. Arches, surcharge, pendentives and piers are modelled as solid elements; while domes, tympanum walls are represented by shell elements. Ribs of the main dome, columns and beams are modelled as frame elements. In the unstrengthened FE model, there are 7139 solid, 1012 shell and 216 frame elements as given in Table 2.2. Tendon elements used as reinforcement in the strengthened models are explained in Chapter 4.1. The mechanical behaviour and particulars of the element types are explained in the following sections.

Table 2.2. Element types used in the finite element model of Hagia Sophia

Structural Element	Type of Element	Shape of Element	Number of Element
Piers,arches,surcharge,pendentives	Solid	Hexahedral/Pentahedral	7139
Main, semi and exedrea domes	Shell	Quadrilateral/Triangular	1012
Beams and columns	Frame	-	216

2.3.1. Frame Elements

For frame elements, SAP2000 software uses a general, three-dimensional, beam-column formulation including the effects of biaxial bending, torsion, axial and biaxial shear deformations. A frame element is modelled as a straight line connecting two joints. It has its own local coordinate system to define its section properties, loads, forces and stresses (SAP2000, 2007).

A frame element has six degrees of freedom at each end. Three of them are translational and the remaining three are rotational. Internal forces of the frame element, corresponding to these degrees of freedom, are calculated by integrating stresses over its cross section. These internal forces are:

- P, axial force
- V2, shear force in the 1-2 plane
- V3, shear force in the 1-3 plane
- T, axial torque
- M2, bending moment in the 1-3 plane (about the 2 axis)
- M3, bending moment in the 1-2 plane (about the 3 axis) (SAP2000 Manual, 2007).

The internal forces and axes used in the definition of the frame element can be seen in Figure 2.4.

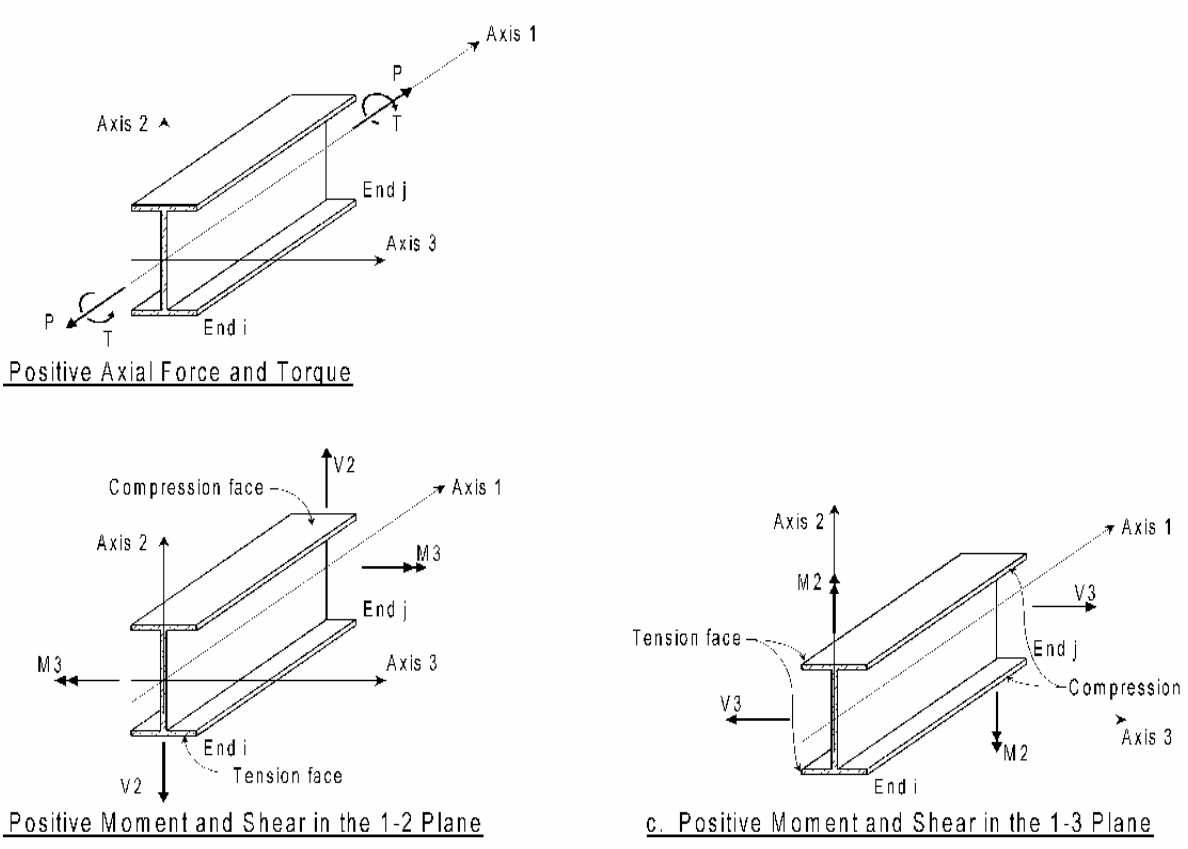

Figure 2.4. Positive directions of internal forces for the frame element in SAP2000

2.3.2. Shell Elements

Shell element is a three or four node formulation that combines membrane and plate-bending behaviour. The membrane behaviour uses an isoparametric formulation including translational in-plane stiffness components and a rotational stiffness component in the direction normal to the plane of the element. On the other hand, the plate bending behaviour includes two-way, out-of-plane, plate rotational stiffness components and a translational stiffness component in the direction normal to the plane of the element. For plate bending, thin-plate (Kirchhoff) formulation which neglects transverse shearing deformation, or thick-plate (Mindlin/Reissner) formulation which includes the effects of transverse shearing deformation can be taken in account. SAP2000 software offers three types of behaviour for shell elements:

- Three-dimensional full shell behaviour for both thin and thick formulation (e.g. domes)
- Pure plate behaviour for both thin and thick formulation (e.g. floor slabs)
- Pure membrane behaviour (e.g. shear walls) (SAP2000, 2007).

In this study, full shell behaviour with thin plate assumption is adopted.

A shell element has six degrees of freedom at each of its connected joints. Three of them are translational and others are rotational degrees of freedom. Available internal stresses for the shell element in SAP2000 are as follow:

- S11, stress acting on the positive and negative 1 faces in the 1-axis direction - Hoop stress.
- S22, stress acting on the positive and negative 2 faces in the 2-axis direction - Radial stress.
- S12, shearing stress acting on the positive and negative 1 faces in the 2-axis direction and acting on the positive and negative 2 faces in the 1-axis direction.
- SMAX, maximum principal stress.
- SMIN, minimum principal stress. By definition, principal stresses (SMAX and SMIN) oriented such that the associated shearing stress is zero. Generally, tensile

regions are represented by SMAX, while compression regions by SMIN. Directions of SMAX and SMIN are independent of direction in either global or local axes.

- SVM, Von Mises stress. Von Mises stress provides a scalar value of the shear stress in an element. For plates, Von Mises stress is identified in terms of the principal stresses as; $SVM=(S11^2-S11xS22+S22^2)^{0.5}$. In a state of pure tension, S11, when all other stresses are zero, then S11=SVM and in a case of pure shear, S12, when all other stresses are zero, then $SVM=\sqrt{3}S12$. For materials, initial yielding can be expected when $SVM=\sigma y$, where σy is the tensile yield stress, or when $SVM=\sqrt{3}\tau y$, where τy is the yield stress in shear. Von Misses stress is important for ductile materials like steel. For materials, particularly frictional materials such as masonry and concrete, Von Mises stress are not used to predict yield or failure. Instead, principle stresses are essential when cracking is the case.
- S13; Out-of-plane shearing stress acting on the positive and negative 1 faces in the 3-axis direction.
- S23; Out-of-plane shearing stress acting on the positive and negative 2 faces in the 3-axis direction.
- SMAXV; Maximum principal shearing stress. By definition, principal shearing stress is oriented on faces of the element such that the associated shears on perpendicular faces are zero. Principal stresses (SMAX and SMIN) are available for analysis cases and combinations that are single valued. So these stresses are shown for only static linear analysis, response spectrum analysis is not applicable (SAP2000, 2007).

In this study, the results of analysis are given as S11 and S22. S11 denotes hoop stress, while S22 denotes radial stress for shell elements. Additionally, the principle stresses SMAX, SMIN and SVM are checked out for the static linear analysis. The internal stresses and axes used in the definition of the shell element can be seen in Figure 2.5.

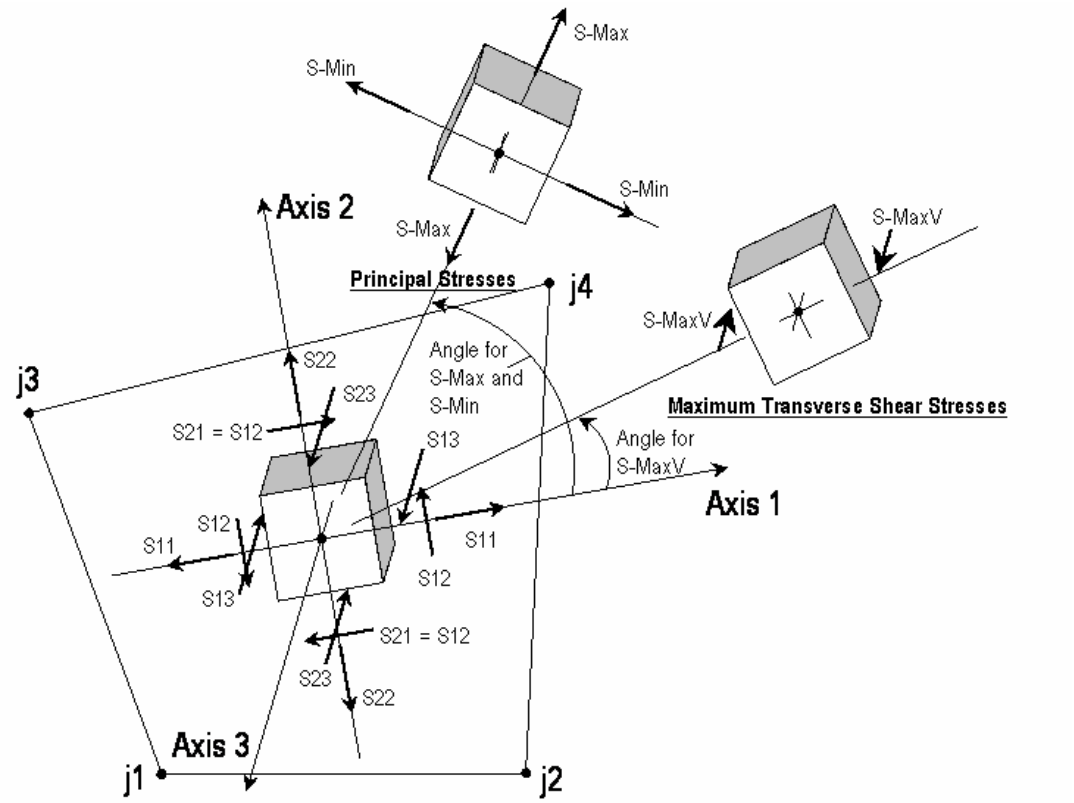

Figure 2.5. Positive directions of internal stresses for the shell element in SAP2000

2.3.3. Solid Elements

A solid element is an eight node element which is used to model three-dimensional structures. It is employed in the case that frame or shell elements are not able to represent the structural element, due to geometrical problems. Solid element's stiffness tensor is based on an isoparametric formulation that includes nine optional incompatible bending modes. The element is named according to its node number such as; hexahedral having 8 nodes, pentahedral having 6 nodes and tetrahedral having 4 nodes. In the FE model used in this study, hexahedral elements exist generally, also pentahedral elements represent pendentives. Solid element's local coordinate system is identical to the global one (SAP2000, 2007).

Accuracy of meshing of solid elements can be estimated from the difference in values calculated from different elements connecting to a common joint. By checking this, the problematic regions are assessed and more accurate FE models can be generated (SAP2000, 2007). Available stress components for solid elements in SAP2000:

- S11, stress acting on the positive and negative 1 faces in the 1-axis direction.
- S22, stress acting on the positive and negative 2 faces in the 2-axis direction.
- S33, stress acting on the positive and negative 3 faces in the 3-axis direction.
- S12, shearing stress acting on the positive and negative 1 faces in the 2-axis direction and acting on the positive and negative 2 faces in the 1-axis direction.
- S13, out-of-plane shearing stress acting on the positive and negative 1 faces in the 3-axis direction.
- S23, out-of-plane shearing stress acting on the positive and negative 2 faces in the 3-axis direction.
- SMAX, maximum principal stress.
- SMIN, minimum principal stress.
- SVM, Von Mises stress (SAP2000, 2007).

The results of the analysis are displayed for S11 and S22. For solid element S11 represents stress in X direction, while S22 represents stress in Y direction. The internal stresses and axes used in the definition of the solid element can be seen in Figure 2.6.

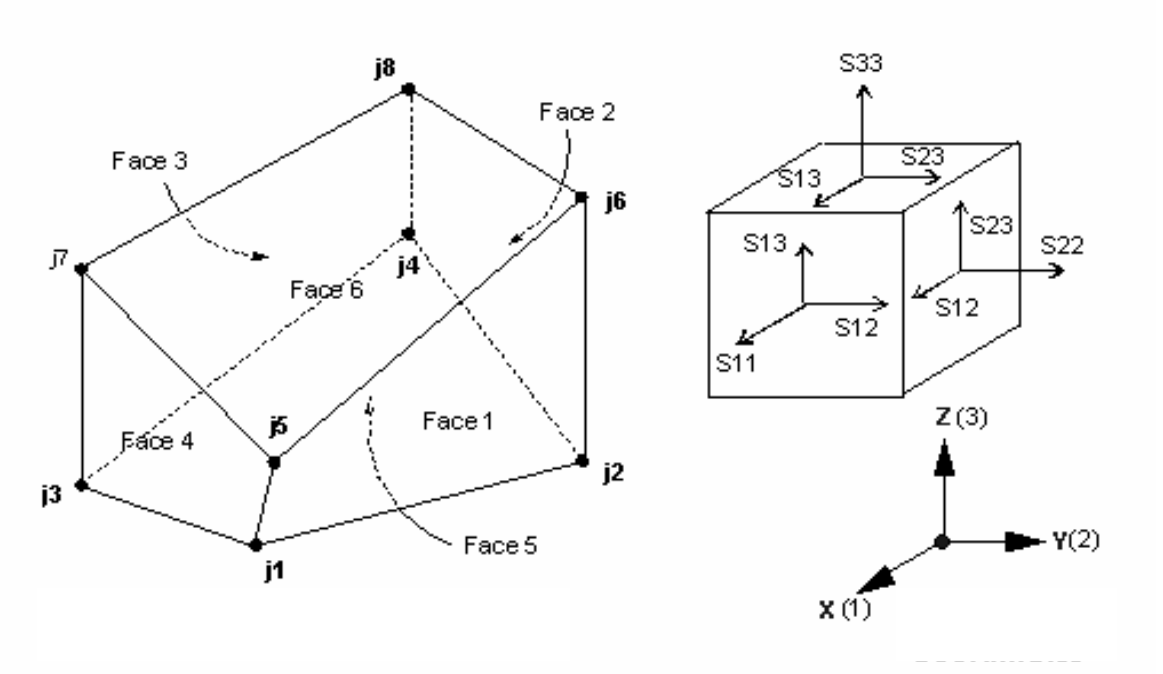

Figure 2.6. Positive directions of internal stresses for the solid element in SAP2000

3. STRUCTURAL ANALYSIS OF THE UNSTRENGTHENED MODEL

All structural analyses are carried out with SAP2000 Structural Analysis Program Version 10 software. The performed analyses are;

- Linear static analysis; self-weight,
- Modal eigenvalue analysis,
- Response spectrum analysis,

All analyses are performed assuming linear behaviour. In SAP2000, linear analyses enable superposition of displacements and stresses caused by different loadings. The additive combination option is used to exhibit a common response for the self-weight and response spectrum analyses. The maximum (positive) results are considered to underline the tensile stress. Also the minimum (negative) results are checked out to be sure whether the compression strength is exceeded.

3.1. Linear Static Analysis

The linear static analysis of a structure requires the solution of a linear equations system represented as, $K \times U = R$ where K is the stiffness matrix, R is the applied load vector, and U is the displacement vector. During linear analysis, SAP2000 assumes structural properties remain the same. Analysis starts with zero stress and displacements and stresses caused by different types of loading can be superposed due to linear response of the structure (SAP2000, 2007).

The static analysis is performed under Hagia Sophia's self-weight. It is ensured that the deformation shape of the FE model is similar to the ones observed on the actual structure; i.e. east and west semidomes abut to the east and west main arches which cause them to move inward, while the north and south crowns of the main arches lean outward. The crowns of the arches display vertical drops and the outward inclination occurs at all piers. Although the order of the real displacements could not be captured, the current

deformation shape could be represented by the linear static analysis. The displacements at specified locations and corresponding measured ones are given in Table 3.1. The top and side views of the deformed shape can be seen in Figures 3.1 and 3.2.

Table 3.1. Comparison of analytical and real displacements

Cross section	FE Model (mm)		Measured* (cm)	
Top of the main dome	7.3	Downward	25.8	Downward
East Arch Crown in Vertical direction	8.9	Downward	13.7	Downward
East Arch Crown in E-W direction	2.3	Inward	13.4	Inward
West Arch Crown in Vertical direction	8.6	Downward	14.8	Downward
West Arch Crown in E-W direction	1.8	Inward	8.9	Inward
North Arch Crown in Vertical direction	5.5	Downward	60	Downward
North Arch Crown in N-S direction	0.9	Outward	17.8	Outward
South Arch Crown in Vertical direction	5.5	Downward	57.9	Downward
South Arch Crown in N-S direction	0.9	Outward	40.5	Outward
Top of the N-E Pier in N-S direction	1.6	Outward	8.5	Outward
Top of the N-E Pier in E-W direction	0.5	Outward	45.5	Outward
Top of the N-W Pier in N-S direction	1.7	Outward	8.5	Outward
Top of the N-W Pier in E-W direction	0.7	Outward	40.5	Outward
Top of the S-E Pier in N-S direction	1.6	Outward	7.4	Outward
Top of the S-E Pier in E-W direction	0.5	Outward	45.5	Outward
Top of the S-W Pier in N-S direction	1.7	Outward	7.4	Outward
Top of the S-W Pier in E-W direction	0.7	Outward	25.8	Outward

* Davidson, 1993

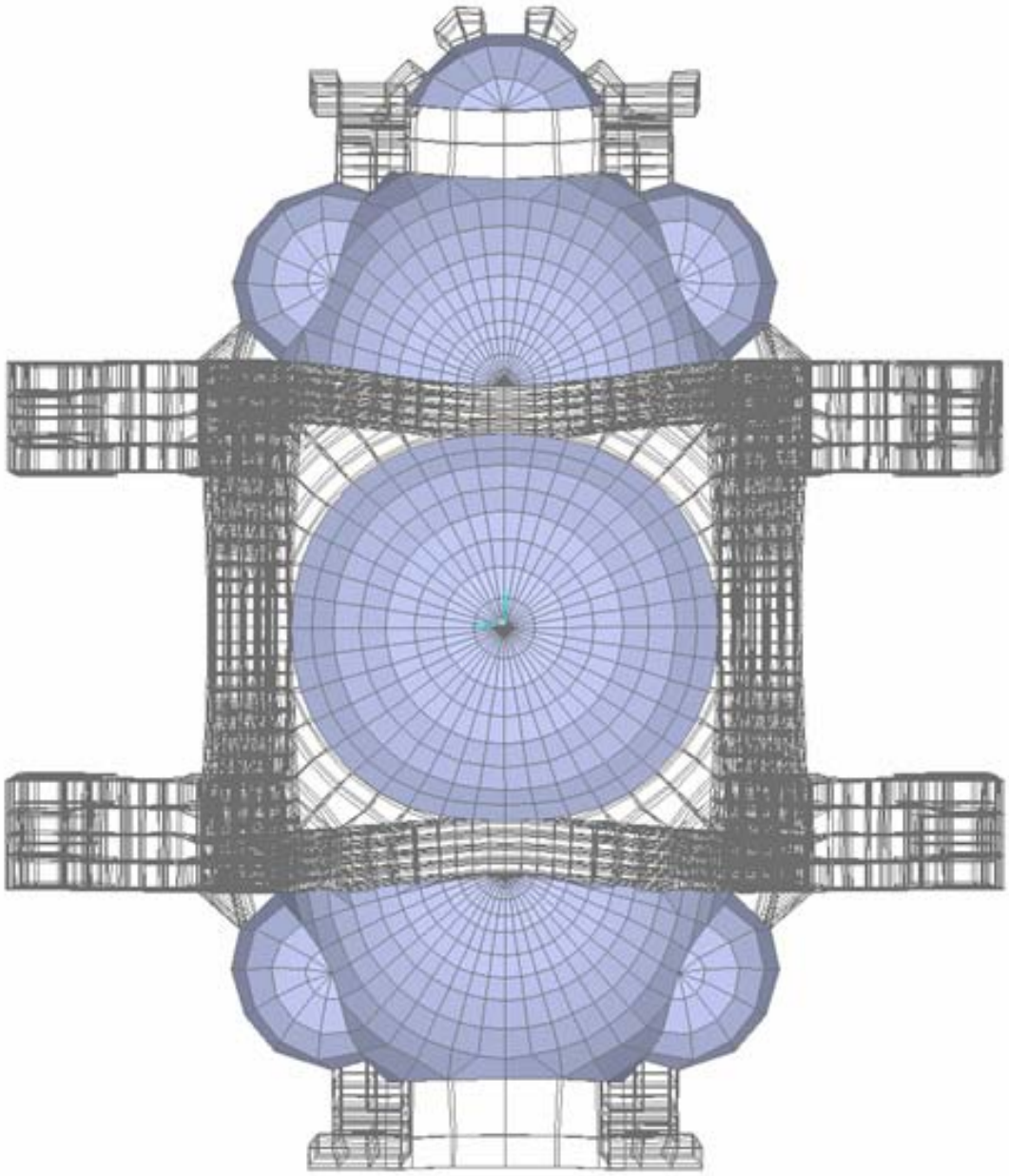

Figure 3.1. Deformation under self-weight, top view

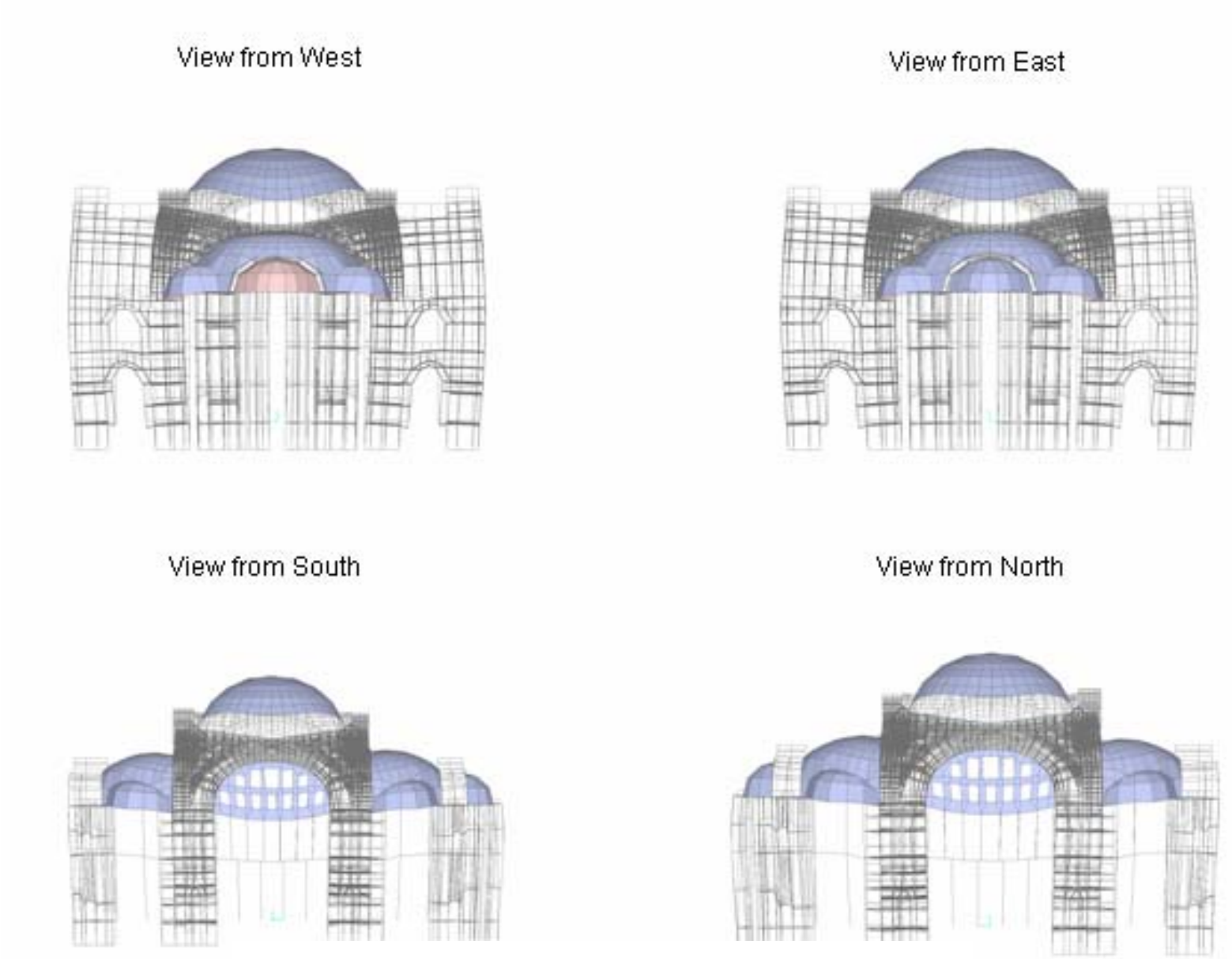

Figure 3.2. Deformations under self-weight, views from four sides

The stresses caused by self-weight are determined as lower than the assumed limit tensile strength of the brick-masonry; 1 MPa. The stress concentrations are observed mostly at the underside of the crowns of the main arches, above the surcharge and springing regions of the arches from the piers as can be seen in Figures 3.8 and 3.9. The upper portions of the crowns of the main arches exhibit compression, while the lower sides are in tension, consistent with the deformation. The maximum tensile and minimum compression stresses observed at the cross-sections of the crowns of the arches are 0.55 and -1.07 MPa for the east-west (Global Y) and 0.34 and -0.41 MPa for the north-south (Global X) directions respectively. The main dome is mostly in compression except four symmetric regions close to the pendentives where tensile stresses lower than 0.15 MPa occurs. Like the main dome, the semidomes are mostly in compression except the lower parts close to the exedrea domes, where tensile stresses have a maximum value of 0.5 MPa. The lower parts of the exedrea domes display tensile stress not exceeding 0.25 MPa. In Figures 3.3 to 3.12, the stresses for the shell and solid elements are shown.

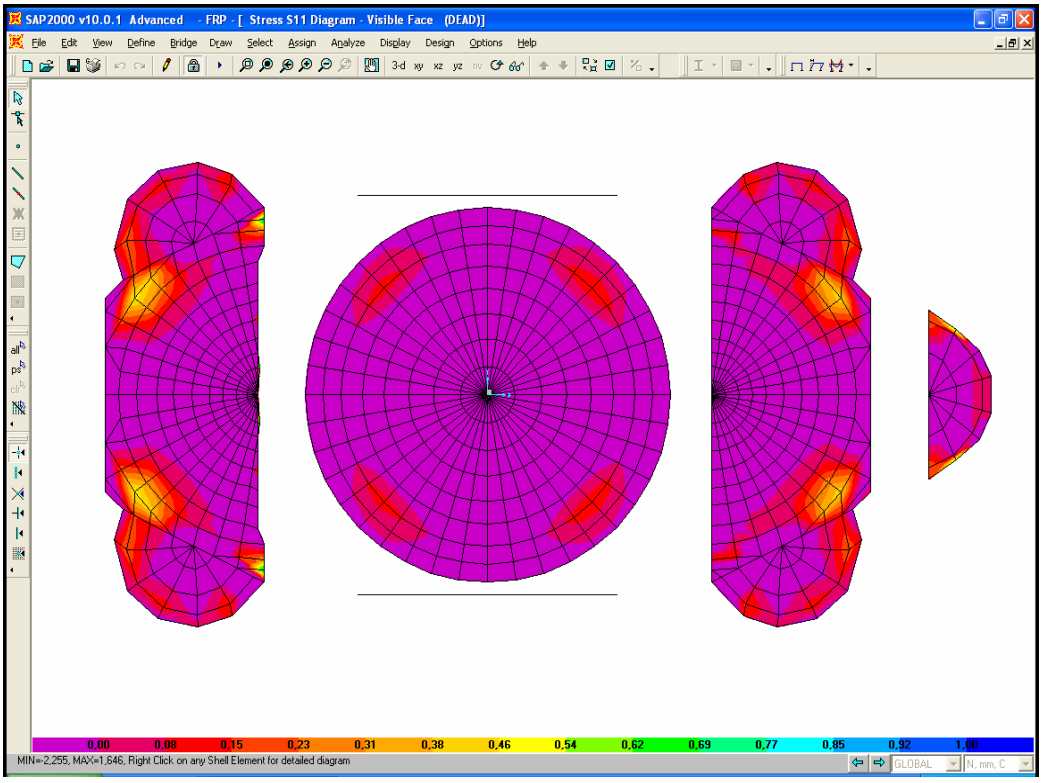

Figure 3.3. Hoop stresses of the shell elements under self-weight (0-1 MPa)

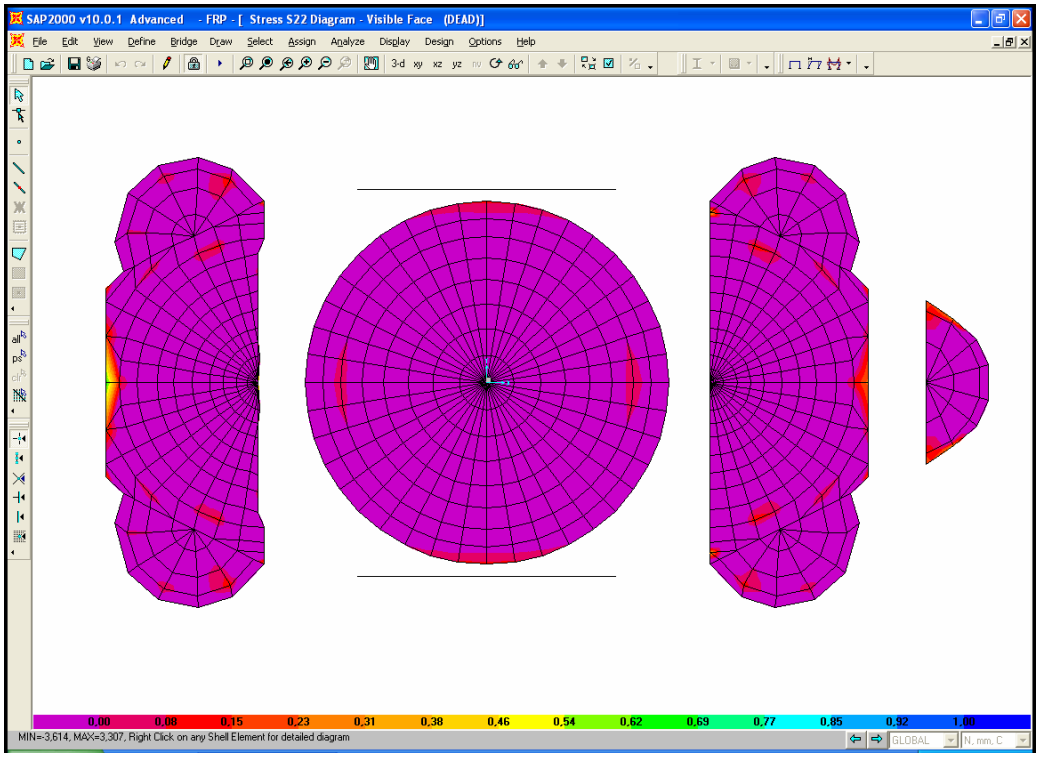

Figure 3.4. Radial stresses of the shell elements under self-weight (0-1 MPa)

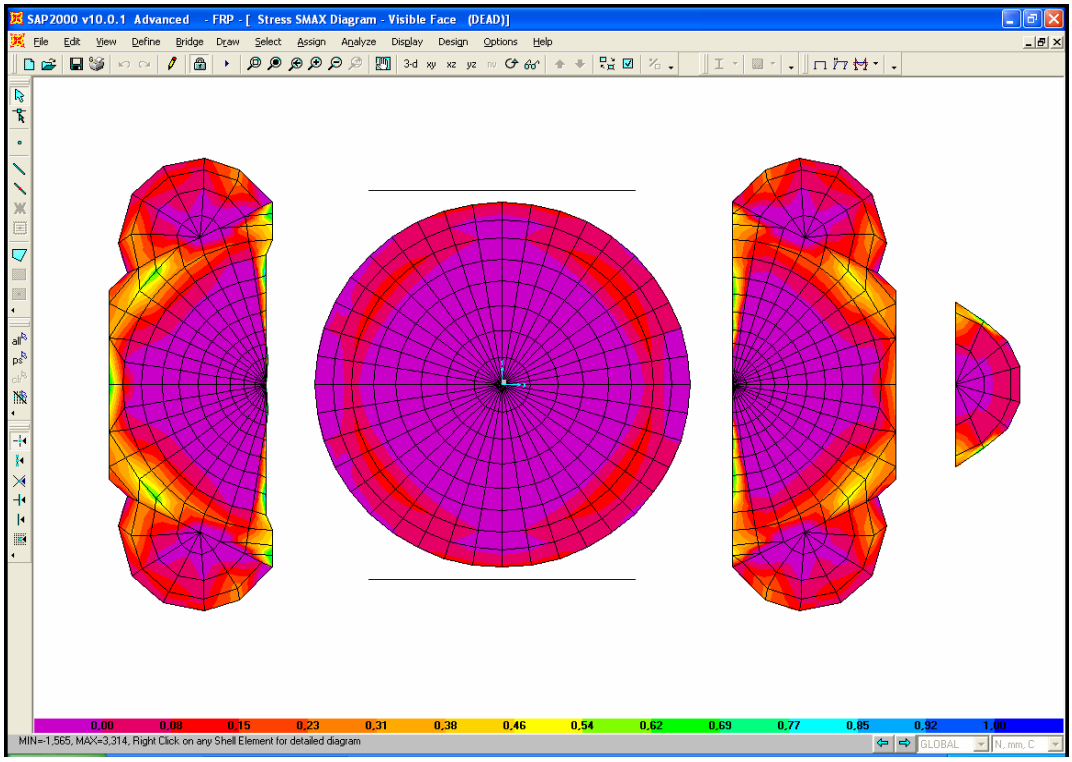

Figure 3.5. Maximum principle stresses of the shell elements under self-weight (0-1 MPa)

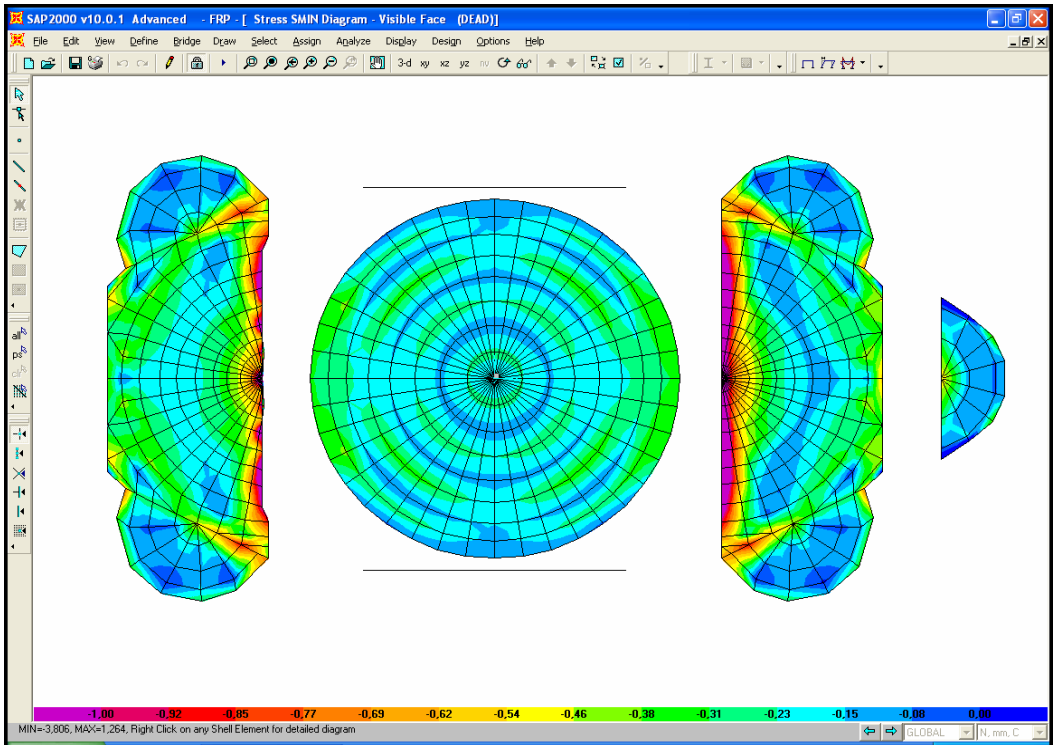

Figure 3.6. Minimum principle stresses of the shell elements under self-weight ((-1)-0 MPa)

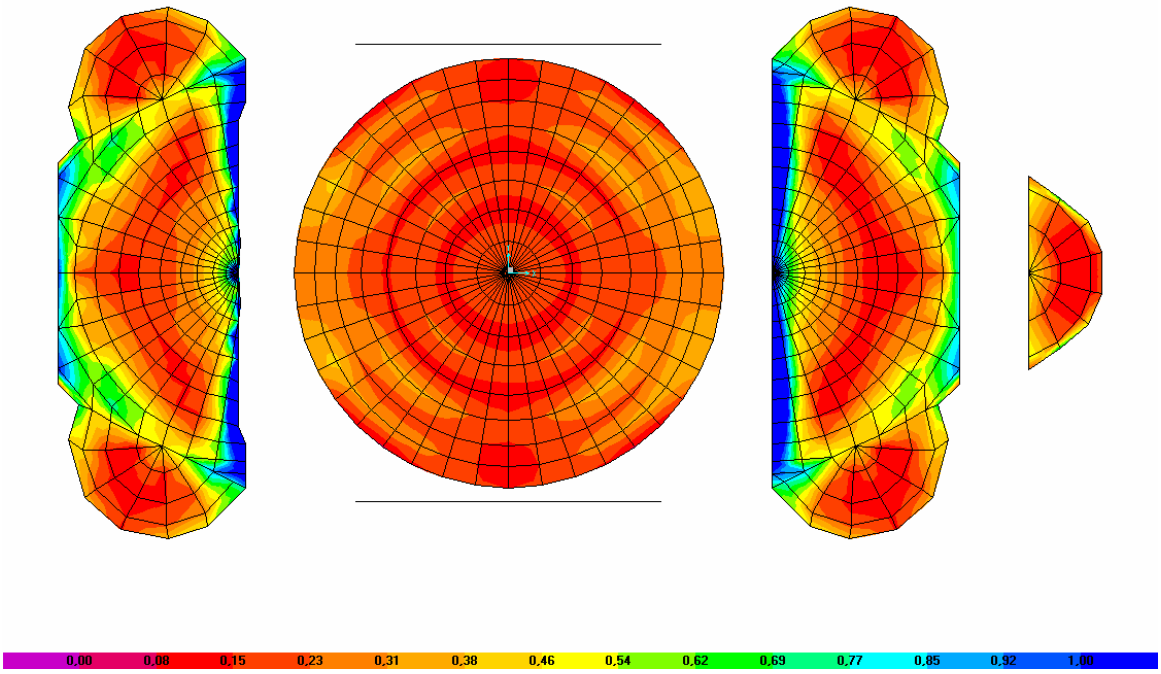

Figure 3.7. Von Mises stresses of the shell elements under self-weight (0-1 MPa)

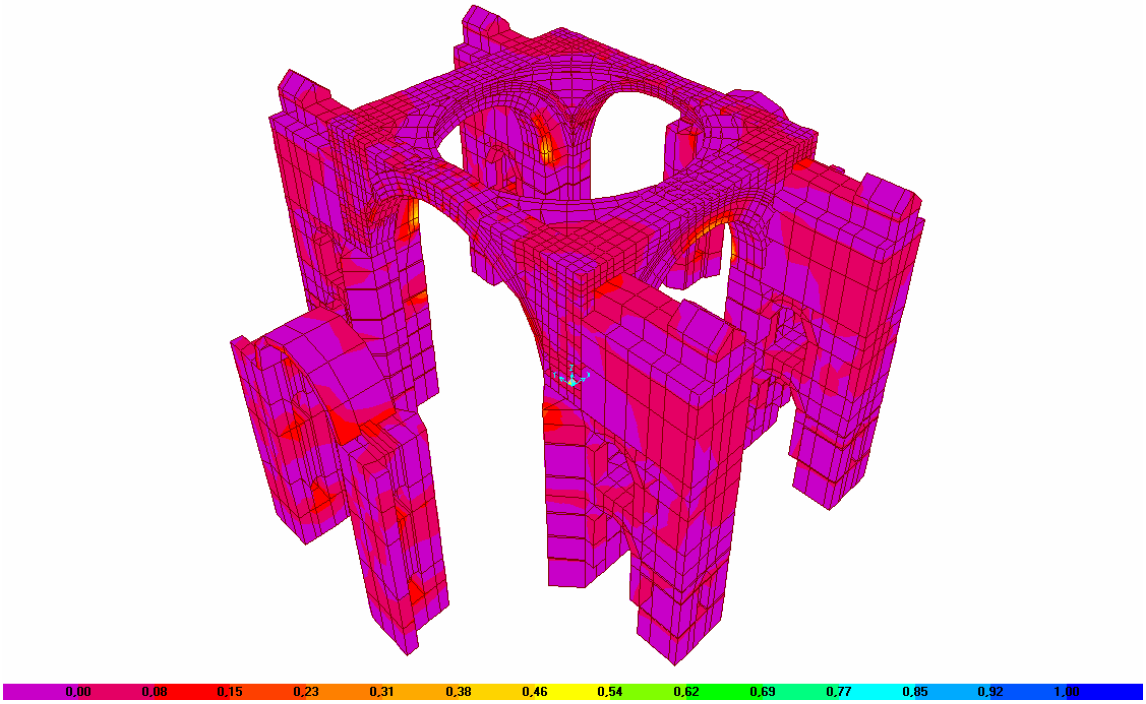

Figure 3.8. SXX stresses of the solid elements under self-weight (0-1 MPa)

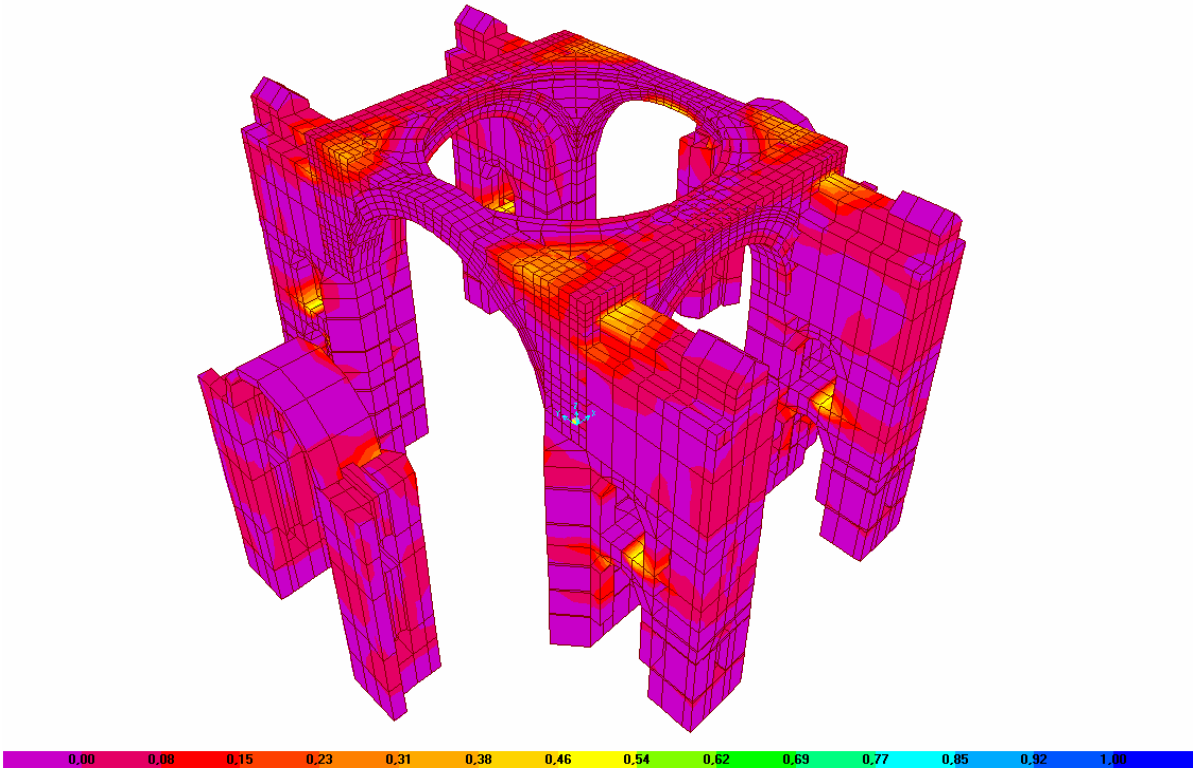

Figure 3.9. SYY stresses of the solid elements under self-weight (0-1 MPa)

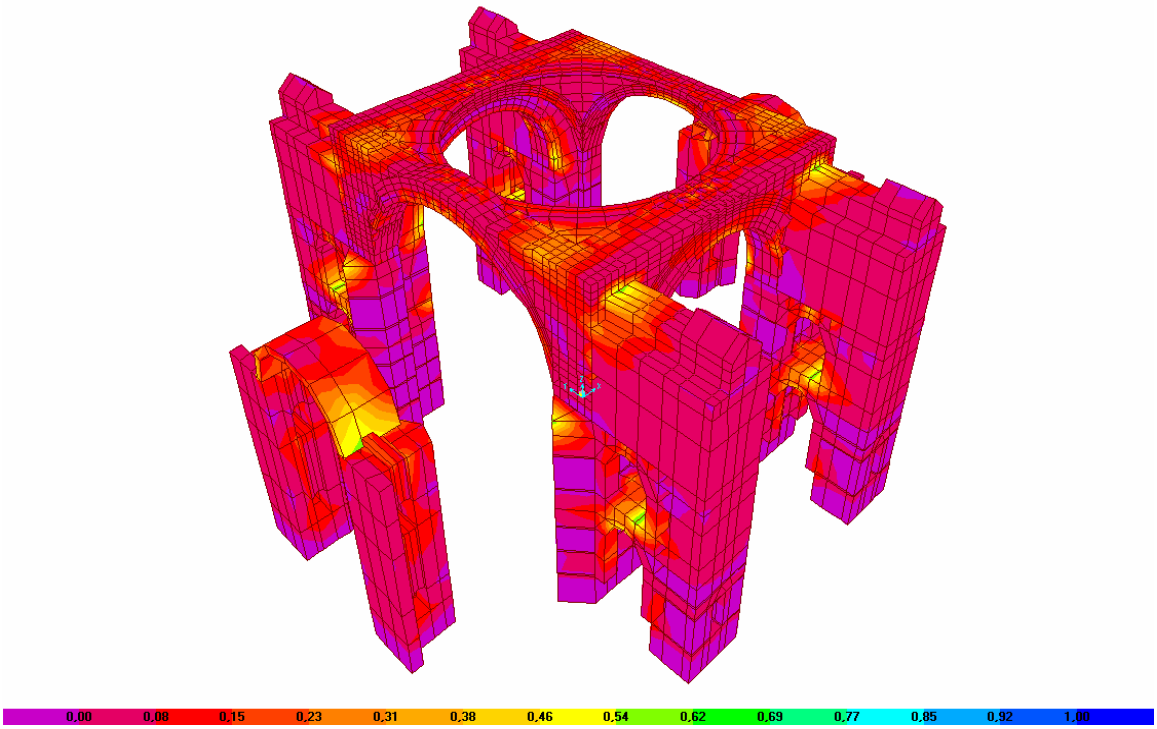

Figure 3.10. Maximum principle stresses of the solid elements under self-weight (0-1 MPa)

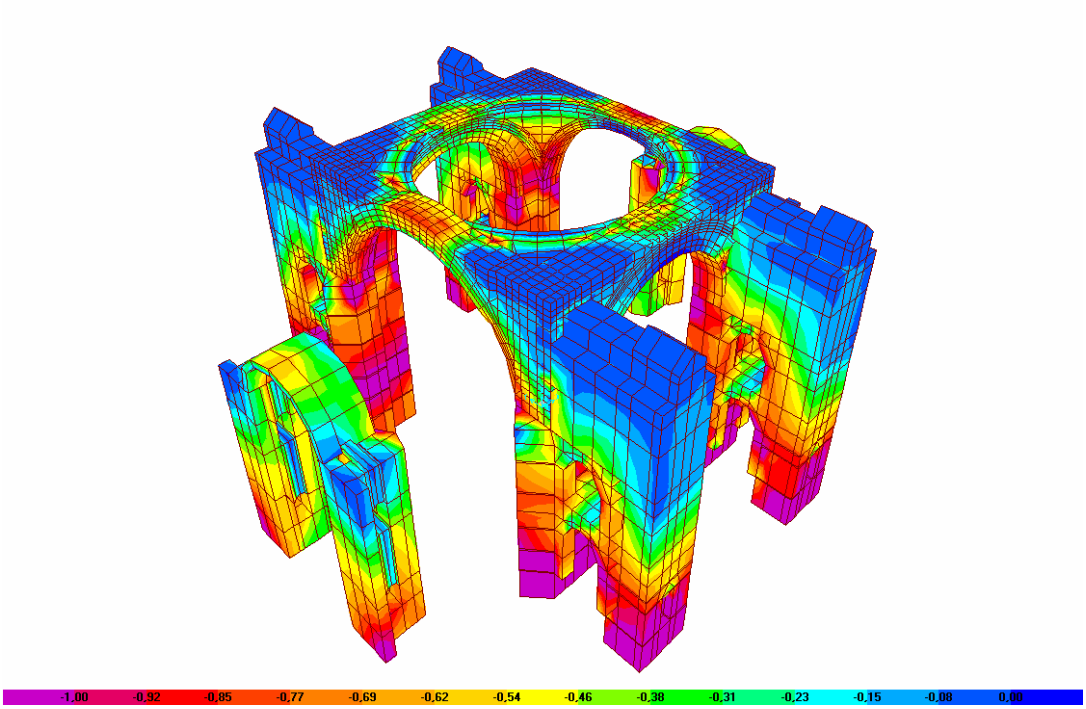

Figure 3.11. Minimum principle stresses of the solid elements under self-weight ((-1)-0 MPa)

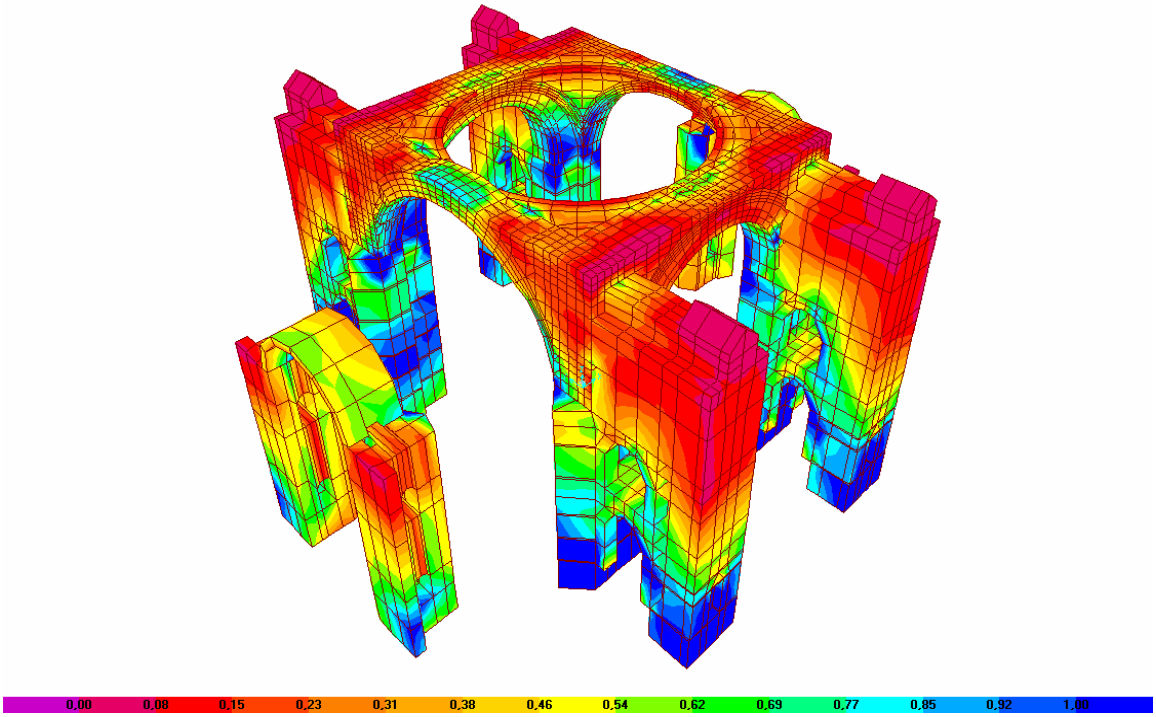

Figure 3.12. Von Mises stresses of the solid elements under self-weight (0-1 MPa)

3.2. Eigenvalue Analysis

Modal eigenvalue analysis provides to understand the dynamic behaviour of a structure by determining the natural frequencies and mode shapes. These modes are used for modal superposition in response spectrum and time-history analyses. Eigenvalue analysis is solved with the following equation;

$$[K - \Omega^2 M]\ \Phi = 0 \tag{3.1}$$

Where K is the stiffness matrix, M is the diagonal mass matrix, Ω^2 is the diagonal eigenvalue matrix, and Φ is the matrix of corresponding eigenvectors (mode shapes). Each eigenvalue with the corresponding eigenvector is named as the natural vibration mode of the structure. An eigenvalue is the square of circular frequency, ω, for that mode. The cyclic frequency, f, and period, T, of a mode are found as;

$$T = 1 / f \text{ and } f = \omega / 2\pi \tag{3.2}$$

The modes, which are numbered from *1* to *n*, have a participating mass ratio which measures how important to compute the response occurred by the corresponding mode to an acceleration load in each of the three global directions – X, Y and Z. By this way, an idea about the accuracy of response spectrum and time-history analyses can be obtained. The participating mass ratios for mode *n* corresponding to acceleration loads in the global X, Y, and Z directions are given by;

$$fxn = \varphi n^{T} mx \qquad rxn = (fxn)^2 / Mx \tag{3.3}$$

$$fyn = \varphi n^{T} my \qquad ryn = (fyn)^2 / My \tag{3.4}$$

$$fzn = \varphi n^{T} mz \qquad rzn = (fzn)^2 / Mz \tag{3.5}$$

where *fxn*, *fyn*, and *fzn* are the participation factors in the global X, Y, and Z directions, *n* is the corresponding mode number, *φn* is the mode shape, *mx*, *my*, and, *mz* are the unit acceleration loads*, Mx*, *My*, and *Mz* are the total unrestrained masses and *rxn, rxn* and *rzn* are the participating mass ratios acting in the global X, Y, and Z directions. If all modes of a structure are calculated, the cumulative participating mass ratio for each direction should be 100 per cent (SAP2000, 2007).

The eigenvalue analysis performed for Hagia Sophia represents a dominant motion along the east-west axis for the first mode. The second mode corresponds to a dominant motion in the north-south axis. Also, a small rotation is seen in this mode. The third mode shape is dominantly torsional. The fourth and fifth modes exhibit breathing respectively in northeast-southwest and east-west axes. It can be said that the model's and the real structure's dynamic behaviours satisfactorily correspond to each other, having two horizontal motions as the first two modes and pure torsion in the third mode. The first five natural frequencies of the FE model are compared with the ambient vibration results in Table 3.2.

Table 3.2. Modal frequencies of Vibration of Hagia Sophia from ambient vibration experiments and eigenvalue analysis

Mode	Ambient vibration freq.	Eigenvalue freq.	Dominant motion
1	1.85* - 1.75**	1.79	East-West
2	2.10* - 2.01**	2.11	North-South including slight torsion
3	2.35*	2.26	Torsional
4	2.50*	3.26	Northeast-Southwest breathing
5	2.80*	3.38	East-West breathing

* Obtained from ambient vibration survey done before 1999 Kocaeli Earthquake, Durukal, 1992.
** Obtained from ambient vibration survey done after 1999 Kocaeli Earthquake, Durukal, 2003.

In this study, the number of the modes taken into account is 5. The first five modes provide 75 per cent of participating mass ratios in translational directions. In Table 3.3, the modes and corresponding percentage of participating mass ratios are given. The first five mode shapes are shown in Figure 3.13.

Table 3.3. Modal frequencies and participating mass ratios

			X direction		Y direction		Z direction	
Mode	Period (t)	Frequency (Hz)	MPF	Sum of MPF	MPF	Sum of MPF	MPF	Sum of MPF
1	0.56	1.79	0.75	0.75	0.00	0.00	0.00	0.00
2	0.47	2.11	0.00	0.75	0.76	0.76	0.00	0.00
3	0.44	2.26	0.00	0.75	0.02	0.78	0.00	0.00
4	0.31	3.26	0.00	0.75	0.00	0.78	0.00	0.00
5	0.30	3.38	0.00	0.75	0.00	0.78	0.00	0.00
6	0.27	3.66	0.00	0.75	0.00	0.78	0.00	0.00
7	0.26	3.81	0.00	0.75	0.00	0.78	0.00	0.00
8	0.26	3.89	0.00	0.75	0.00	0.78	0.00	0.00
9	0.26	3.89	0.00	0.75	0.00	0.78	0.00	0.00
10	0.25	3.98	0.00	0.75	0.00	0.78	0.00	0.00
11	0.25	3.99	0.00	0.75	0.00	0.79	0.00	0.00
12	0.25	4.02	0.00	0.75	0.00	0.79	0.00	0.01
13	0.25	4.06	0.00	0.75	0.00	0.79	0.00	0.01
14	0.24	4.18	0.00	0.75	0.00	0.79	0.00	0.01
15	0.23	4.29	0.00	0.75	0.00	0.79	0.00	0.01
16	0.23	4.39	0.00	0.75	0.00	0.79	0.00	0.01
17	0.23	4.43	0.00	0.75	0.00	0.79	0.00	0.01
18	0.22	4.49	0.00	0.75	0.00	0.79	0.00	0.01
19	0.21	4.79	0.00	0.75	0.00	0.79	0.00	0.01
20	0.19	5.15	0.00	0.75	0.00	0.79	0.02	0.03
21	0.19	5.21	0.00	0.75	0.00	0.79	0.00	0.03
22	0.19	5.28	0.00	0.75	0.00	0.79	0.00	0.03
23	0.18	5.69	0.02	0.77	0.00	0.79	0.00	0.03
24	0.18	5.70	0.00	0.77	0.00	0.79	0.00	0.03
25	0.16	6.43	0.00	0.77	0.05	0.85	0.00	0.03

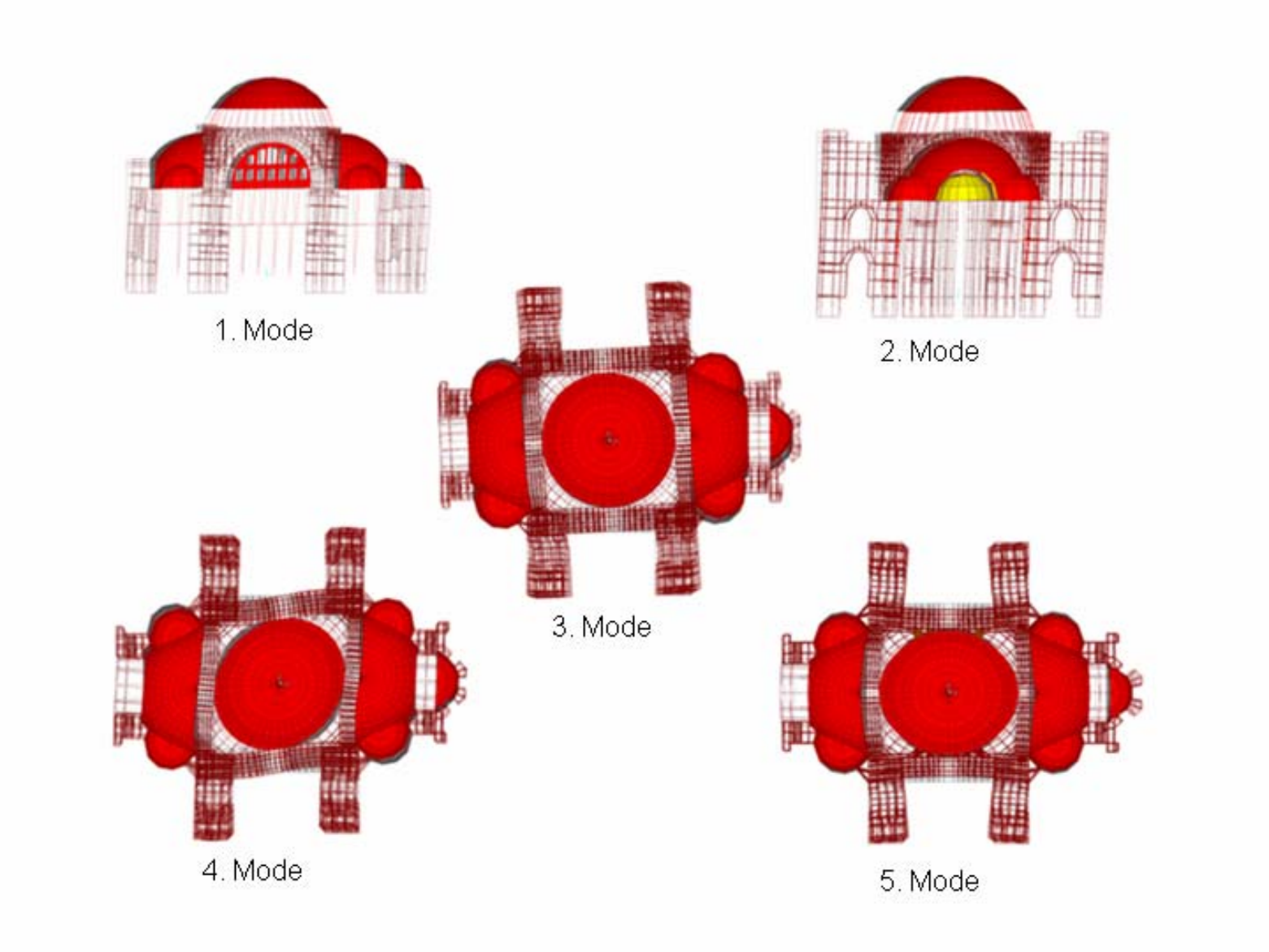

Figure 3.13. Modal shapes associated with the first five modes

3.3. Response Spectrum Analysis

Response spectrum analysis is a statistical method used to determine the likely response of a structure under a specific seismic loading. Analysis is performed by solving the dynamic equilibrium equation given as;

$$K\,x(t) + C\frac{dx(t)}{dt} + M\ddot{x}(t) = m_x \ddot{u}_{gx}(t) + m_y \ddot{u}_{gy}(t) + m_z \ddot{u}_{gz}(t) \qquad (3.6)$$

Where K is the stiffness matrix; C is the proportional damping matrix; M is the diagonal mass matrix; x, $\frac{dx}{dt}$, and $\ddot{x}$ are the relative displacements, velocities, and accelerations with respect to the ground; m_x, m_y, and m_z are the unit acceleration loads; and $\ddot{u}_{gx}$, $\ddot{u}_{gy}$ and $\ddot{u}_{gz}$ are the components of uniform ground acceleration. Response spectrum analysis aims to determine the maximum response rather than a full time history response to an earthquake (SAP2000, 2007).

To use an appropriate dynamic load, response spectrum curves are employed. Response spectrum curve is defined as; a set of values – whether acceleration, velocity or displacement – consisting of the maximum responses of single mass oscillators varying with natural frequencies and a given damping. Here, a spectrum of pseudo-spectral acceleration response versus period is considered. For each direction of the structure, horizontal and vertical, a spectrum can be utilized, but only a single positive response is produced by SAP2000. This response indicates a statistical magnitude of the likely maximum response for the considered earthquake. The actual response will change within a range from this positive value to its negative according to the application direction whether positive or negative (SAP2000, 2007).

Response spectrum analysis is a successor analysis which follows a modal analysis. For a specific direction, the loads obtained from spectrum curve for each mode of the structure are applied and corresponding responses whether displacement, force or stress are calculated. Then these calculated responses for each mode are superposed by using Complete Quadratic Combination method, so that a unique value for that direction is

estimated. The same procedure is repeated for the other directions. Finally responses calculated for each direction are combined with Square Root of the Sum of Squares method to ensure a single result. Response spectrum analysis is completed with two results by SAP2000; one is the maximum, positive, value and the other is the minimum, negative, value whose absolute value is same with the positive one. These two values correspond to the direction of the load applied. To figure out tensile stress, the maximum (positive) results are added to the self-weight results. To calculate compression, the minimum (negative) results are added to the self-weight results.

Hereby, to represent the seismic hazard at the site of Hagia Sophia, a response spectrum with a 0.4 peak ground acceleration and 5 per cent damping is employed. For the horizontal directions (X, Y) full loading is considered. This spectrum represents a 7.5 magnitude earthquake assumed to take place on the segments of the North Anatolian Fault in the Marmara Sea to the south of Istanbul. The response spectrum curve is shown in Figure 3.14 (Erdik *et al*., 2004). Seventy per cent of the response spectrum is applied in the vertical (Z) direction.

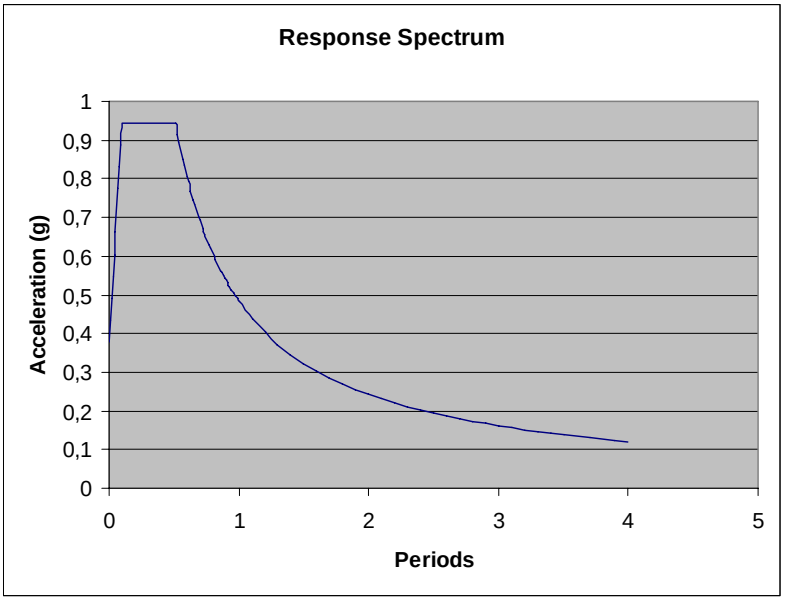

Figure 3.14. Response spectrum curve

It can be said that the domebase has a rigid body motion under the combined effect of self-weight and spectral loading. All crowns of the arches move in the same range, approximately 65 mm in N-S and 80 mm in E-W directions. The top of the main piers are

excited in a similar manner with a displacement of 50 mm and 60 mm in N-S and E-W directions respectively as shown in Table 3.4. The top, south and west views of the deformed shape under static and earthquake loading can be seen in Figures 3.15, 3.16 and 3.17 respectively.

Table 3.4. Displacements under self-weight and spectral forces

Location	North-South (mm)	East-West (mm)	Vertical (mm)
Top of the main dome	65.4	86.5	-6.6
East Arch Crown	64.0	75.2	-5.6
West Arch Crown	68.4	82.6	-5.8
North Arch Crown	67.2	83.9	-0.2
South Arch Crown	65.4	83.9	-0.2
Top of the N-E Pier	48.0	61.8	+5.5
Top of the N-W Pier	51.7	60.9	+5.7
Top of the S-E Pier	44.8	61.8	+5.5
Top of the S-W Pier	48.3	60.9	+5.7

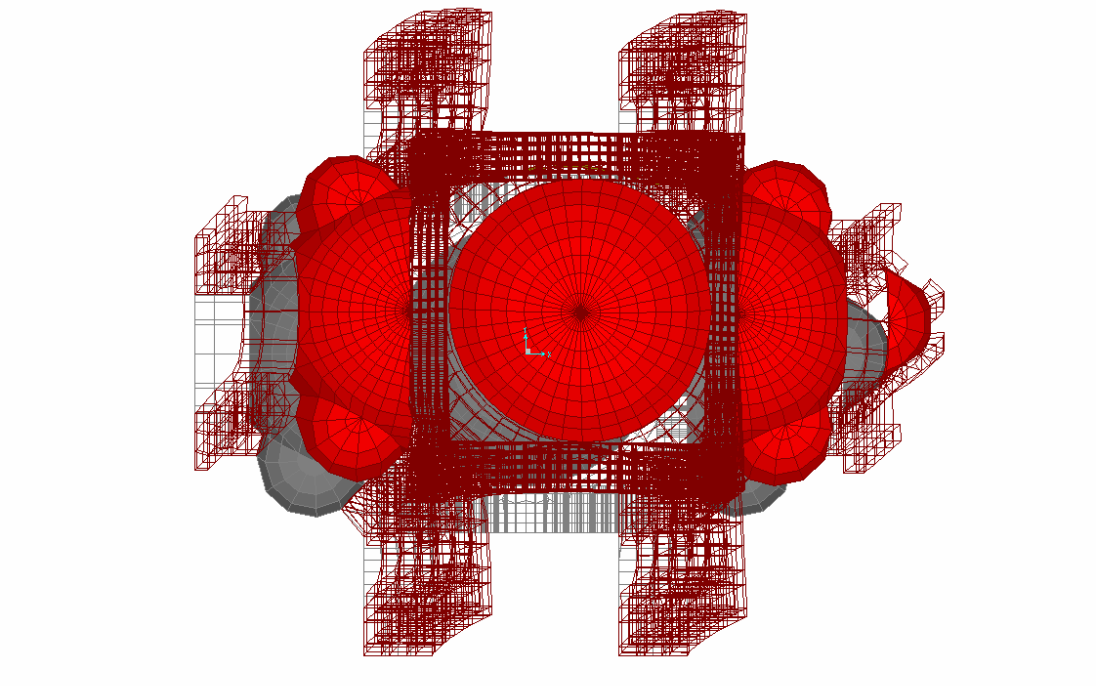

Figure 3.15. Deformations under self-weight and response spectrum loading, top view

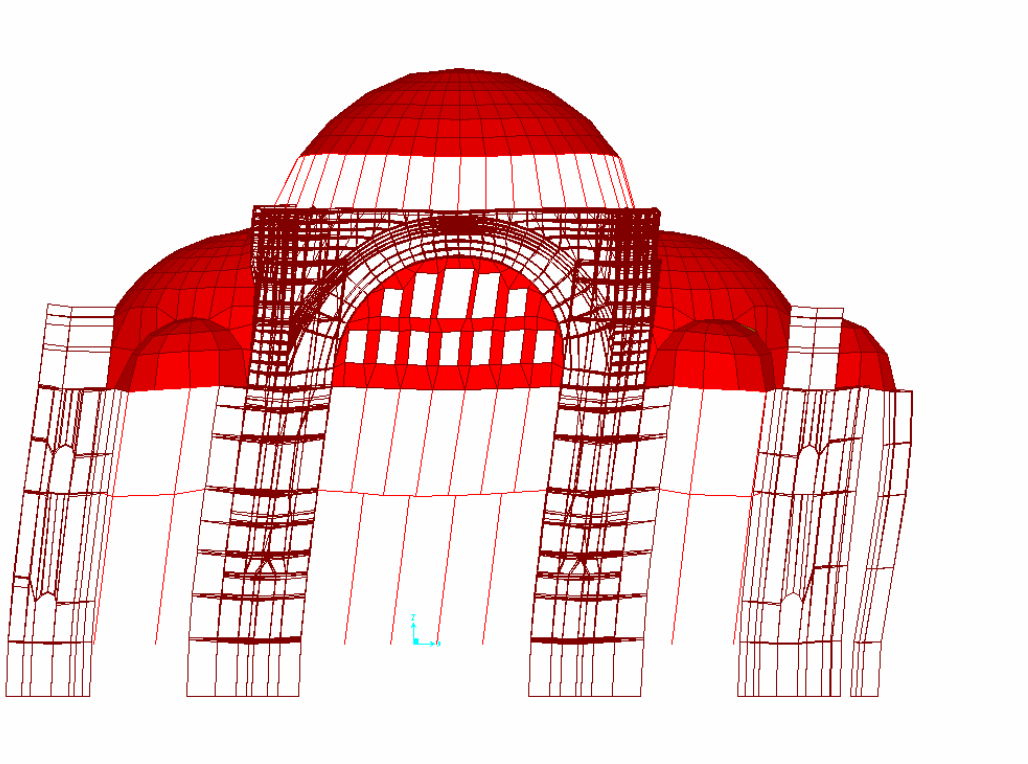

Figure 3.16. Deformation under self-weight and response spectrum loading, view from south

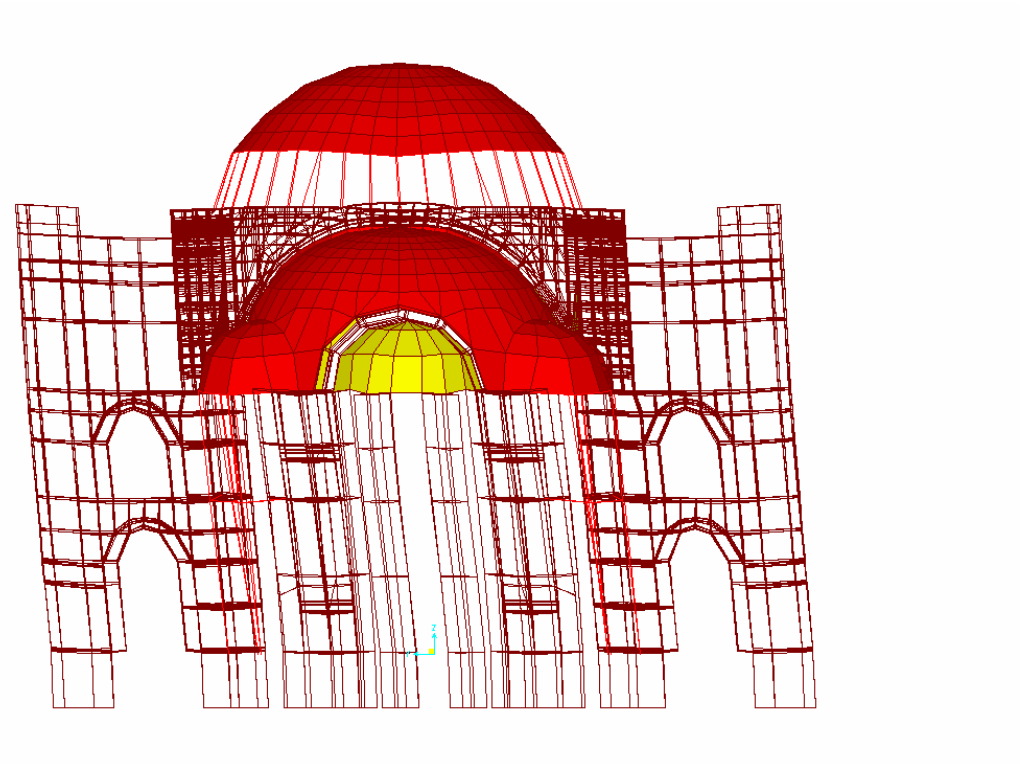

Figure 3.17. Deformation under self-weight and response spectrum loading, view from west

Large portions of the structure exhibit tensile stresses exceeding 1 MPa, especially on the surface of surcharge, undersides of voussoir and the springing regions of the arches. The maximum tensile stresses observed in the east-west (Global Y) direction are 3.9 MPa at the surface of the surcharge and 4.4 MPa at the intrados of voussoir and in the north-south (Global X) direction, it is 4.5 MPa at the surface of the surcharge and 5.0 MPa at the intrados of voussoir. In Figures 3.18 and 3.19, the stresses for the solid elements are shown.

Except the top regions, the main dome is mostly in tension not exceeding 1.5 MPa and 1 MPa for hoop and radial directions respectively. Compared to the main dome, semidomes display very high tensile stresses. The most critical regions are the lower portions of the semidomes especially the areas close to the exedra domes and barrel vaults where the stress values raise to 5 MPa and the upper parts close to the main arches where tensile stresses raise to 7 MPa for both hoop and radial directions. It should be underlined that these values should be approached carefully. Particularly, the regions connecting shell and solid elements or elements of different shapes, or adjacent shell elements having largely different local axes may display stress values much larger than the limit strength. Accuracy of the stress distribution in these regions can be estimated from the difference in values calculated from adjacent elements connecting to a common joint. By checking this, the reliability of stresses is assessed. The hoop and radial stresses of shell elements under static and dynamic loading can be seen in Figures 3.20 and 3.21. In SAP2000, principal stresses (SMAX and SMIN) and Von Mises stress are available for analysis cases and combinations that are single valued. So these types of stresses can be given for only static linear analysis. They are not applicable for response spectrum analysis (SAP2000, 2007).

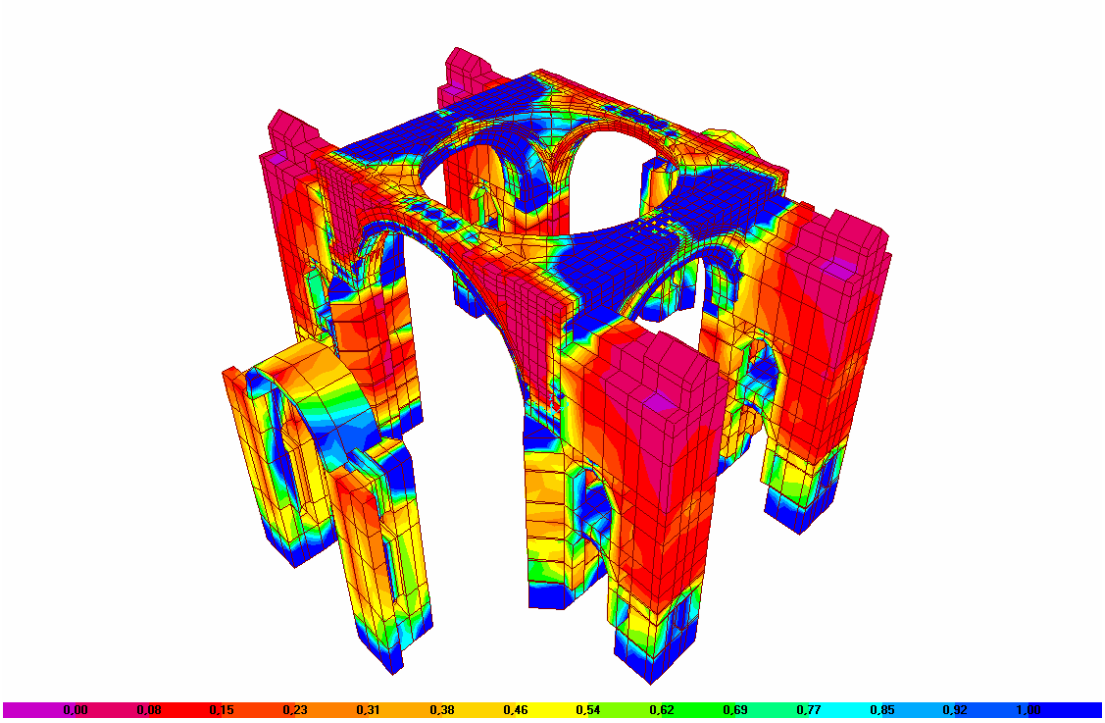

Figure 3.18. SXX stresses under self-weight and response spectrum loading (0-1 MPa)

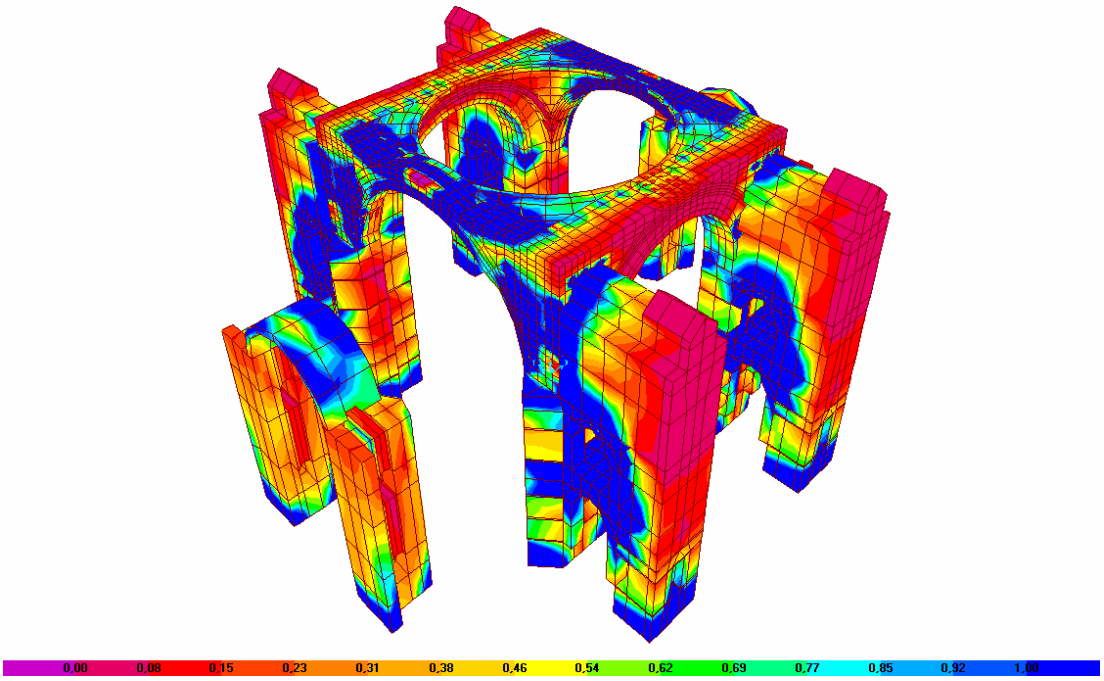

Figure 3.19. SYY stresses under self-weight and response spectrum loading (0-1 MPa)

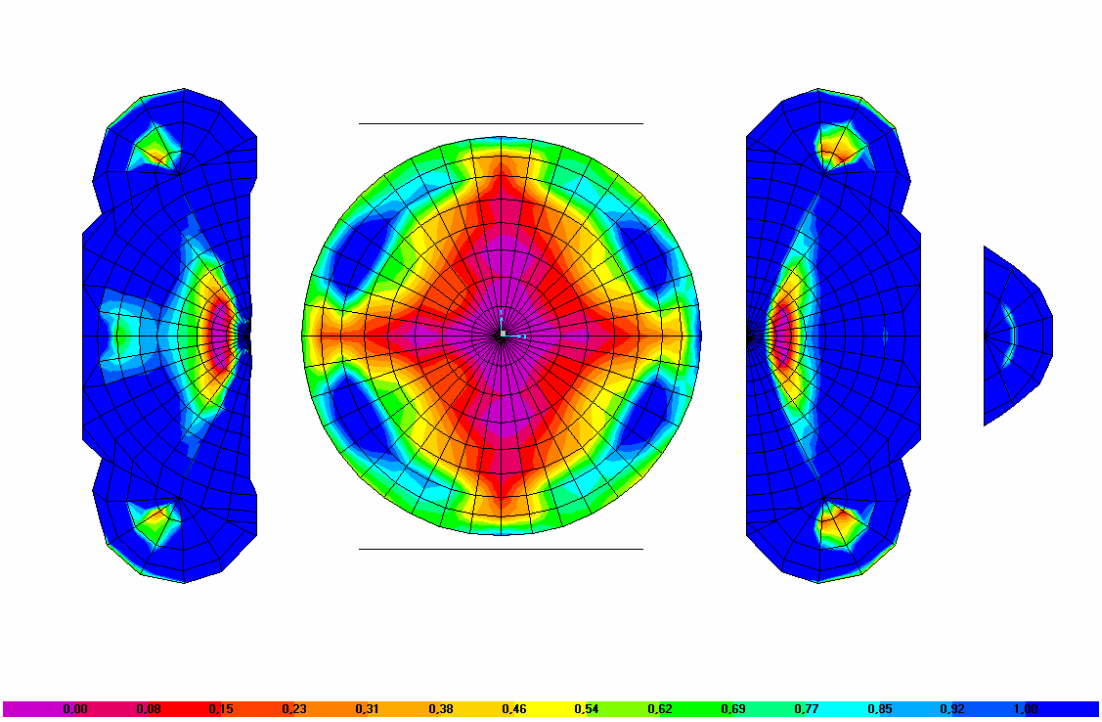

Figure 3.20. Hoop stresses under self-weight and response spectrum loading (0-1 MPa)

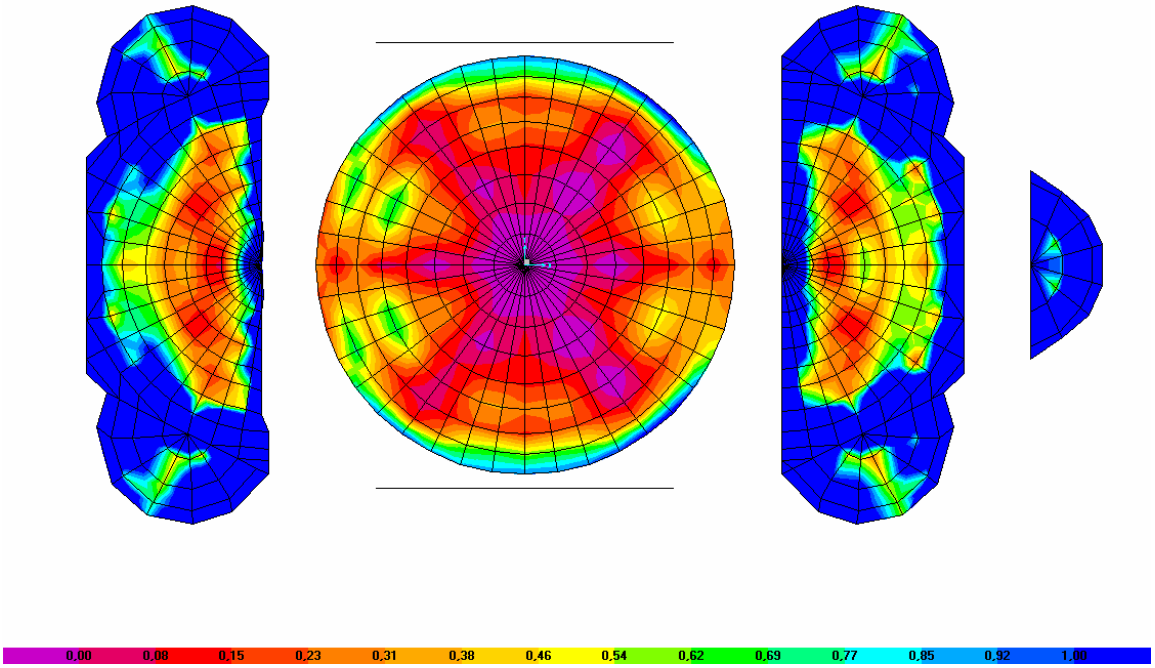

Figure 3.21. Radial stresses under self-weight and response spectrum loading (0-1 MPa)

4. THE STRENGTHENING STRATEGIES

The response spectrum analyses performed on the unstrengthened model determine the regions under risk during a strong earthquake. Particularly, main arches, semidomes and domebase exhibit high tensile stress concentrations. Reducing tensile stresses under the strength of brick masonry, which is assumed as 1 MPa, will lower the risk of failure under a seismic incident. To achieve this, two retrofitting methods are chosen; post-tensioned steel bars and fiber reinforced polymers (FRPs). Two models that represent these alternatives are created. In the first model, steel bars are used to strengthen the domebase to reduce the arches' responses to seismic loading. By implementing post-tensioning, additional compressive strength to counteract high tensile stresses are aimed for. The second model representative of application of FRPs is created to investigate the improvement in resistance of the semidomes and that of the domebase to seismic forces. Tension is intended to be carried by FRP laminates rather than the brick-masonry.

Same analyses carried out for the unstrengthened model are repeated for the two strengthened models. Successively, self-weight and response spectrum analyses, with the same input data are performed. Reinforcements with different post-tension values, cross sections and material properties are tested until the most reasonable responses are obtained. The stresses calculated in the intervened models are aimed to remain in the range (-10 MPa) and 1 MPa. The obtained stress changes are tabled to compare with the unstrengthened model.

4.1. Retrofit with Post-tensioned Bars

The reinforcement bars used for strengthening are modelled with tendon elements provided in SAP2000. Tendons are used to represent the effect of prestressing or post-tensioning applied upon frame, shell or solid elements. They can be modelled as either a load or an element. For linear analysis it will be satisfactory to model them as loads, but if the internal forces acting on tendons are needed, they must be modelled as elements. Tendons should be discretized with an adequate length. This discretion length is important for the accuracy of analysis. The length must be chosen according to the geometry of the

elements which the tendons pass through. The elements containing tendons are determined by a bounding box. The bounding box refers to the volume of the element, so it will be calculated by SAP2000, whether the tendon is connecting with it or not. Like frame elements, tendons have six degrees of freedom which transmit forces and moments to the elements they pass through. The cross sectional shape is always circular. Although, the stiffness properties for shear, bending and torsion can be assigned, the major interest is for the axial behaviour. The internal forces of tendons are same as frame elements. (SAP2000, 2007).

To define a post-stress load applied to a tendon, the following parameters are needed;

- Tension value in the tendon,
- Jacking location; at which end of tendon the tensioning will occur,
- Curvature coefficient; to specify the fraction of tension loss (due to friction) per unit of angle change (in radians) along the length of tendon measured from the jacking end,
- Wobble coefficient; to specify the fraction of tension loss (due to friction) per unit of tendon length measured from the jacking end, due to imperfect straightness of tendon,
- Anchorage set slip; to specify the length of slippage at the jacking end of tendon due to the release of the jacking mechanism (SAP2000, 2007).

In the study, tendons are model as elements to observe the internal forces which they deal with. The parameters assumed for the analysis is summarized as follows;

- For each arches 4 tendons and totally 16 tendons are employed in the model.
- 10 MN post-tension force for each tendon in East and West arches and 20 MN post-tension force for the ones in North and South arches are applied.
- Tendons' material is selected as steel
- cm diameter is chosen for each tendon.
- Maximum discretization length is 50 cm
- No tendon profile is given.

- Jacking location at both ends of tendon is selected.
- The default values of SAP2000 for wobble coefficient - 8,333e-7 1/cm and anchorage set slip - 25 cm are set.

The locations of the tendons are decided after a set of trial runs. Two types of arrangements for the tendons have been tried. In the first model three tendons are placed in the parts of the main arches close to their lower faces to counteract the observed tensile stress concentrations in these zones. This first model can be seen in Figure 4.1. In the second model, concerned about the bowing that this non-uniform placement of tendons may cause, they are distributed uniformly in cross-sections as seen in Figure 4.2. However no distinct difference between these two models could be observed from displacements presented in Figure 4.3. Thus it was decided to continue with the model where four tendons are distributed uniformly over the cross-section of the main arches.

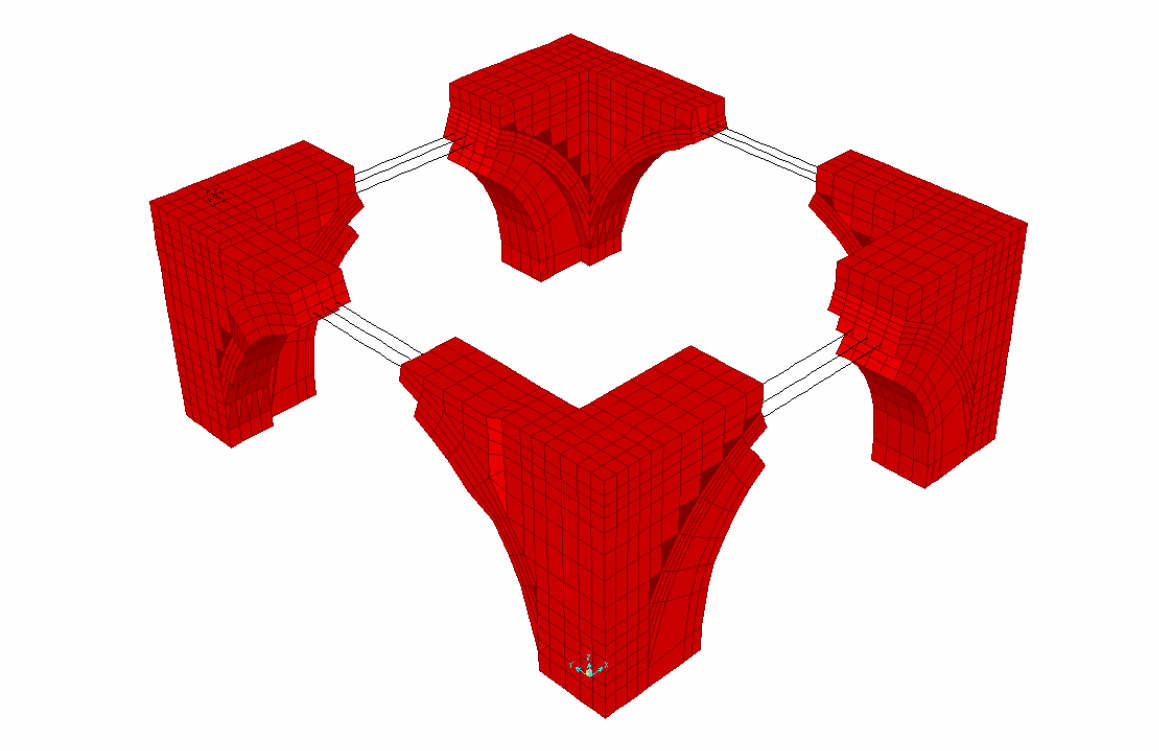

Figure 4.1. Strengthened model I

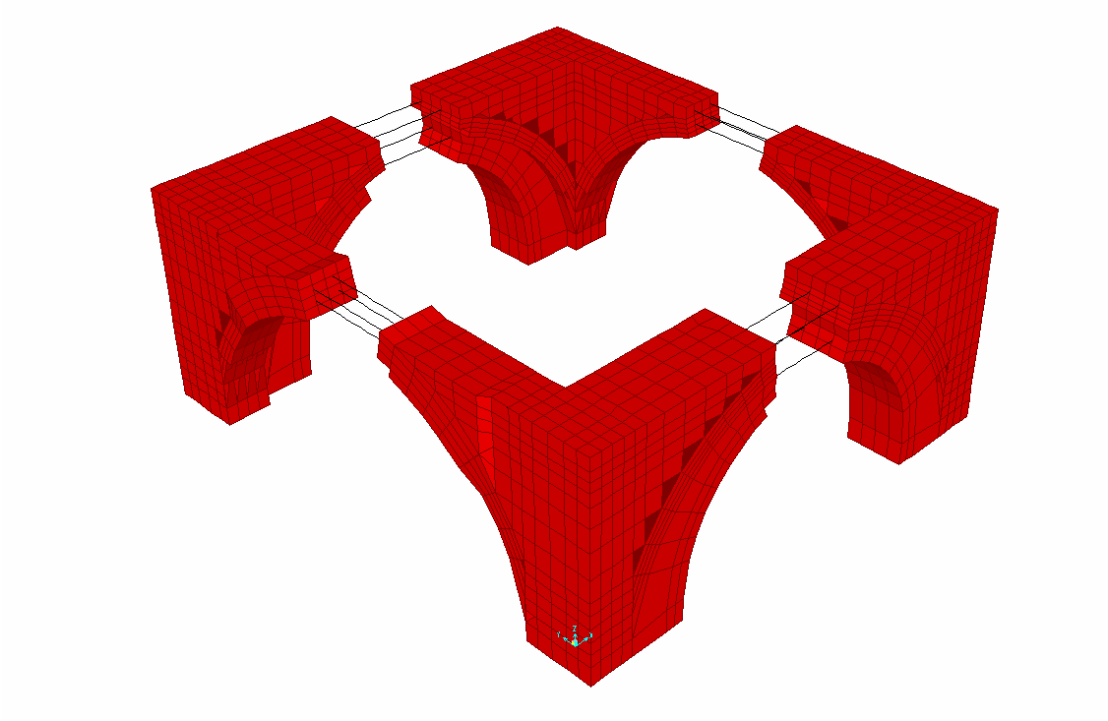

Figure 4.2. Strengthened model II

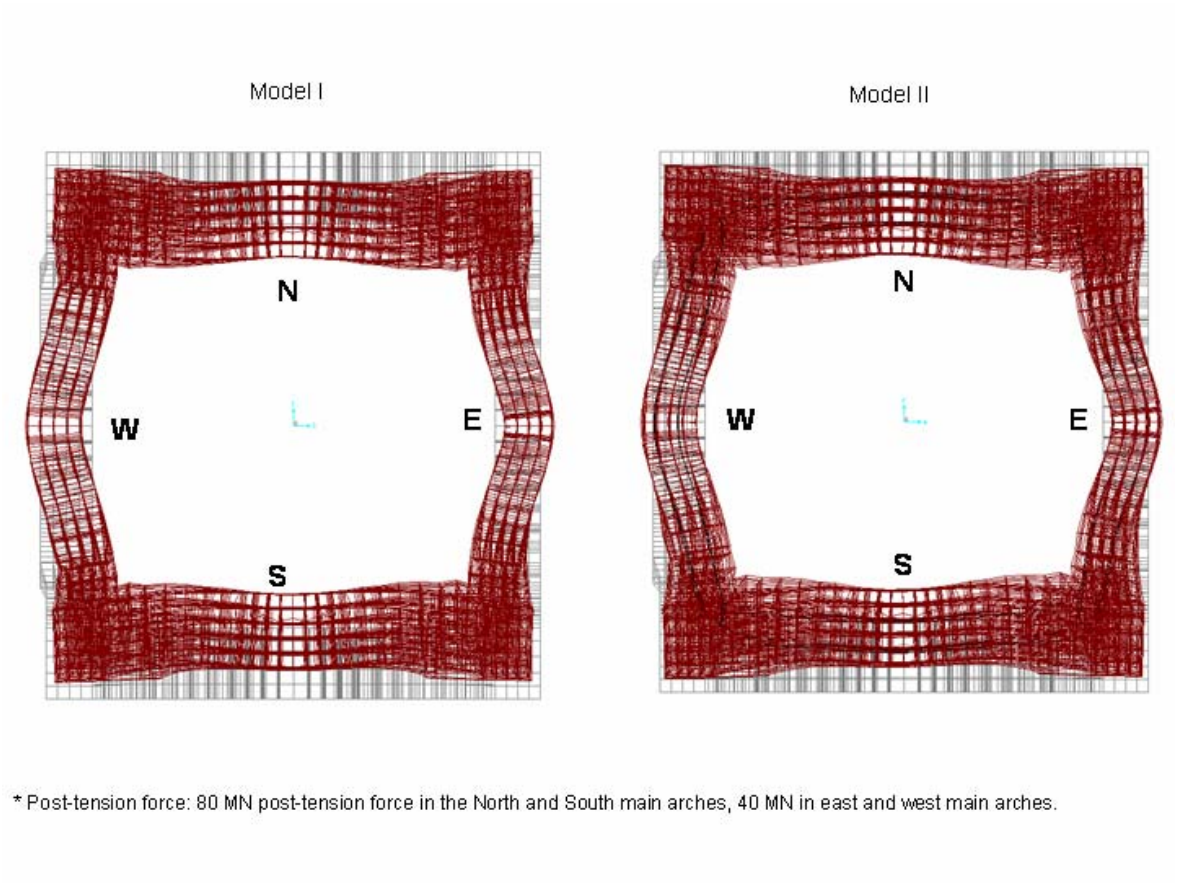

Figure 4.3. Displacements for the strengthened models: model I (left side), model II (right side)

Moreover, different forces are applied to inner and outer tendons passing through the arches to overcome the bowing occurred at the crowns, but again it was observed that the responses remain the same. The major parameter affecting deformations and stresses is the magnitude of post-tension force. If total post-tension force acting to an arch remains constant, all alternatives of locations give similar results. To understand the character of the behaviour, the post-tension forces are increased incrementally. For this purpose, three models are tried. They can be described as follows:

(i) 60 MN in north-south arches and 30 MN in east-west arches
(ii) 80 MN in north-south arches and 40 MN in east-west arches
(iii) 120 MN in north-south arches and 60 MN in east-west arches

The most appropriate one is chosen to ensure the strength limits of masonry. The final values used for the post-tension forces are 40 MN for east and west arches and 80 MN for north and south arches. Here, the post-tension forces are total, i.e. as an example in the model to achieve 40 MN post-tension in an arch, 10 MN post-tension is applied per tendon.

The static linear analysis performed for the post-tensioned model reveals that the deformation pattern of the domebase changes fundamentally as compared to the case under self-weight only as shown in Figures 4.4, 4.5 and 4.6. Unlike self-weight analysis this time all arches are forced to move inward. On the other hand, the crowns of east and west arches – which have thinner cross sections - bow towards outward at their crowns i.e. the corners of the domebase move inward whereas the crowns move outward. Because north and south arches have larger cross section and higher rigidity, bowing of these two arches is less than the bowing at east and west arches. The displacements are in the order of mm similar to the ones obtained from the analysis due to self-weight only, but directions of displacements are reversed. Displacements at all joints in the cross sections are taken to calculate the average displacements of the crowns given in Table 4.1.

Table 4.1. Displacements under self-weight and post-tensioning

Location*	Self-weight					Self-weight and Post-tension**				
	North-South		East-West		Vertical	North-South		East-West		Vertical
	mm		mm		mm	mm		mm		mm
Top of main dome	0.0	-	0.1	West	-7.3	0.0	-	0.1	West	-5.1
East Arch Crown	-	-	2.3	Inward	-8.9	-	-	0,7	Outward	-3.4
West Arch Crown	-	-	1.8	Inward	-8.6	-	-	0,7	Outward	-3.2
North Arch Crown	0.9	Outward	-	-	-5.5	5.6	Inward	-	-	-6.7
South Arch Crown	0.9	Outward	-	-	-5.5	5.6	Inward	-	-	-6.7
Top of the N-E Pier	1.6	Outward	0.5	Outward	-2.7	3.4	Inward	2.4	Inward	-3.5
Top of the N-W Pier	1.7	Outward	0.7	Outward	-2.7	3.1	Inward	2.2	Inward	-3.5
Top of the S-E Pier	1.6	Outward	0.5	Outward	-2.7	3.4	Inward	2.4	Inward	-3.5
Top of the S-W Pier	1.7	Outward	0.7	Outward	-2.7	3.1	Inward	2.2	Inward	-3.5

* All joints existing at cross section are taken into account to calculate the average displacement
** Post-tension forces: 80 MN in north-south arches and 40 MN in east-west arches

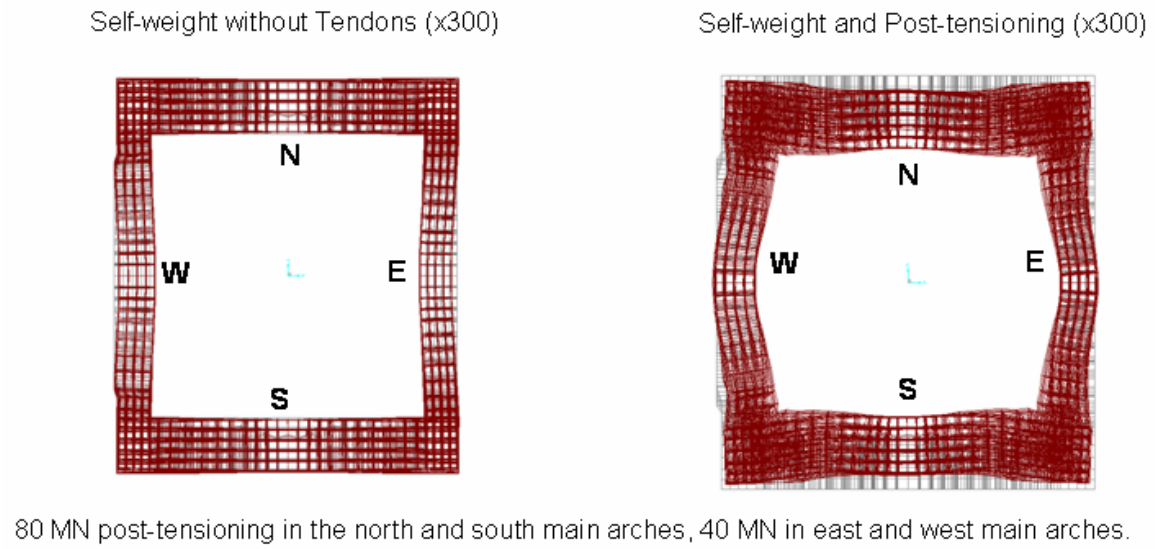

Figure 4.4. Deformations under self-weight and post-tensioning, top view

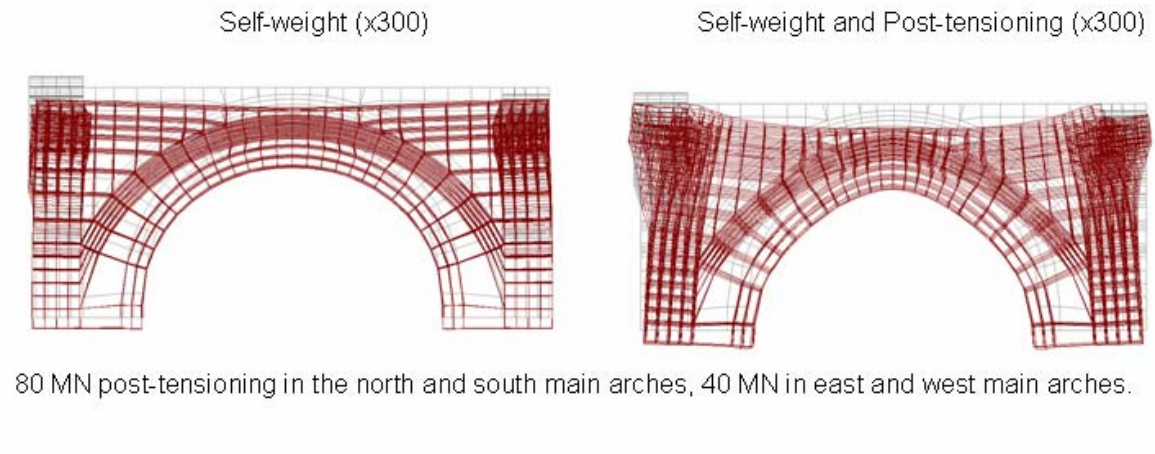

Figure 4.5. Deformations under self-weight and post-tensioning, south view

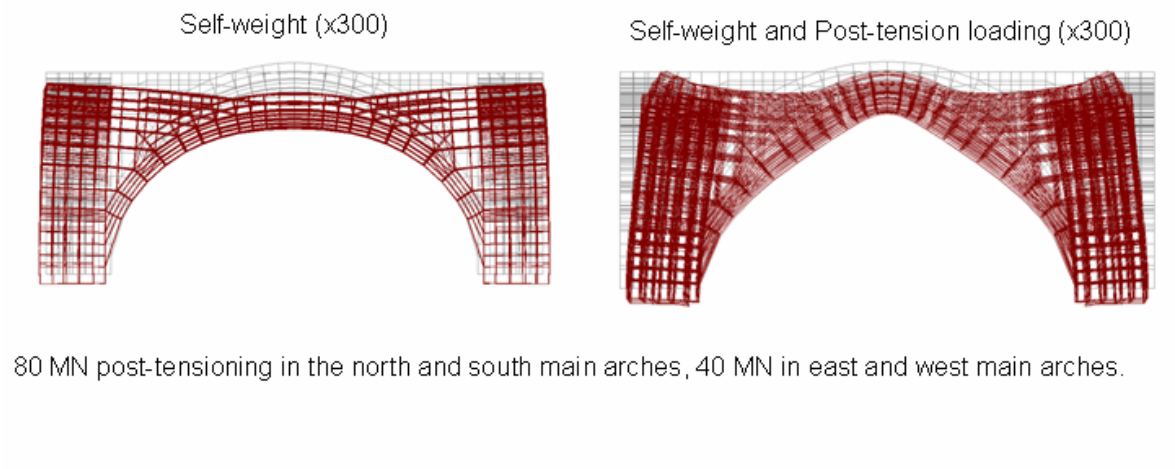

Figure 4.6. Deformations under self-weight and post-tensioning, west view

The compressive stresses caused by both self-weight and post-tensioning are lower than the assumed limit compressive strength of the brick-masonry; 10 MPa throughout the structure. All arches exhibit compressive stresses along their spans, especially high stress concentrations are observed at the crowns (Figures 4.7 and 4.8). The maximum compressive stresses observed are 5.6 MPa for east arch (Global Y), 5.1 MPa for west arch (Global Y), and 3.9 MPa for both north and south arches (Global X). Tension caused due to bowing, not exceeding 1 MPa, occurred on the outside surfaces of the crown of the west main arch. The stresses in X and Y directions can be seen in Figures 4.7 and 4.8 respectively.

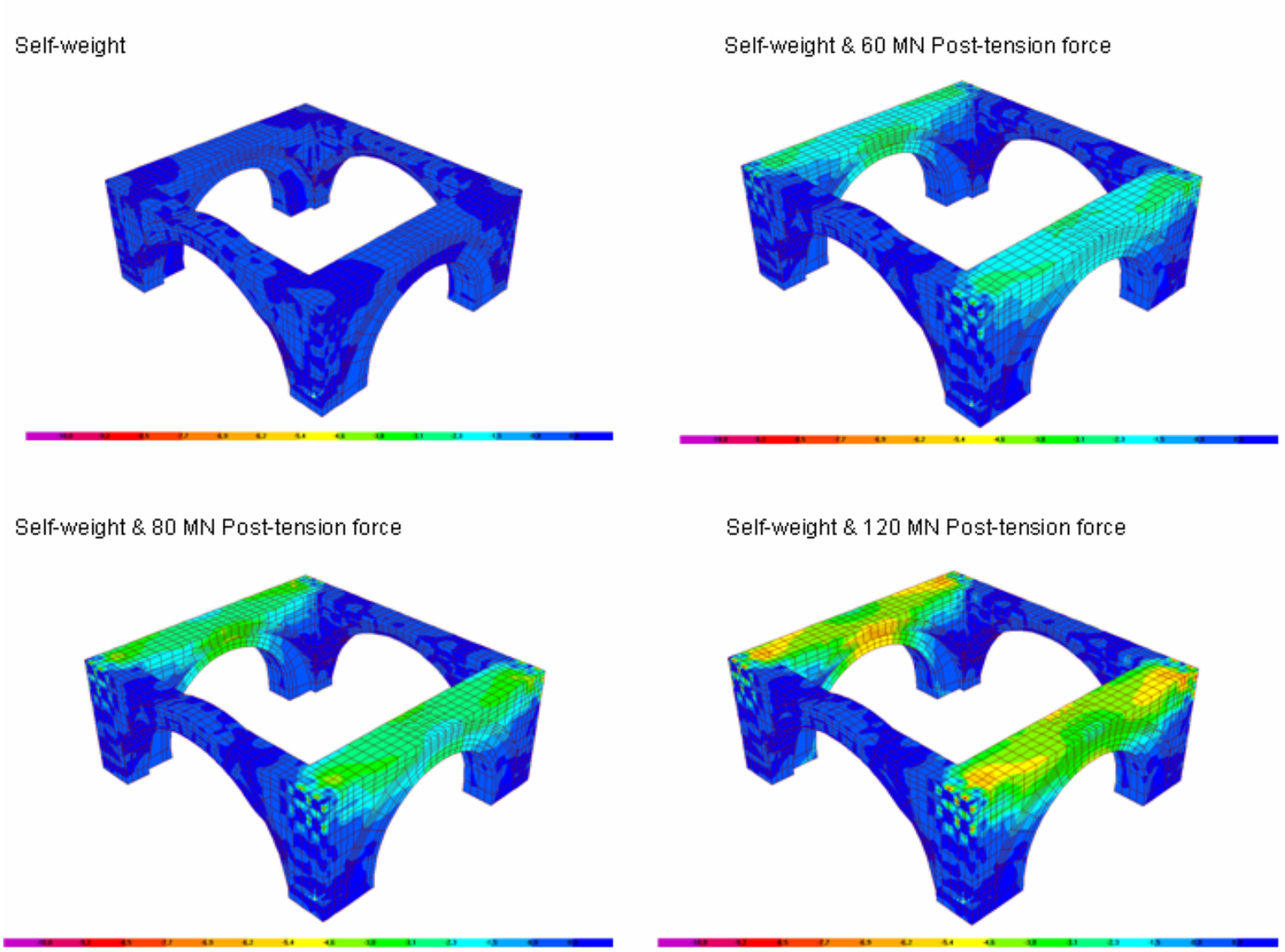

Figure 4.7. SXX stresses at the domebase under self-weight and post-tensioning ((-10)-0 MPa)

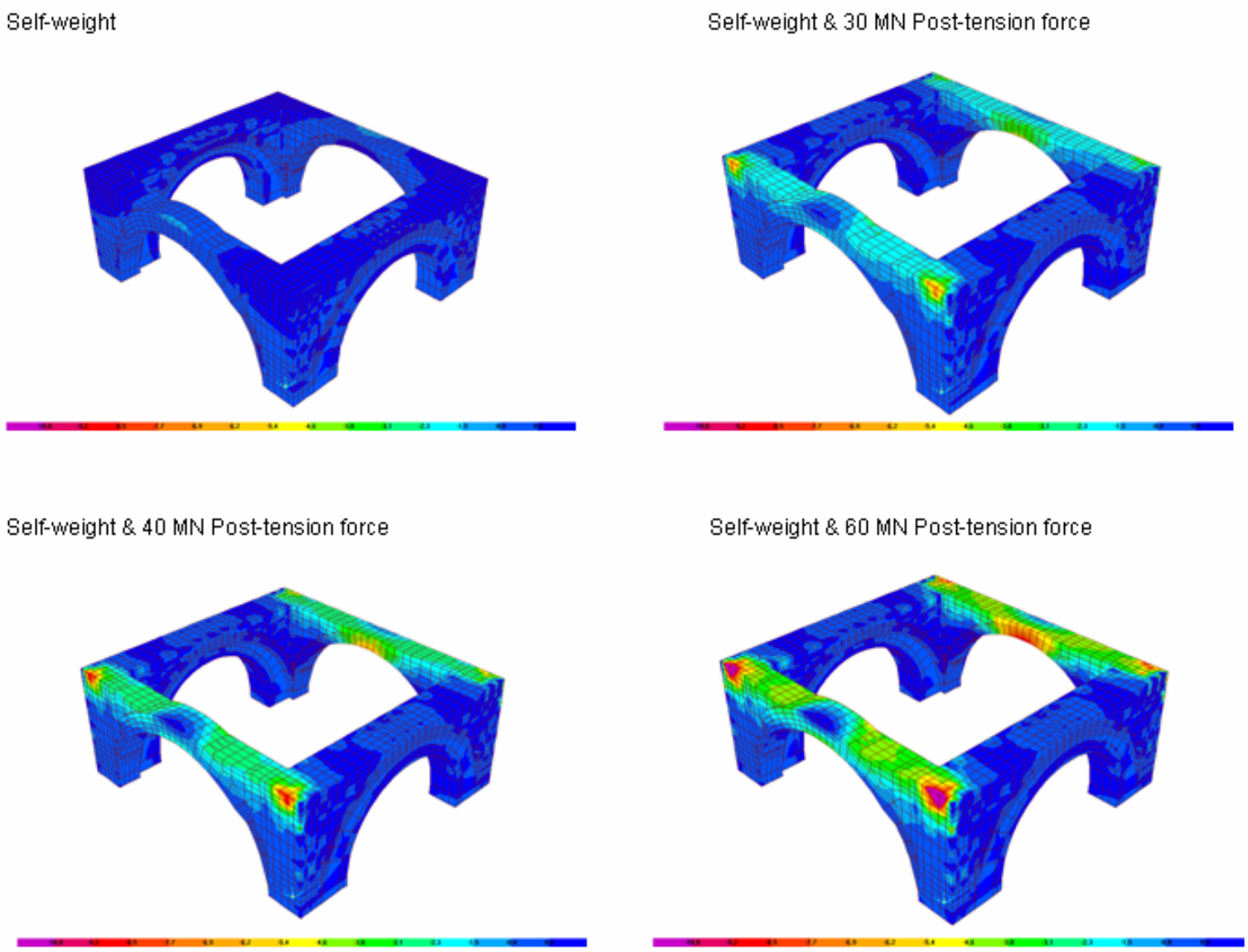

Figure 4.8. SYY stresses of the domebase under self-weight and post-tensioning ((-10)-0 MPa)

The response spectrum analysis performed using the post-tensioned model reveals a deformation shape in general terms similar to the deformation shape of the unstrengthened model. The effect of post-tensioning becomes evident particularly in the vertical deformations of the crowns of the east and west main arches and that of the top of the main dome. In the main dome vertical deformation reduces by about 30 per cent. At the crowns of the north and south main arches we observe a decrease in the north-south deformation by about 10 per cent, on the other hand the deformations of the crowns of the north and south arches increase. The effect of post-tensioning is the horizontal east-west deformation of the east and main arches is less pronounced probably due to the trust of the semidomes. The major displacements under the combination of self-weight, spectral loading and post-tension forces - which are 80 MN in north-south arches and 40 MN in east-west arches - are given in Table 4.2.

Table 4.2. Displacements under self-weight, spectral and post-tension forces

	Self-weight and Response spectrum			Self-weight, Resp. Spec. and Post-tension**		
	North-South	East-West	Vertical	North-South	East-West	Vertical
Location*	mm	mm	mm	mm	mm	mm
Top of main dome	65.4	86.5	-6.6	65.4	86.5	-4.4
East Arch Crown	64.4	75.1	-5.6	64.3	78.4	-0.1
West Arch Crown	68.4	82.6	-5.8	68.4	80.1	-0,4
North Arch Crown	67.2	83.9	-0.2	60.7	83.9	-1.5
South Arch Crown	65.4	83.9	-0.2	72.9	84.0	-1.5
Top of the N-E Pier	48.0	61.8	5.5	42.9	58.8	4.7
Top of the N-W Pier	51.7	60.9	5.7	46.8	63.9	4.9
Top of the S-E Pier	44.8	61.8	5.5	49.8	58.8	4.7
Top of the S-W Pier	48.3	60.9	5.7	53.1	63.9	4.9

* All joints existing at cross section are taken into account to calculate the average displacement
** Post-tension forces: 80 MN in north-south arches and 40 MN in east-west arches

Post-tensioning lead to significant stress reductions in the response spectrum analysis. Although the stresses on the surcharge can not be decreased under 3 MPa, the stresses at the cross sections of the crowns reach reasonable values. The limiting value of 1 MPa is reached at these sections. Assuming the earthquake loading acting in positive directions, the maximum compressive stress observed is 3.4 MPa for north and south arches (Global X), while it is 4.8 MPa for east arch and 4.4 MPa for west arch (Global Y).

If the earthquake forces act in negative directions, the maximum compression stresses become 5.8 MPa for north and south arches (Global X), 6.4 MPa for east arch and 5.8 MPa for west arch (Global Y). The stresses in X and Y directions can be seen in Figures 4.9 and 4.10 respectively.

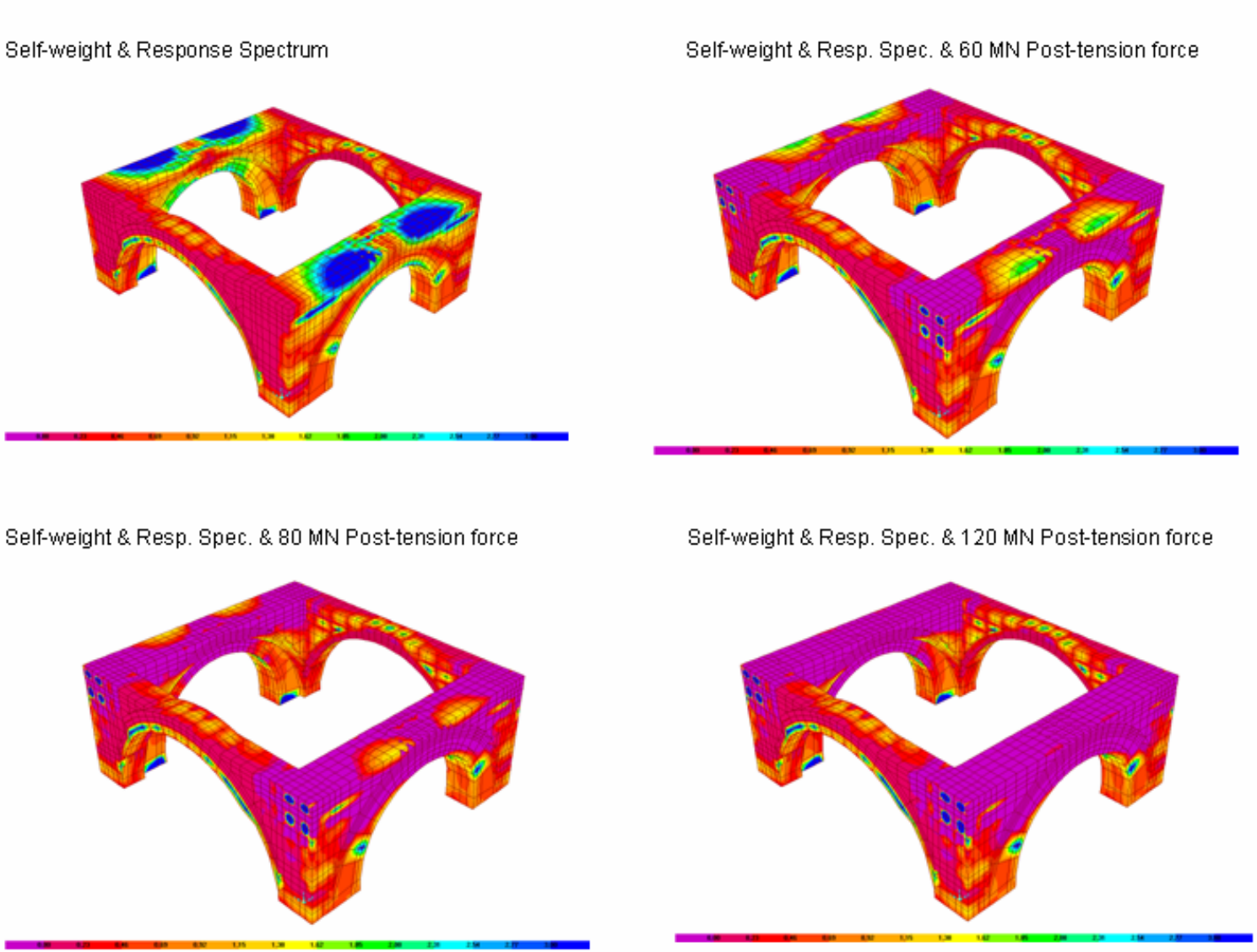

Figure 4.9. SXX stresses at the domebase under self-weight, response spectrum, post-tensioning (0-3 MPa)

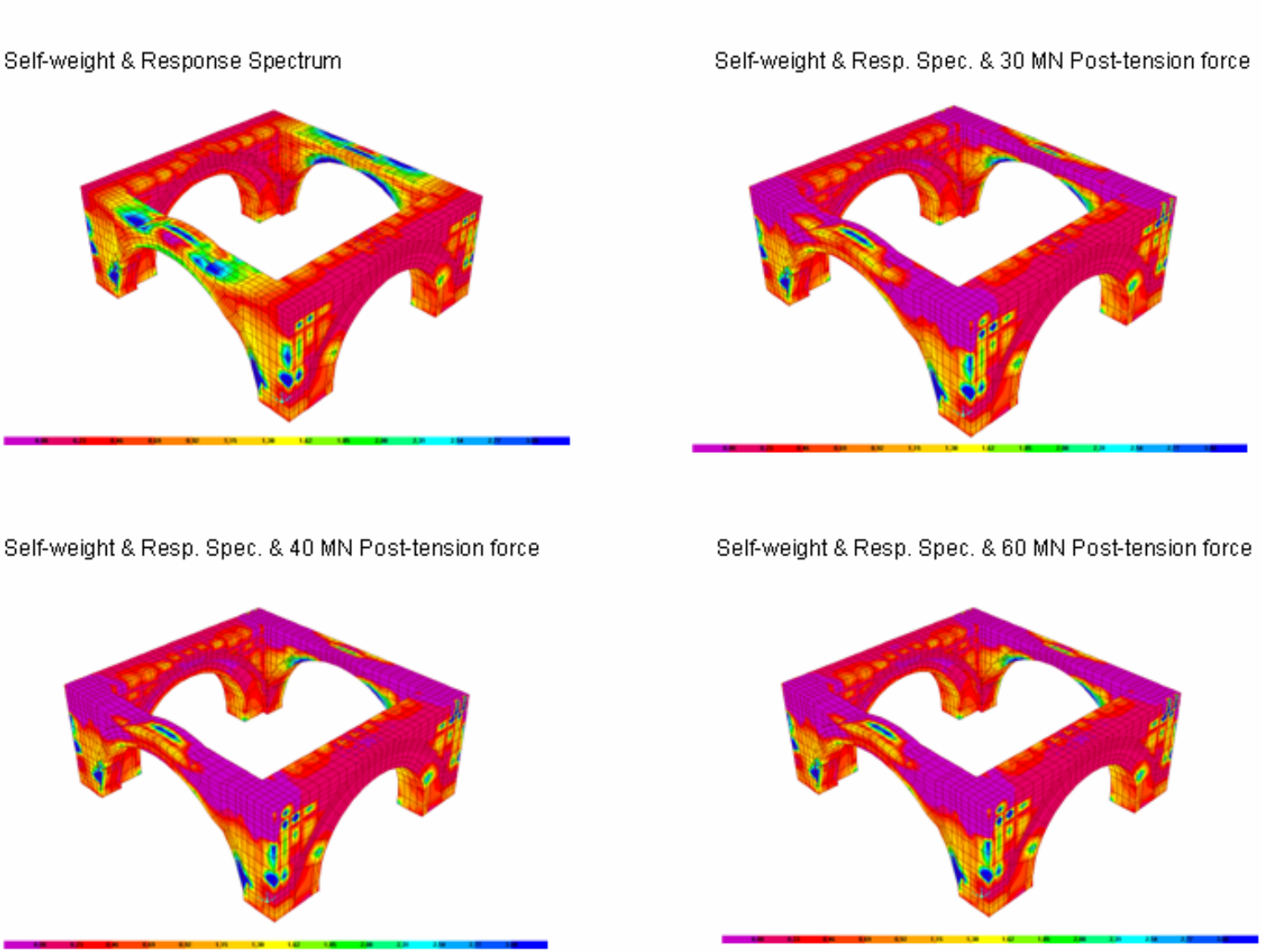

Figure 4.10. SYY stresses at the domebase under self-weight, response spectrum, post-tensioning (0-3 MPa)

The stresses due to post-tensioning at the crown cross-sections of the main arches are summarized in Table 4.3. The stresses are calculated as the average value of stresses obtained from the joints representing a depth of 70 cm from bottom of the crowns of the main arches – where the tensile stress is concentrated, except at east arch where a depth of 35 cm is considered. These depths correspond to the regions where the tensile stresses concentrated. Figures 4.11 and 4.12 display the difference between the stresses obtained from unstrengthened and strengthened models.

Table 4.3. Stresses at the cross-section of crowns under self-weight, spectral and post tension forces (MPa)

Location*	Stress	Self-weight	Self-weight and Post-tension	Self-weight and Spectral	Self-weight and Spectral and Post-tension
North Arch Crown	SXX	0.125	-3.730	1.027	-2.828
	SYY	-	-	-	-
	Smax	0.154	0.054	N/A	N/A
	Smin	-0.040	-3.743	N/A	N/A
South Arch Crown	SXX	0.125	-3.730	1.026	-2.829
	SYY	-	-	-	-
	Smax	0.154	0.054	N/A	N/A
	Smin	-0.040	-3.743	N/A	N/A
East Arch Crown	SXX	-	-	-	-
	SYY	0.128	-4.724	1.402	-3.450
	Smax	0.173	0.001	N/A	N/A
	Smin	-0.050	-4.728	N/A	N/A
West Arch Crown	SXX	-	-	-	-
	SYY	0.108	-3.941	1.278	-2.771
	Smax	0.197	0.050	N/A	N/A
	Smin	-0.104	-3.950	N/A	N/A

*Earthquake forces acting in positive directions.

The intervention using the post-tensioned tendons cause also changes in stress distribution at the semidomes. Although the order of the stress values remain the same, the distribution of stresses differs from the unstrengthened model for both static and spectral analyses as shown in Figures 4.13 and 4.14.

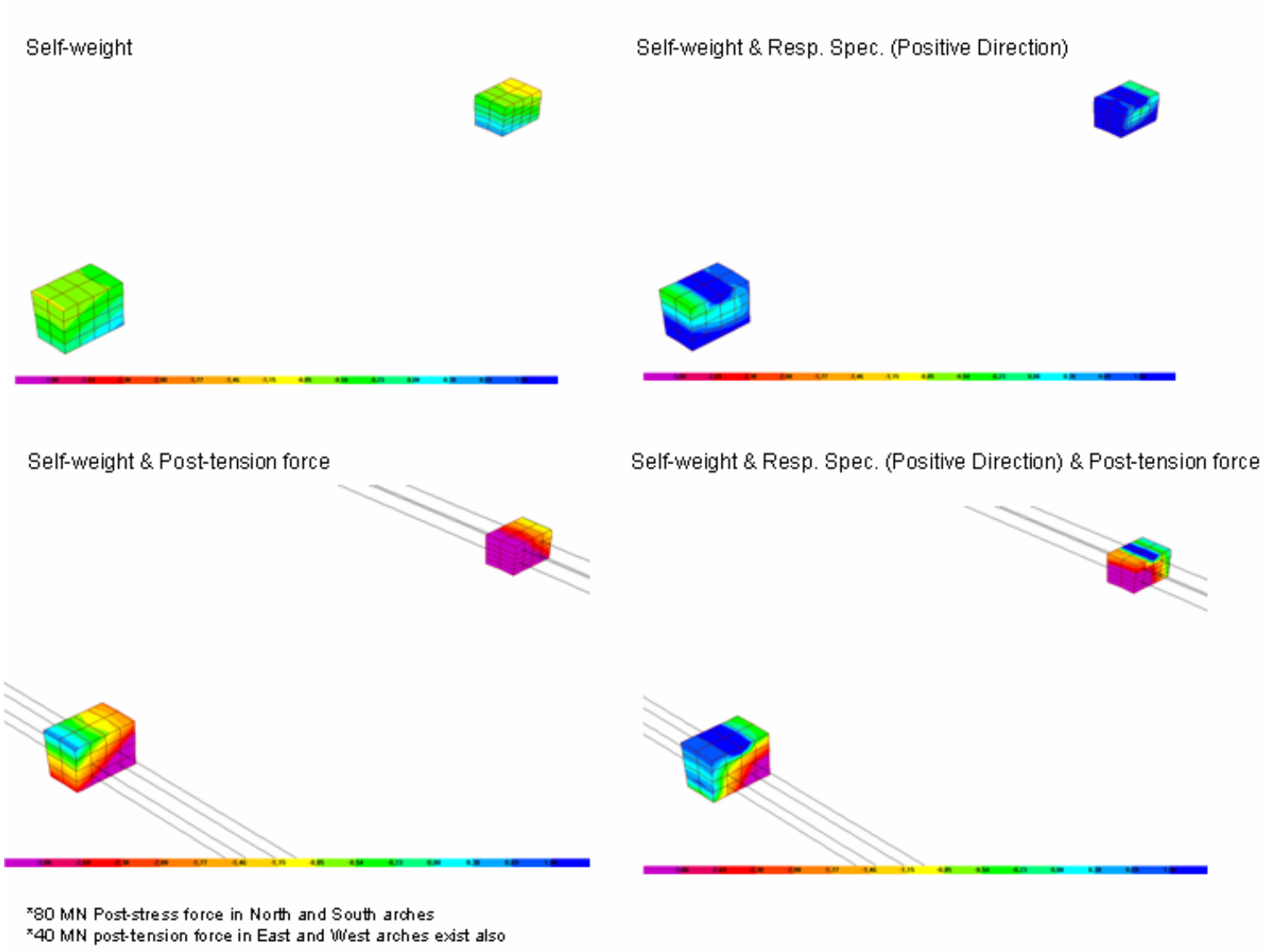

Figure 4.11. SXX stresses of the crowns of east and west arches ((-3)-1 MPa)

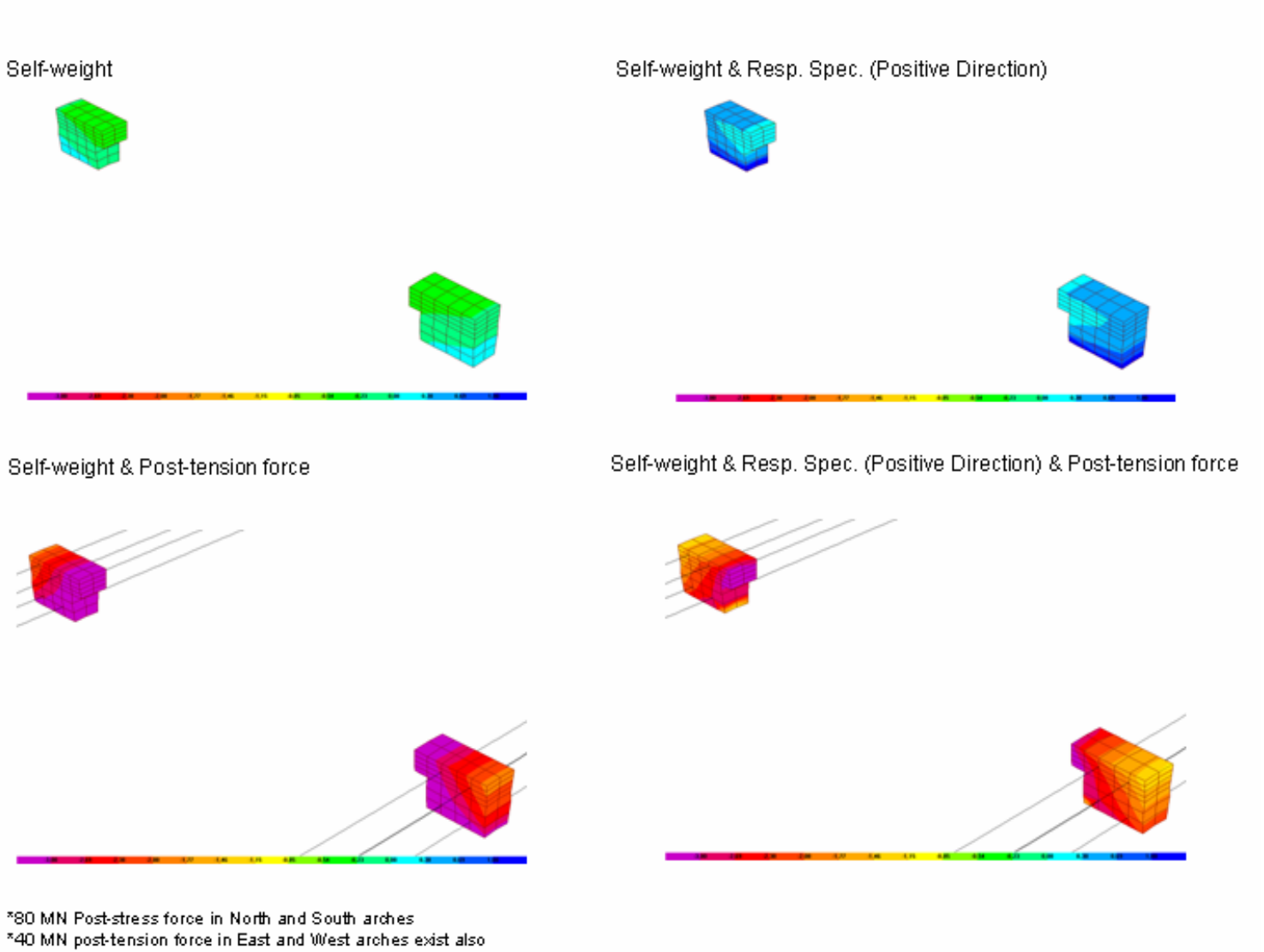

Figure 4.12. SYY stresses of the crowns of north and south arches ((-3)-1 MPa)

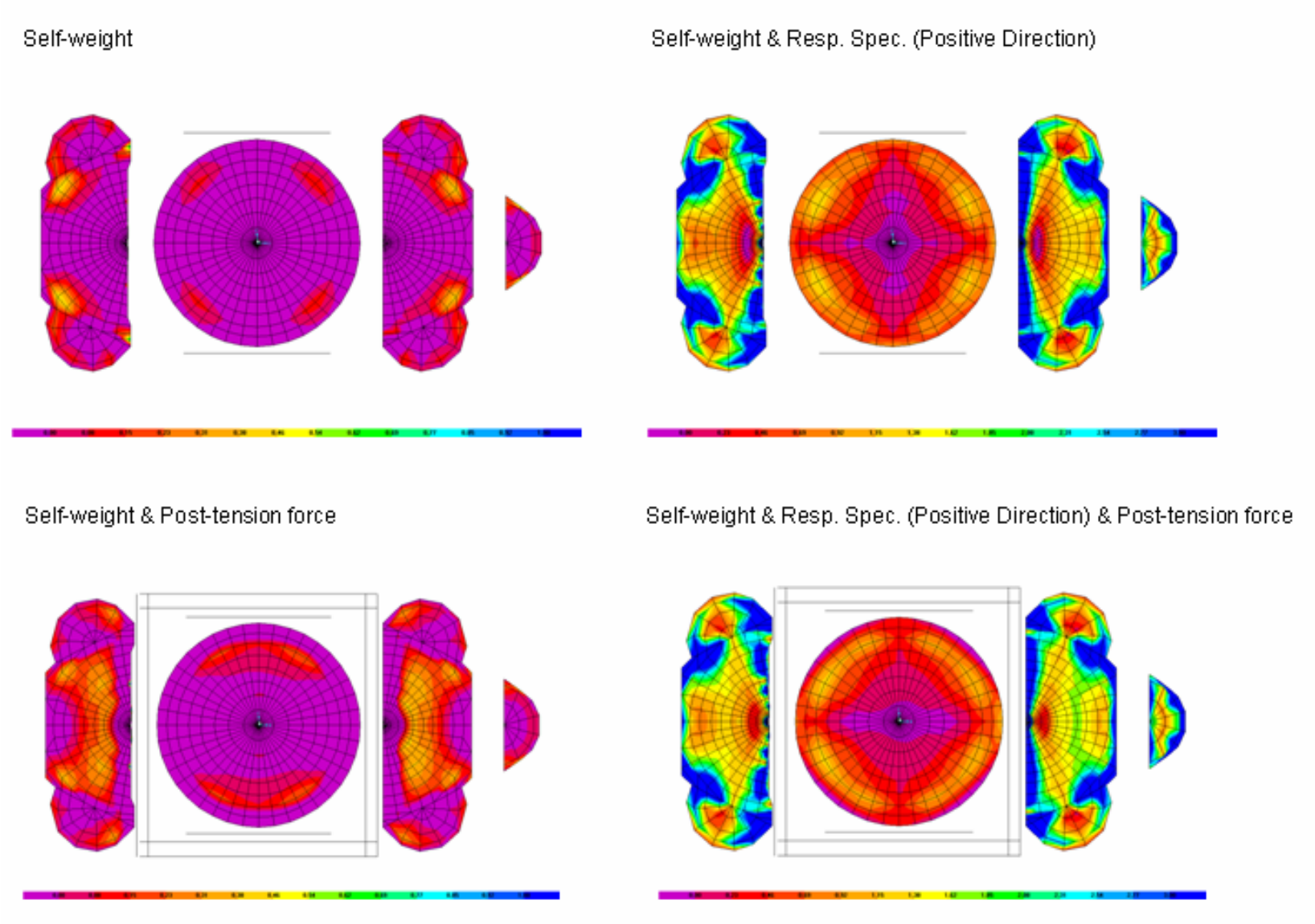

Figure 4.13. Hoop stresses at the shell elements of strengthened model (0-1 MPa for static and 0-3 MPa for dynamic analysis)

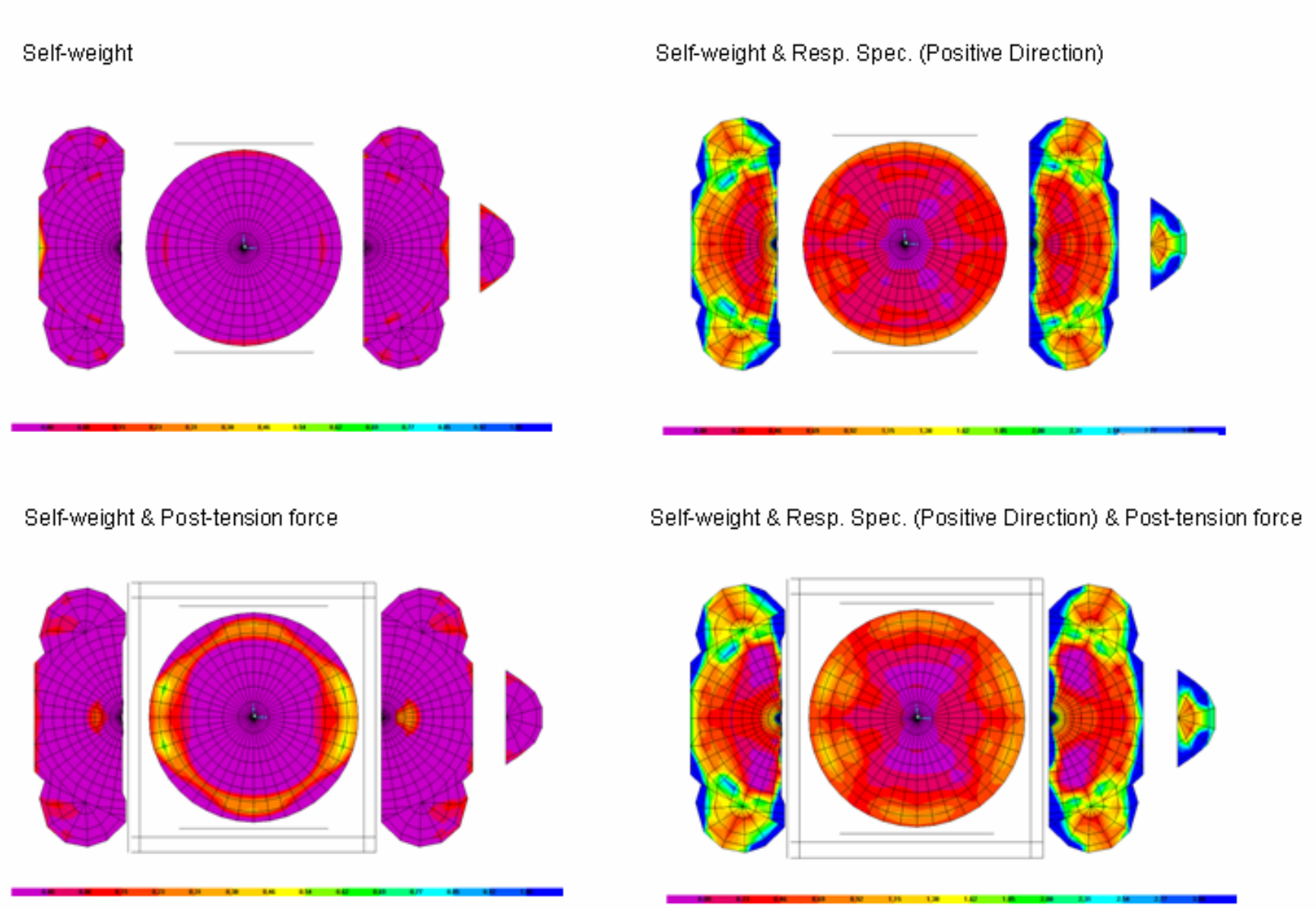

Figure 4.14. Radial stresses at the shell elements of strengthened model (0-1 MPa for static and 0-3 MPa for Dynamic analysis)

4.2. Retrofit with FRPs

4.2.1. Introduction to FRPs

In the last decade, externally bonded fiber-reinforced polymer (FRP) systems are accepted as an efficient alternative for strengthening of existing buildings. The FRP systems are used for improving structural behaviour against both static and seismic forces. They respond well to cyclic loading. Although generally the FRP systems are applied for strengthening of concrete structures, they are applicable also to masonry structures.

The advantages that the FRP systems offer can be listed as: Lower costs, corrosion resistance, flexibility of use, minimum disturbance to structure, minimum loss of free space, resistance to chemicals, impermeability to water and light weight which means the dynamic properties would not change. Moreover when it is needed, they can be removed. These features make the FRP systems an important alternative to the conventional intervention techniques such as steel plate bonding, section enlargement and external post-tensioning (Ipek, 2004).

A FRP system is a composite material made of fibers and resin. Here, fibers act like reinforcement which is embedded in resin, a continuous polymer called as matrix. The fibers are typically stiffer than the resin. The FRP composites are anisotropic materials. A unidirectional lamina has three mutually orthogonal planes of material properties. The material properties of a FRP system are related with individual fibers, fabric architecture of fiber laminate, and the method used to create the composite. The safest way to determine the mechanical properties of a FRP system is testing of laminate samples on-site (ACI 440.2R-02).

The characteristics of a FRP system are specified by factors such as fiber volume, type of fiber, type of resin, fiber orientation and thickness. The main properties of a FRP system can be summarized as in the following;

Constituents: A FRP system consists of two main constituent materials; resins and fibers (Figure 4.15). A wide range of polymeric resins exist such as; putty fillers, saturants,

and adhesives. And fibers have three common types; continuous glass (GFRP), aramid (AFRP) and carbon (CFRP). Fibers are the main constituent which gives the FRP system its strength and stiffness.

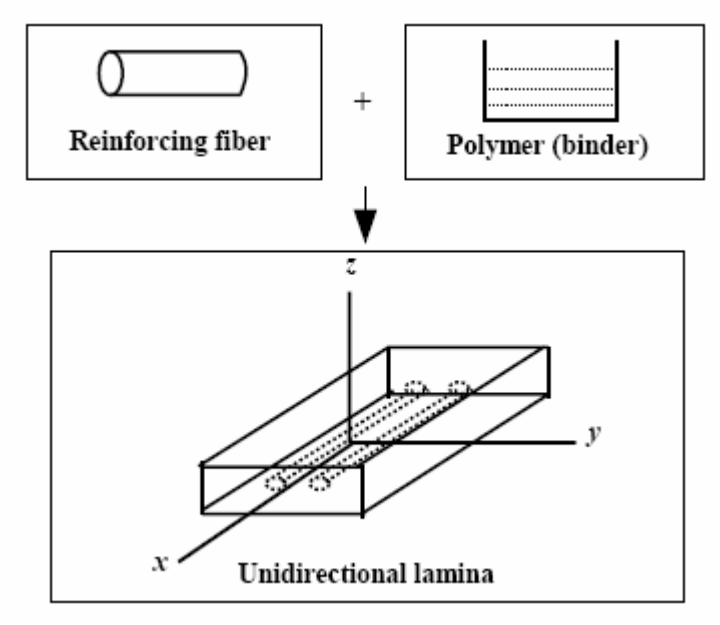

Figure 4.15. Fiber and resin composite employed in fiber reinforced polymer (FRPs) (Kachlakev, 2001)

Density: Fibers' density can range between 1.2 to 2.1 g/cm^3 as shown in Table 4.4, which means four to six times lower than density of steel.

Table 4.4. Typical densities of fibers used in fiber-reinforced polymers (g/cm^3) (ACI 440.2R-02)

Steel	Glass	Aramid	Carbon
7.9	1.5 – 1.6	1.2 – 1.5	1.2 – 2.1

Tensile behaviour: The FRP systems have linear-elastic stress-strain relationship. They do not represent any plastic behaviour and display a sudden failure under tension. The tensile strength and stiffness of a FRP material is mostly dependent on type, orientation and quantity of fibers. They display excellent tensile strength in the direction of the fibers and negligible strength in the transverse direction to the fibers. The mechanical properties of fibers and composites are given in Table 4.5 and 4.6.

Compression behaviour: The FRP systems are not supposed to be used for improving compression strength capacity. The compressive modulus of elasticity is smaller than the tensile modulus of elasticity of FRPs.

Stiffness: Stiffness of a FRP system mostly depends on its fiber content (Figure 4.16). Because the fiber content of the FPR system changes according to application method, two area definition are used named as net-fiber area and gross-laminate area. The gross-laminate area of a FRP system is calculated using the total cross-section area of the cured FRP system, including all fibers and resin. On the other hand, the net-fiber area of a FRP system is equal to net area of fiber, excluding resin. The net-fiber area is used for wet lay-up systems, while the gross-laminate area used for pre-cured systems. So the pre-cured systems, using the gross-laminate area, have higher thickness, lower strength and modulus values, while wet lay-up systems, using the net-fiber area, have lower thickness, higher strength and modulus values. Regardless of which system is preferred, the load-carrying strength (fxA; Tensile strength x Area) and stiffness (ExA; Elasticity modulus x Area) remain constant (ACI 440.2R-02). For the commercially available FRP systems, a table is given in Appendix B.

Table 4.5. Mechanical properties of fibers (ACI 440.2R-02)

	Elasticity Modulus	Ultimate Strength	Rupture Strain
	GPa	MPa	Per cent
Carbon	220 - 690	1380 - 6200	0.2 – 1.5
E-Glass	69 - 72	1860 - 2680	4.5
Aramid (High performance)	110 - 124	3440 - 4140	1.6

Table 4.6. Mechanical properties of FRP composites (ACI 440.2R-02)

	Elasticity Modulus	Ultimate Strength	Rupture Strain
	GPa	MPa	Per cent
Carbon (High-Strength)	100 - 140	1020 - 2080	1.0 – 1.5
E-Glass	20 - 40	520 - 1020	1.5 – 3.0
Aramid (High performance)	48 - 68	700 - 1720	2.0 – 3.0

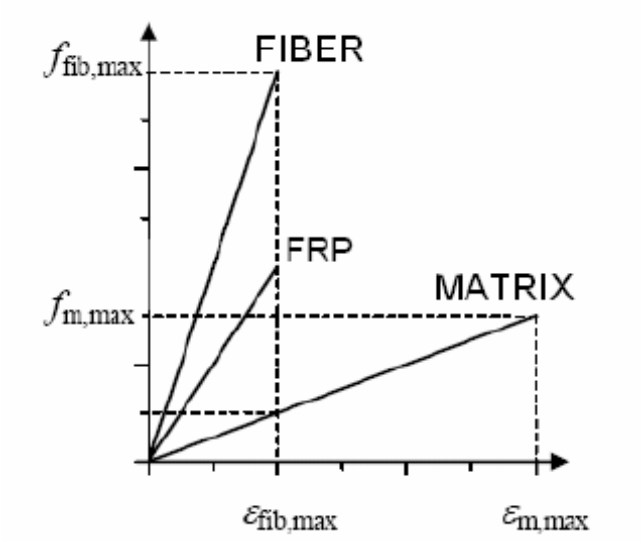

Figure 4.16. Stress-strain relationships of fibers, matrix and FRP (INRC)

4.2.2. Application Methods of FRPs

Two main forms of FRP system exist, externally bonded laminates and near surface mounted (NSM) bars.

Externally bonded FRP laminates can be used for flexural and shear strengthening of masonry members. The possible failure modes for the strengthened masonry with FRP laminates occur in three phases:

- Debonding of the FRP laminate from the masonry due to surface characteristics such as roughness, soundness and porosity,
- Flexural failure (rupture of the FRP laminate in tension or crushing of the masonry in compression)
- Shear failure (Ipek, 2004)

The externally bonded FRPs have three major application methods; wet lay-up, prepreg, and procured which are explained briefly below:

Wet lay-up systems: Fiber sheets or fabrics impregnated with a saturating resin on-site. The saturating resin, along with the compatible primer and putty, is used to bond the

Fiber sheets to the concrete surface. Wet lay-up systems are saturated in-place and cured in-place. They can be considered as analogous to cast-in-place concrete.

Prepreg systems: Fiber sheets or fabrics are pre-impregnated with a saturating resin in the manufacturer's facility. Prepreg systems are bonded to the concrete surface with or without an additional resin application, depending upon specific system requirements. Prepreg systems are saturated off-site, but cured in place.

Precured systems: These FRP systems are saturated and shaped off-site. An adhesive along with the primer and putty is used to bond the precured shapes to the concrete surface. Precured systems are analogous to precast concrete (ACI 440.2R-02).

Near surface mounted (NSM) bars are another form of FRP systems. These bars do not require any surface preparation or long installation time like FRP laminates. For the installation of this type of FRP system, firstly a groove is created, then it is filled partially with epoxy or cement-based paste and the bar is embedded into groove surrounded by the paste. Mostly to maintain the flexural and shear strength of unreinforced masonry walls, this technique is employed via installing the FRP bars into mortar bed joints (ACI 440.XR).

Prestressing is an applicable technique for the FRP systems. Both FRP bars and laminates can be subjected to prestressing. By this way, the FRP material can be used more efficiently against tensile stress. It is recommended a prestress value of 50 per cent of the laminate strength to achieve a reasonable improvement for structural stiffness and load-carrying capacity. At the same time, high level of prestress tension can generate high shear stresses which lead to shear peeling failure. To avoid this failure, the shear strength of the structure should be also ensured. The long-term stress loses are less than the traditional steel tendons, which is another skill of the FRP. Prestressing technique is more common for FRP bars, but also it can be applied to laminates. First the central portion is bonded to surface using heating elements, and then prestress level is reduced progressively as the curing moves towards the ends of laminates. So a prestress tension which is maximum in the middle and minimum at the ends of the laminate is generated. By this method no anchor is required to transfer the prestress at release of jacking (ACI 440.XR).

4.2.3. Finite Element Modelling for FRP laminates

In a research implemented by Oregon Department of Transportation (Kachlakev, 2001), a reinforced concrete beam and a horsetail creek bridge retrofitted with FRP laminates modelled using finite element analysis. ANSYS structural analysis software is used for this purpose. In the FE model, concrete, reinforcement steel and FRP laminate are simulated. An eight-node solid element is used to model concrete. This solid element has eight nodes with three translation degrees of freedom at each node. The element is capable of displaying nonlinear behaviour including plastic deformation, cracking in three orthogonal directions, and crushing. Steel reinforcement is represented by a link element. Two nodes of the link element have three translation degrees of freedom. Steel rebars are assumed to be an elastic-perfectly plastic material and identical in tension and compression. The FRP composites are simulated via a layered solid element. This element allows different material layers with different orientations and orthotropic material properties in each layer. The element has three translation degrees of freedom at each node. Linear elastic properties of the FRP composites are assumed. Perfect bond between concrete and FRP laminates is assumed. To achieve this assumption, FRP laminates, modelled as layered solid elements, are connected to those of adjacent concrete solid elements' nodes directly.

The properties needed for the FRP composites in the FE models are; number of layers, thickness of each layer, orientation of the fiber direction for each layer, elastic modulus of the FRP composite in three directions (Ex, Ey and Ez), shear modulus of the FRP composite for three planes (Gxy, Gyz and Gxz), and major Poisson's ratio for three planes of the solid element. Here a local coordinate system for the FRP layered solid elements is defined where X direction is the same as the fiber direction, while Y and Z directions are perpendicular to X direction.

The horsetail creek bridge was also modelled in SAP2000 software besides ANSYS model due to linear behaviour of the structure. The comparison of the models is reported. While the FRP laminates are modelled as layered solid elements in ANSYS, truss elements with isotropic material properties are used to represent the FRP laminates in SAP2000. It is reported that modelling the FRP laminates as truss elements compared to solid elements

with orthotropic material properties caused reduce of the overall structural stiffness. But the linear behaviour of the bridge is captured similarly within two softwares.

In the present study, the challenge is how to model the FRP composites in SAP2000. For this purpose, frame elements and layered shell elements are taken into consideration. Before taking into consideration the full model of Hagia Sophia, only the main dome is investigated with these two element types. The bottom portions of the dome, where high tension zones are observed under earthquake loading, are strengthened with FRPs. Two different models are generated for this purpose: One with layered shell elements and one with frame elements as shown in Figure 4.17. For the layered shell a 1 mm thick of rebar layer with isotropic material properties is used. To obtain the same cross-section with the model strengthened with layered shell elements, frame elements with a 40 mm cross-section are defined for the model strengthened with frame elements. The dome strengthened with frame elements did not display any apparent difference of stress distribution or reduction as compared to the dome without frame intervention. On the other hand the model with rebar shell layer displayed reduced tensile stresses in the lower portions of the dome. In Figure 4.18 the stresses of two models can be seen. With the help of these exploratory analyses, it is decided to model FRP laminates on the semidomes with layered shell elements in further analyses.

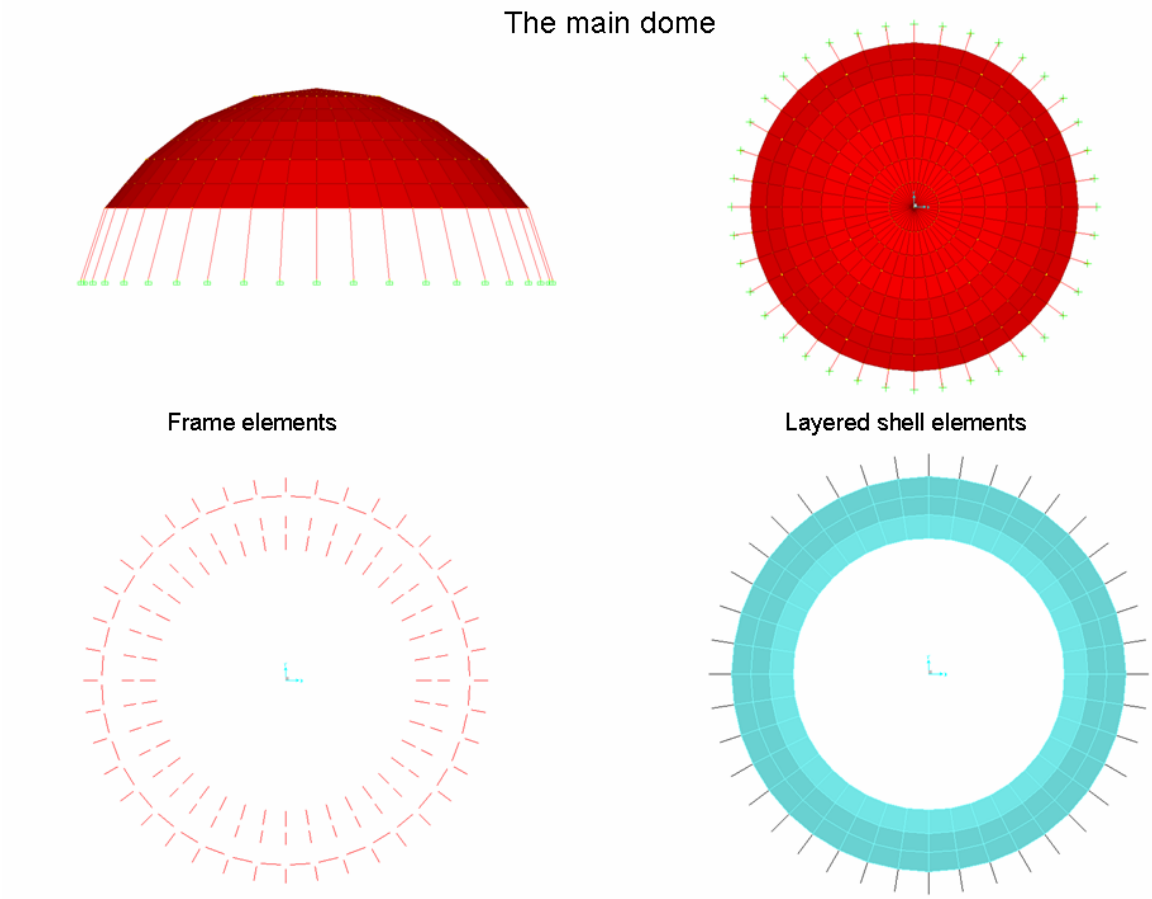

Figure 4.17. Strengthening of the main dome with FRPs

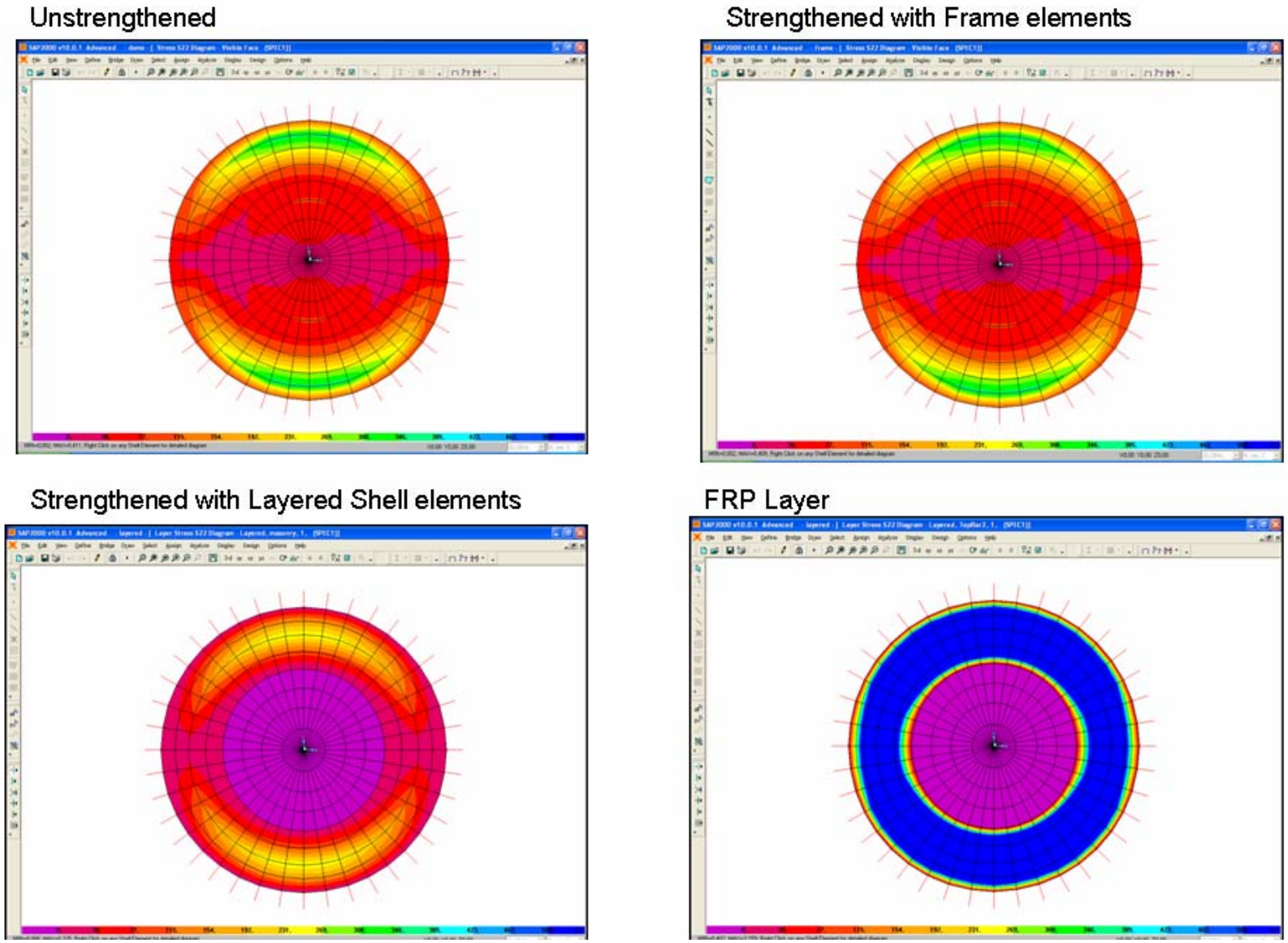

Figure 4.18 Radial stresses at the main dome models: no strengthening (top left), strengthened with frame element (top right), strengthened with layered shell elements (bottom left), FRP layer (bottom right)

Layered shell elements in SAP2000: Before we proceed, there is merit in understanding the layered shell element in SAP2000. It is a shell element with multiple layers having different material, thickness, and locations. This element can support all forces and moments of full shell behaviour. Important properties of the layered shell element are (SAP2000, 2007):

- *Layered section property:* Any number of layers is allowed. Layers are located with respect to a reference surface which can be the middle, top, bottom surfaces or any other location defined. By default, the reference surface contains the element's nodes. The thick-plate (Mindlin/Reissner) formulation, which includes the effects of transverse shear deformation, is always used for bending behaviour the layered shell.
- *Layer distance:* Each layer is located at a distance from the reference surface to the center of the layer, measured in the positive local-3 direction of element.
- *Layer thickness:* Each layer has a single thickness, measured in the local-3 direction of element.
- *Layer material:* Material may be isotropic, uniaxial or orthotropic.
- *Layer material angle:* Each layer can have a different material angle. For instance to model rebar in two orthogonal directions, two layers of uniaxial material with material angles 90° apart can be employed.
- *Layer number of integration points:* Material behaviour is integrated at a finite number of points in the thickness direction of each layer. It is allowed one to three points for each layer. The location of these points follows standard Gauss integration procedures. For a single layer of linear material, one point in the thickness direction will capture membrane behaviour and two points will both membrane and plate behaviour. In the case of multiple layers, a single point for thinner layers will be adequate.
- *Interaction between layers:* Layers are defined independently and overlap of layers or gaps between them are allowed. Ii is assumed that normal to the reference surface remain straight after deformation.

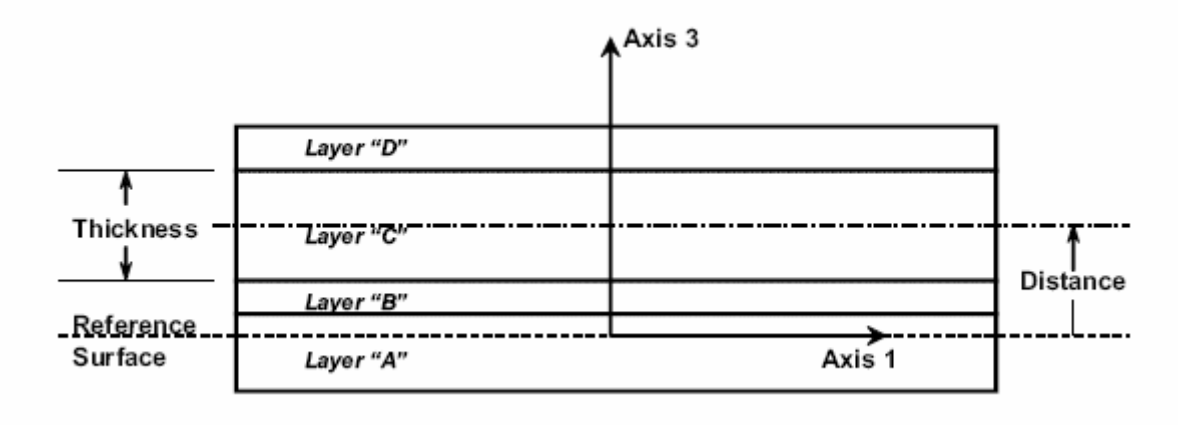

Figure 4.19. Layered shell element showing the properties for "Layer C" (SAP2000, 2007)

4.2.4. Wrapping the semidomes with FRPs

According to the static and dynamic analyses performed in Chapter 3, the lower parts of the semidomes and their parts adjacent to the main arches may be under risk of high tensile stresses. The FRP laminates are modelled for these regions as shown in Figure 4.20. Shell element with three layers is employed; one layer for brick-masonry semidome and the other two layers for FRP laminates with 0° and 90° material angles. The laminate layers are placed on the top surface of the semidomes. Different elasticity moduli and thicknesses are tried out to find out the changes in the response due to elasticity modulus and thickness of the laminates. For the elasticity modulus the values of 50, 100 and 200 GPa and for the thickness 1, 5, 10 mm are employed successively for the laminates. These trial runs provided a judgement about the material properties that should be used for FRPs. The final model of FRP consists of a brick-masonry part with a thickness of 800 mm and two thin layers with 5 mm thickness representing the FRP laminates. Uniaxial material properties are set for the FRP layers. The elasticity modulus, 62000 MPa, used in the research done by Oregon Department of Transportation is set for the FRP layers, the mass density is taken 300 g/m^3 as given for Carbon sheet in ACI 440.2R-02.

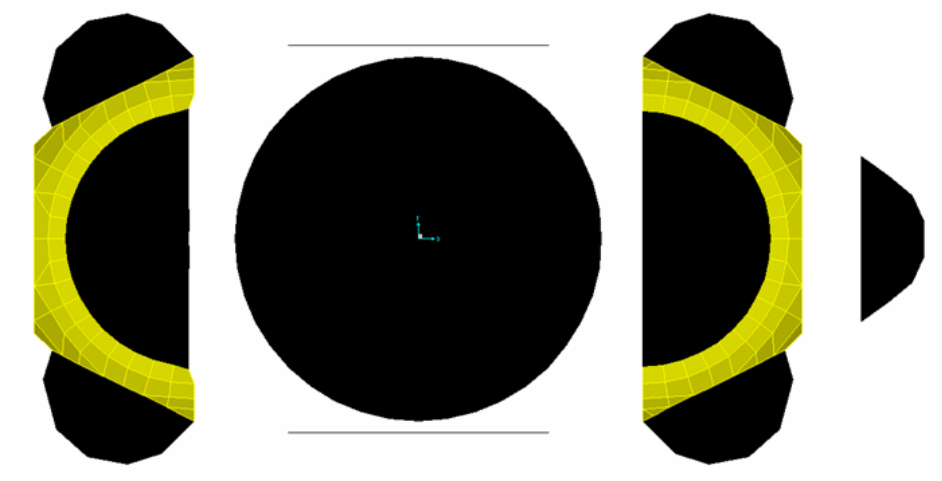

Figure 4.20. Regions strengthened with FRP laminates

The spectral analysis is performed for the model with FRPs. No post-tension force is implemented for the FRPs. The displacements remain the same with the unstrengthened model, no obvious change is observed as given in Table 4.7. On the other hand, stress values change clearly. The stress values at the chest of the semidome reduce from 5.3 to 3.8 MPa (Hoop stress) and 2.5 to 1.5 MPa (Radial stress) under spectral analysis. The stresses in the FRP layers reach high values for their uniaxial directions which are 70 MPa for radial and 100 MPa hoop stresses under seismic loading, but the high tensile strength of FRP composites given as in Table 4.6 will be satisfactory. Also high compressive stresses occurred in the FRP layers. It is non-applicable for the FRPs to cover the compression, so this high compression stresses can be considered to be compensated by the large cross section of the masonry layer of semidome. The hoop and radial stresses obtain during the analyses for each layer – both masonry and FRP laminate – is shown in Figures 4.21 to 4.24. In the regions that are not covered by laminates, no change of stresses is obtained. Implementing FRP layers cause any change of responses in the solid elements.

Table 4.7. Displacements under self-weight and response spectrum loading

	East Semidome*			West Semidome*		
	North-South	East-West	Vertical	North-South	East-West	Vertical
	mm	mm	mm	mm	mm	mm
Without FRPs	60	75	5	69	76	6
With FRPs	58	74	4	68	75	5

* For each main semidome, a particular joint is selected

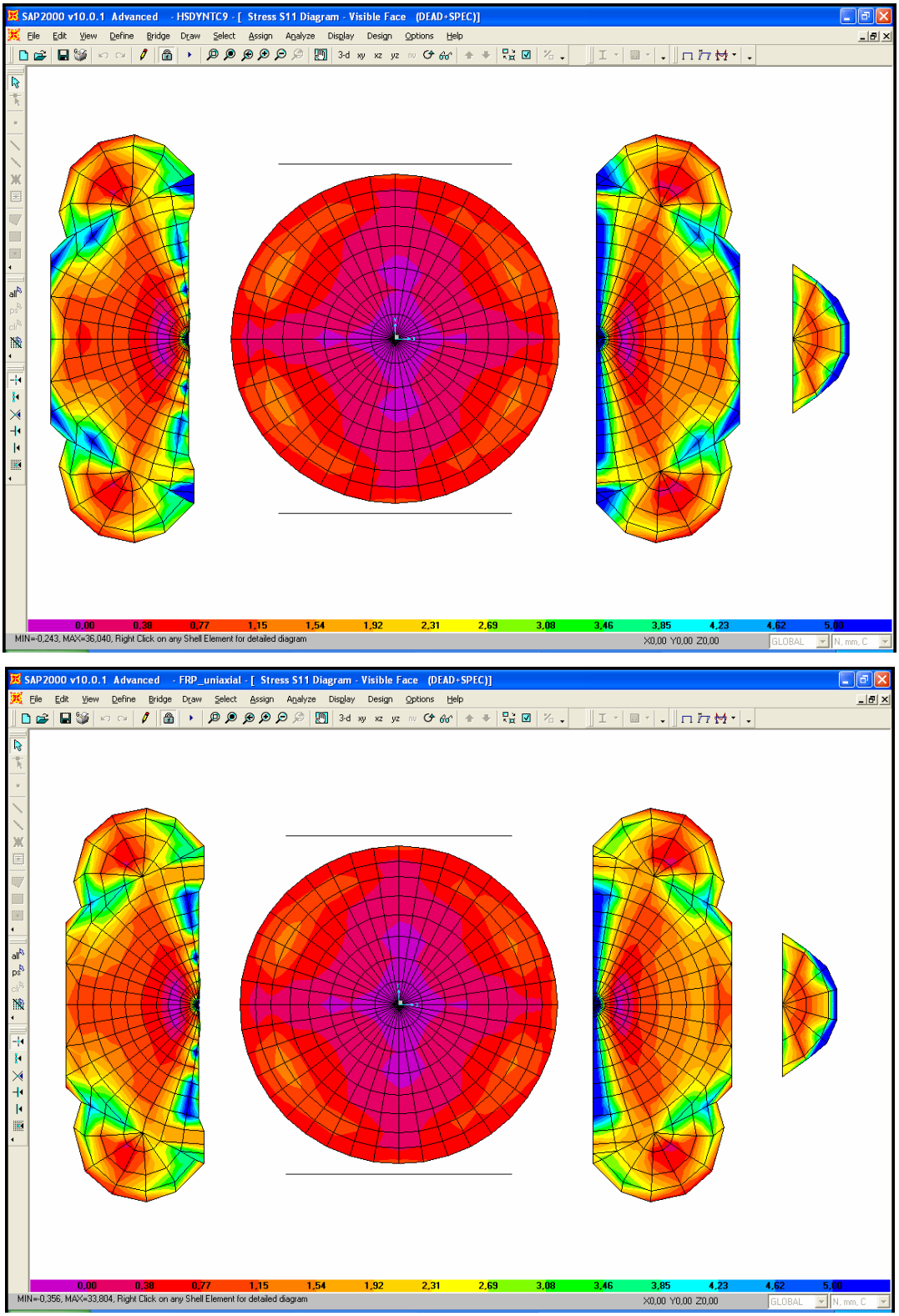

Figure 4.21. Hoop stresses at the shell elements under response spectrum loading, with FRPs (bottom), without FRPs (top)

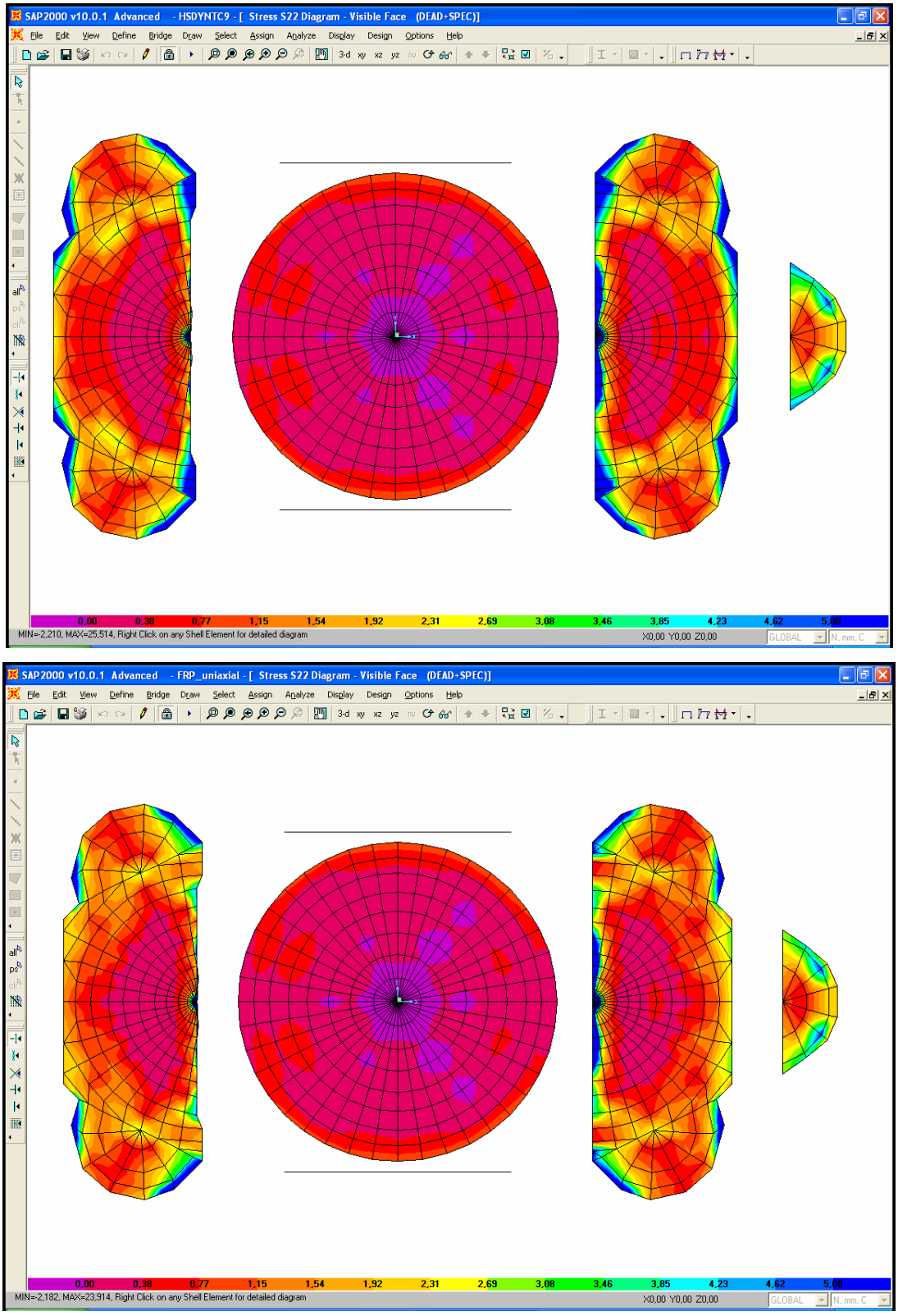

Figure 4.22. Radial stresses at the shell elements under response spectrum loading, with FRPs (bottom), without FRPs (top)

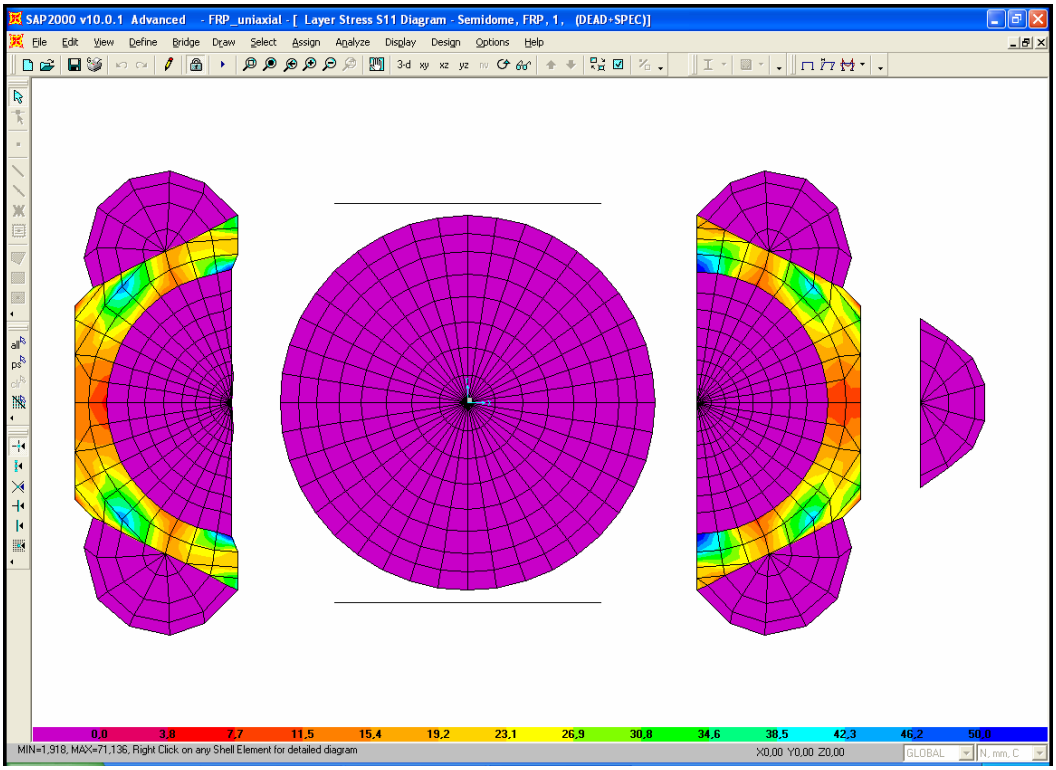

Figure 4.23. Hoop stresses of the FRP with 0° angle under response spectrum loading

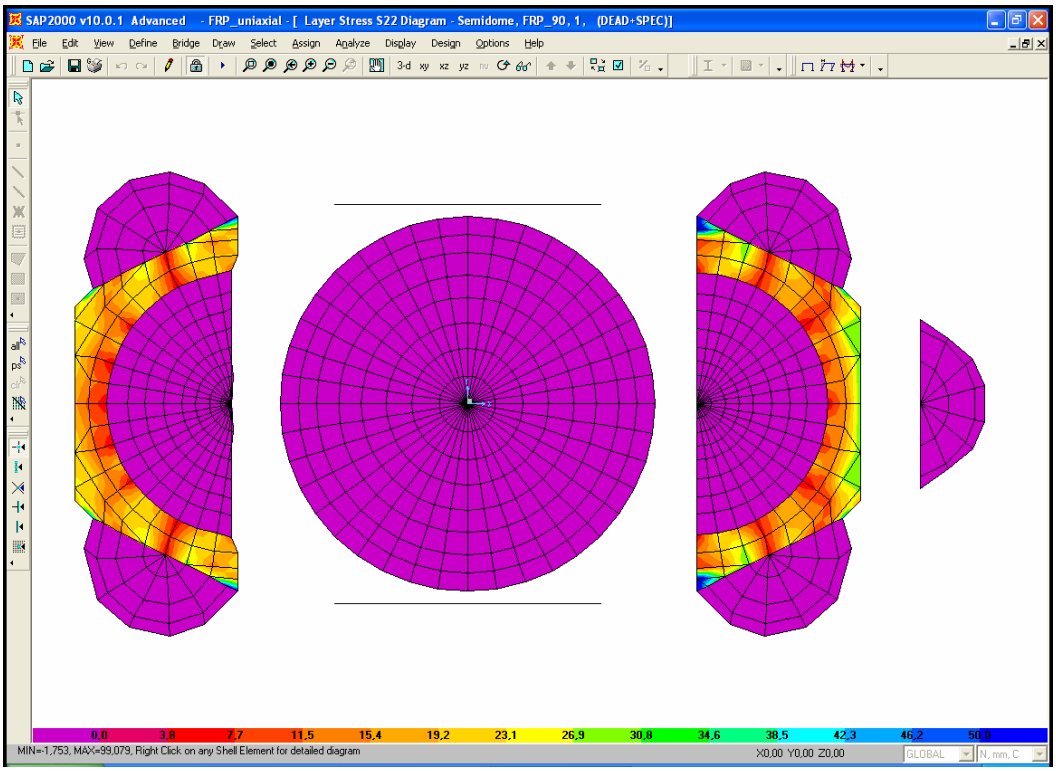

Figure 4.24. Radial stresses of the FRP with 90° angle under response spectrum loading

4.2.5. Wrapping the domebase with FRPs

Response spectrum analysis performed in Chapter 3 reveals that the domebase can be subjected to high tensile stress concentrations under earthquake loading. For this reason, it is considered that it would be suitable to strengthen the domebase by wrapping it with FRP laminates. Here, because domebase consist of solid elements unlike semidomes, solid elements are employed to simulate FRP laminates instead of layered shell elements. The laminate layer is placed on the outside surface of the domebase where it is possible to wrap (Figure 4.25). Different elasticity moduli and thicknesses are tried out to evaluate the changes in the responses. For the trial runs the values of 50, 100 and 200 GPa for the elasticity modulus and 1, 5, 10 mm for the thickness are employed successively at the laminates. The final model of FRPs has an elasticity modulus of 200 GPa and a thickness of 10 cm. The values lower than these material properties did not affect response of the structure. Uniaxial behaviour of material is assumed for three global directions; X, Y and Z. The mass density is taken 300 g/m^3 as given for carbon sheet in ACI 440.2R-02.

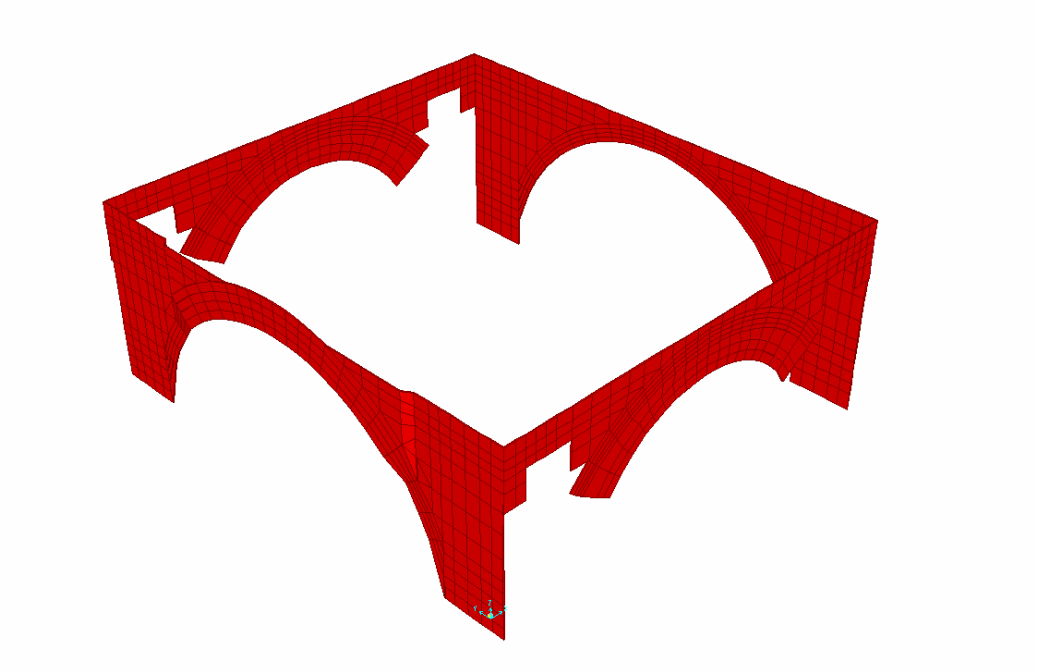

Figure 4.25. Solid elements representing FRP laminates.

The response spectrum analysis is performed for the model. No post-tension force is implemented for the FRPs. The displacements remain the same with the unstrengthened model, no obvious change is observed. On the other hand, stress values change obviously. The stresses at the top of the surcharge reduce from 4.5 to 2.5 MPa in X direction and 3.7 to 1.9 MPa in Y direction under spectral analysis. The stresses in the FRP layers, particularly in the regions close to the top of surcharge and bottom of the crowns of the main arches, reach high values which are 100 MPa in X and 80 MPa in Y directions, but the tensile strengths of FRP composites given as in Table 4.6 will be satisfactory to overcome these high tensile stresses. The stresses obtain from the analysis for each layer – both masonry and FRP laminate – are shown in Figures 4.26 to 4.29. In the regions that are not covered by laminates, no change of stresses is obtained. Also the stress distributions in the main dome and semidomes are not affected from the FRPs.

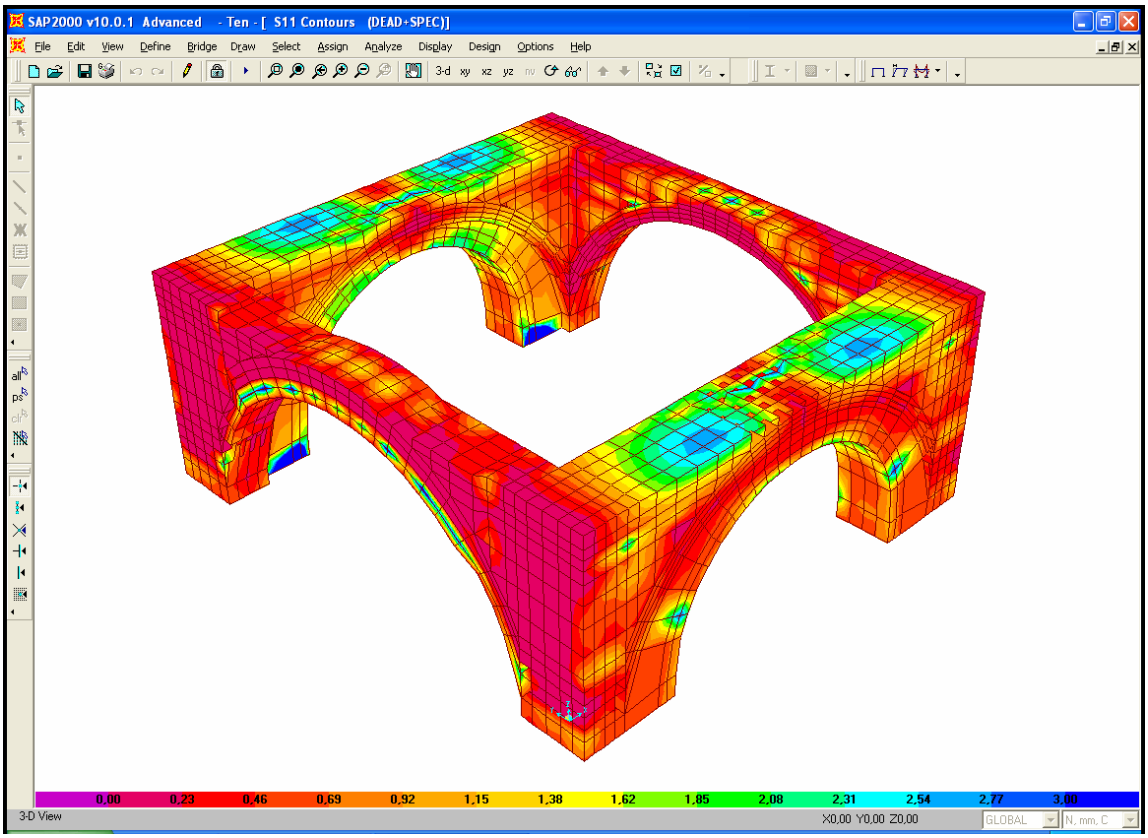

Figure 4.26. SXX stresses at the domebase under self-weight and response spectrum loading

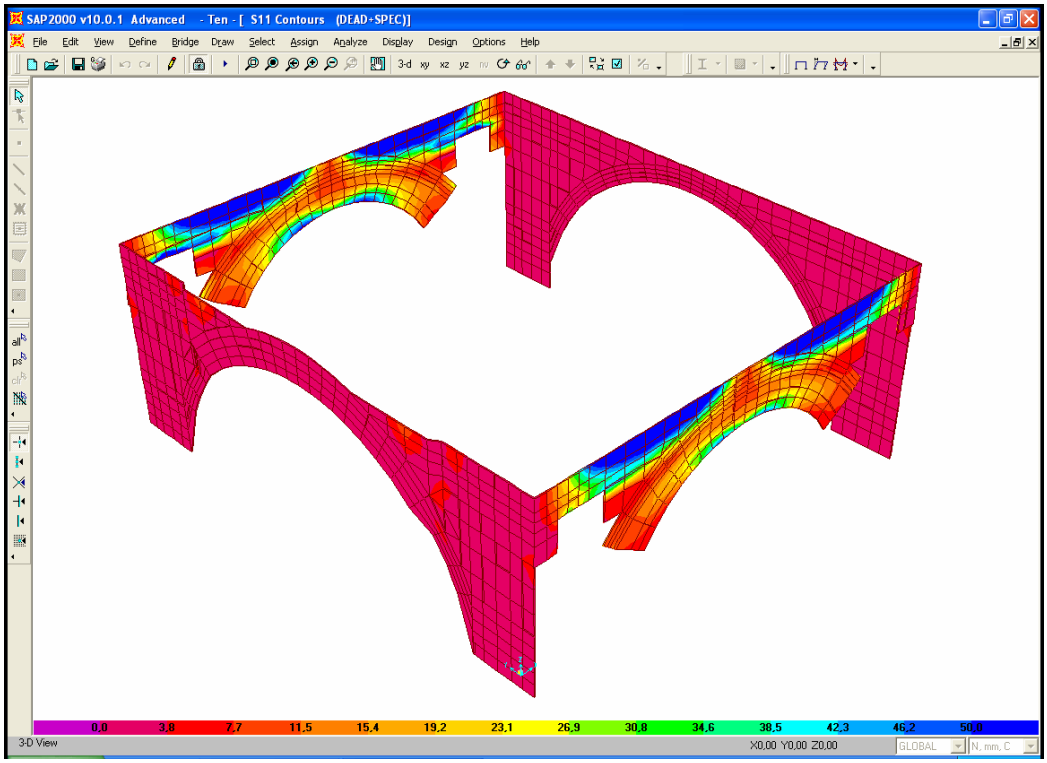

Figure 4.27. SXX stresses at the FRP under self-weight and response spectrum loading

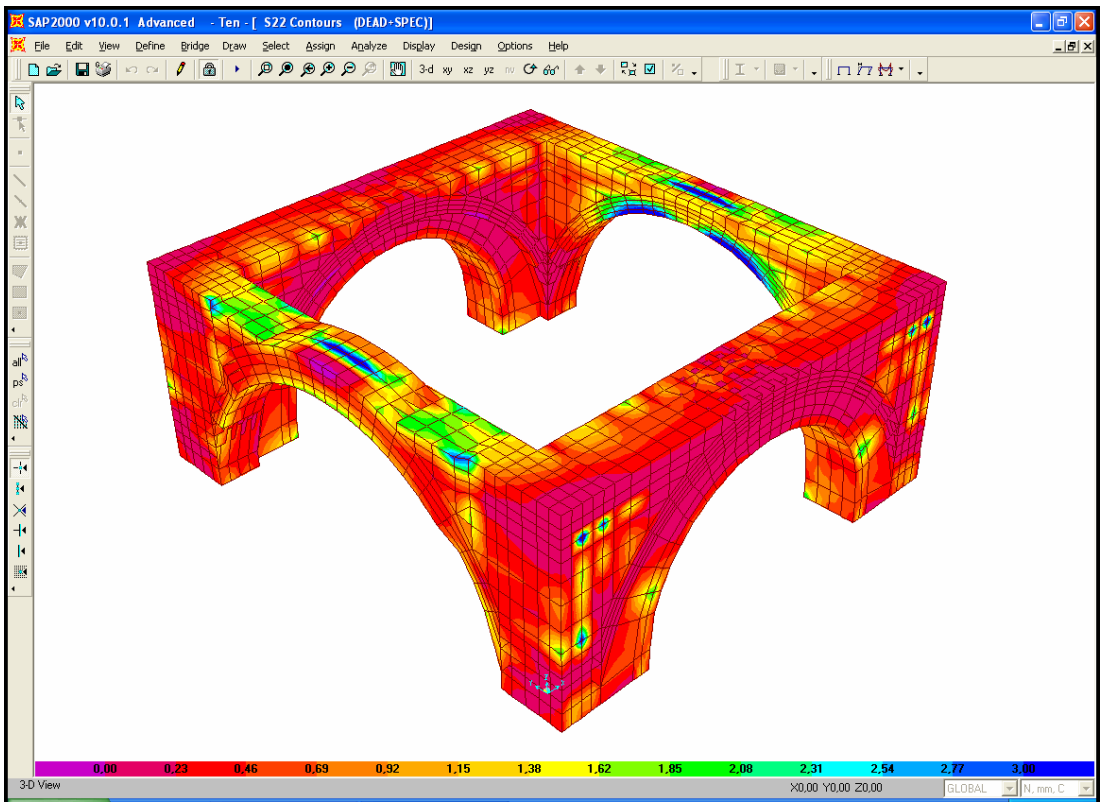

Figure 4.28. SYY stresses at the domebase under self-weight and response spectrum loading

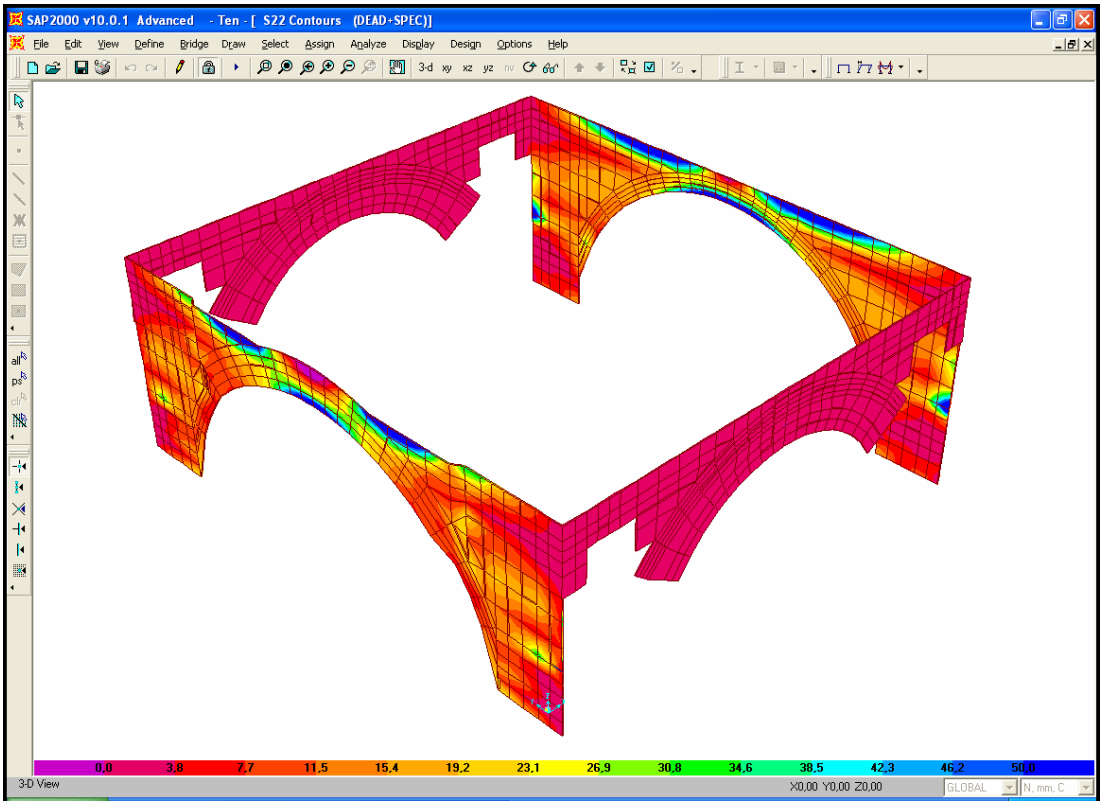

Figure 4.29. SYY stresses at the FRP laminate under self-weight and response spectrum loading

4.3. Implementing Anchorages for the connection of the Semidomes with the Main Arches

It is worth to mention about the responses obtained from the regions of the semidomes that are adjacent to the main arches. The previous researches proposed that one of the critical regions under the risk of seismic hazard is these connecting regions. They predicted that the split of the semidomes with the main arches can cause collapse of the semidomes totally. In the current thesis, the same regions exhibit high tensile stresses under earthquake loading. But, here it is obligatory for the writer to tell about the modelling problems concerning these regions in the FE model. These problem can be listed as follow:

- Connecting different type of elements with different degrees of freedom i.e. the connection regions of the semidomes (shell elements) and the main arches (solid elements),

- Connecting shell elements with different shapes such as quadrilateral and triangular ones,
- Adjacent shell elements having largely different local axes such as the shell elements at the west semidome. Local angles of the elements sharply increase at the regions close to the west main arch.

For the reasons explained here, this type of regions is not subjected to any strengthening procedure in the previous chapters. Here, to determine the forces that should be transmitted by these regions, anchorages are employed. For this purpose, firstly the shell elements close to the main arches assumed to be cracked by setting zero for elasticity modulus. Secondly, frame elements are used to model anchorages in the west and east semidomes. Frames are replaced starting from the inner edge of the east and west main arches ending in the shell elements at the semidomes allow. For the anchorages, material properties of steel are assumed and a diameter of 10 cm is selected. The model with anchorages and the cracked shell elements can be seen in Figure 4.30.

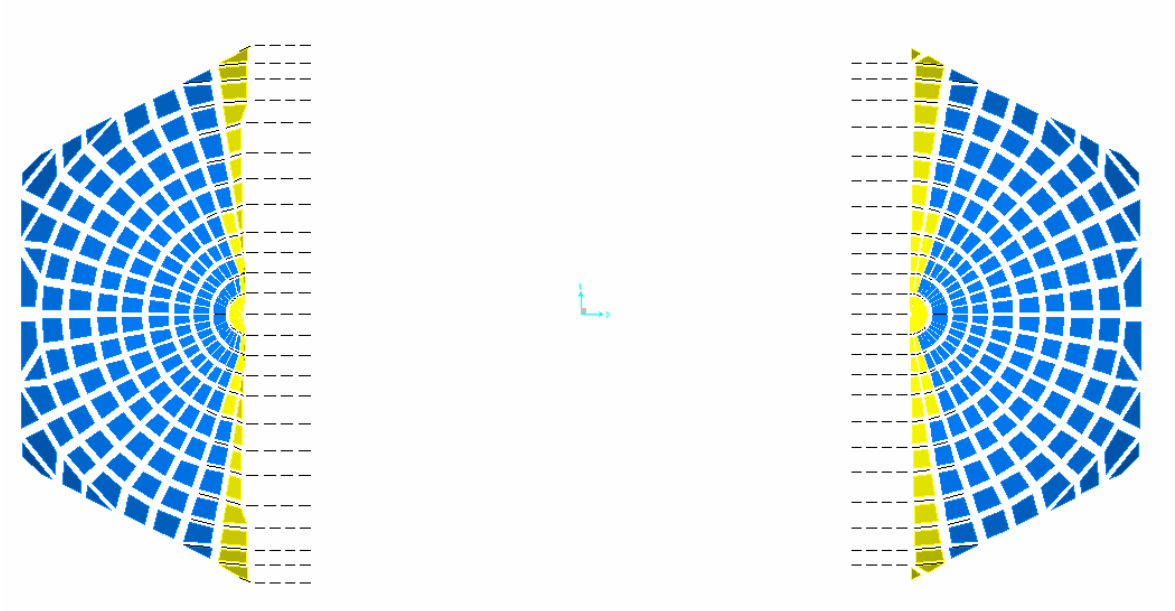

Figure 4.30. Finite element model with anchorage

The self-weight and response spectrum analyses are performed for the model with anchorages. In the unstrengthened model, the section-cuts regarding the total cross-sections of the east and west semidomes reveal the axial forces in compression as 2.6 and

2.3 MN respectively for the self-weight. For the response spectrum analysis, the axial forces are in tension which are 41.0 and 26.8 MN for the east and west semidomes respectively. The axial forces acting along the frame elements are checked to obtain the local normal forces in the semidomes which are given in Figures 4.31 and 4.32. Here the maximum trust force is given in that direction.

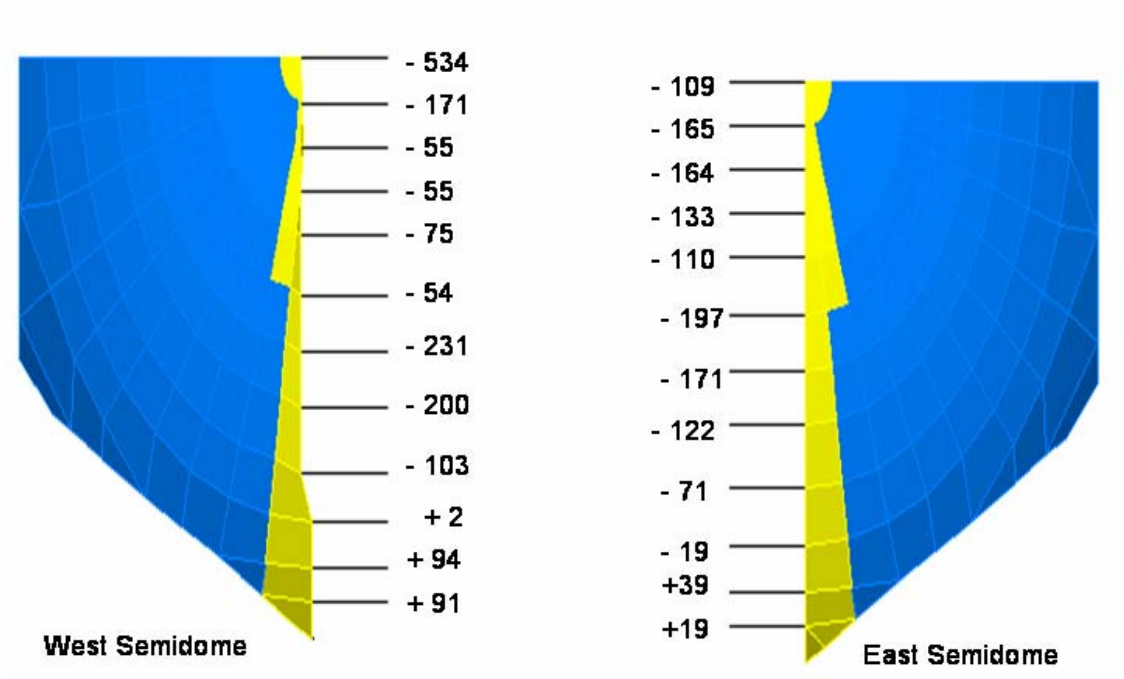

Figure 4.31. Axial forces under self-weight

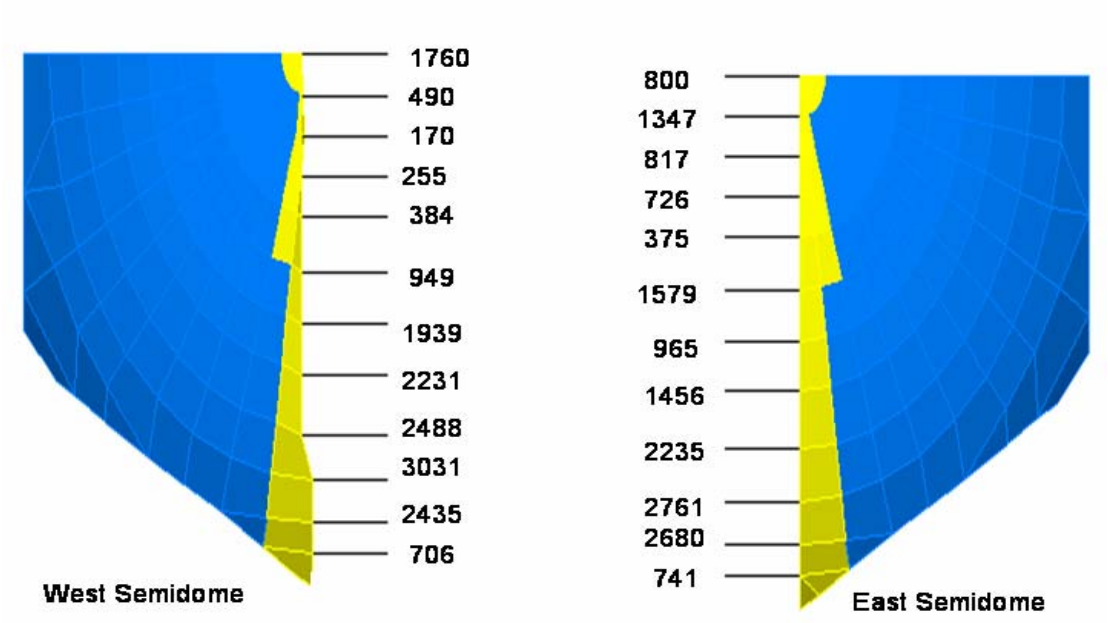

Figure 4.32. Axial forces under self-weight and response spectrum loading

5. CONCLUSION

In this study, intervention alternatives to strengthen Hagia Sophia against earthquakes are investigated. Static and modal–eigenvalue analyses are performed to ensure that the FE model of Hagia Sophia is adequate to represent the structure. Response spectrum analysis revealed that main arches, semidomes and domebase exhibit high stress concentrations. These particular elements were considered for an intervention. It is aimed that the stresses remain in the range of -10 to 1 MPa in the retrofitted models. Two main strategies for retrofitting are considered;

(i) Retrofitting the main arches with post-tensioned bars,
(ii) Wrapping the semidomes and domebase with fiber reinforced polymers – FRPs,
(iii) Implementing anchorages to connect the semidomes with the main arches.

Retrofitting the main arches with post-tensioned bars: Post-tensioned tendons are used to strengthen the main arches against seismic loading. By applying post-tension forces, additional compression force to counteract the high tension is aimed for. Post-tension forces are selected as 80 MN in north-south arches and 40 MN in east-west arches. Static linear analysis performed under post-tensioning yields a deformation pattern fundamentally different from the one due to self-weight loading. The main arches were forced to move inward except the crowns of east and west arches. East and west arches – which have thinner cross sections - bowed at their crowns, the edges of the arches move inward whereas the crowns move outward. It is ensured that the stresses caused by both self-weight and post-tension forces are lower than the assumed limit compressive strength of the brick-masonry; 10 MPa, to avoid any crushing of masonry. All arches exhibit compressive stresses along their spans. Maximum compressive stresses observed are 5.6 MPa for east arch (Global Y) and 5.1 MPa for west arch (Global Y) and 3.9 MPa for north and south arches (Global X). Tension caused due to bowing, not exceeding 1 MPa, observed on the outside surface of west crown.

The response spectrum analysis reveals a deformation shape similar to the one that of the unstrengthened model. The effect of post-tensioning becomes evident particularly in

the vertical deformations of the crowns of the main arches and that of the top of the main dome. In the main dome vertical deformation reduces by about 30 per cent. At the crowns of the north and south main arches, a decrease in the north-south deformation by about 10 per cent is observed, on the other hand the deformations of the crowns of the north and south arches increase unlike the crowns of the east and west arches. The effect of post-tensioning in the horizontal east-west deformation of the east and main arches is less pronounced probably due to the trust of the semidomes. The post-tensioning leads stress reduction as expected. Although the stress on surcharge can not be decreased under 3 MPa, the stresses at the cross sections of the crowns decrease to values desired. Assuming the earthquake loading acting in positive directions, the maximum compressive stress found is 3.4 MPa for north and south arches (Global X), while it is 4.8 MPa for east arch and 4.4 MPa for west arch (Global Y). If the earthquake forces act in negative directions, the maximum compression stresses become 5.8 MPa for north and south arches (Global X), and 6.4 MPa for east arch and 5.8 MPa for west arch (Global Y).

Wrapping the structural elements with fiber reinforced polymers – FRPs: The response spectrum analysis of the unstrengthened model displayed that the lower parts of the semidomes and their adjacent portions to the main arches are exposed to high tensile stresses. The model with FRPs was generated to investigate any improvement that can be achieved in the dynamic response of the model by using FRP laminates. By implementing FRPs, tension was intended to be carried by FRP laminates rather than the brick-masonry. No post-tension force is implemented for the FRPs. Two model with FRPs are created:

(i) The semidomes with FRPs
(ii) The domebase with FRPs

In the first model, the lower parts of the semidomes are wrapped with FRPs. Under earthquake loading, the displacements remain same with the unstrengthened model, no obvious change was observed. On the other hand, stress values changed clearly. The stress values at the chest of the semidome drop from 5.3 to 3.8 MPa (Hoop stress) and from 2.5 to 1.5 MPa (Radial stress) for spectral analysis. At the FRP layers high stress values in their uniaxial directions which are 70 MPa for radial and 100 MPa for hoop stresses were obtained for the seismic loading. Considering the high tensile strength of FRP composites,

these stresses will not create any problem. Also high compressive stresses occurred at the FRP layers. It is non-applicable for the FRPs to cover the compression, so this high compression stresses will be compensated by the large cross section of the masonry semidome. For the regions that are not covered by laminates, no change of stresses is obtained.

In the second model, the domebase is wrapped with FRP laminates. This time, solid elements are used to model the laminates and no post-tension force is employed for the FRPs. The response spectrum analysis revealed the same deformations with the unstrengthened model, again no obvious change was observed. The stresses at the top of the surcharge reduce from 4.5 to 2.5 MPa in X direction and 3.7 to 1.9 MPa in Y direction under spectral analysis. The stresses in the FRP layers, particularly in the regions close to the top of surcharge and bottom of the crowns of the main arches, reach high values which are 100 MPa in X and 80 MPa in Y directions. In the regions that are not covered by laminates, no change of stresses is obtained. Also the stress distributions in the main dome and semidomes are not affected from the FRPs.

*Implementing anchorages to connect the semidomes with the main arches:*The regions of the semidomes that are adjacent to the main arches exhibit high tensile stresses under earthquake loading. It can be predicted that this high tensile stress can cause cracking of the upper parts of the semidomes and the cracking can lead to split of the semidomes with the main arches. Anchorages are employed to evaluate the forces that are transmitted via these connecting regions,. For this purpose, firstly the shell elements in the regions close to the main arches assumed to be cracked by setting zero for elasticity modulus. Then, frame elements are used to model anchorages in the west and east semidomes. The self-weight and response spectrum analyses are performed for this model. As expected, the axial forces reveal in compression under self-weight and in tension under earthquake loading.

In this study, two main strengthening alternatives; post-tensioning and using FRPs are investigated. Post-tensioning seems to be much more effective than FRPs. Implementing post-tensioned tendons in the main arches leads serious stress reductions in the FE model. On the other hand, it causes fundamental changes in the deformation shape

of the structure which could put pressure on the structure's current situation. Although it can be suggested that post-tensioning is the most effective alternative to maintain an improvement for Hagia Sophia, how to succeed this task still needs more investigations for the researchers and engineers.

6. FUTURE WORKS

6.1. Staged Construction Analysis

It is known that Hagia Sophia exhibited large deformations during its construction period due to the long curing time of mortar. Until the mortar took its full strength, the lower levels should have already been deformed due to their self weight before upper portions were constructed (Davidson, 1993). As explained in Chapter 2.2, Hagia Sophia exhibits non-linear behaviour. A unique model conducted to determine the both static and dynamic material properties of the structure could not be achieved. The elastic modulus required to reach the displacements at the actual structure are much lower than those necessary to capture the natural vibration frequencies obtained from ambient vibration surveys. For this reason it is predicted that it will be more reasonable to model the construction period in stages rather than a one stage analysis.

SAP2000 provides an analysis named Staged Construction Analysis which is a pseudo-nonlinear static analysis that allows defining a sequence of stages wherein you can add or remove portions of the structure and consider the time-dependent material behaviour such as aging, creep, and shrinkage. In the analysis, a sequence of stages is needed to be defined. For each stage the followings are specified;

- A duration, in days, to be used for time-dependent effects,
- Groups of objects to be added to the structure and the age of the objects at the time they are added,
- Groups of objects to be loaded by specified load cases.

Each stage to be analyzed is considered in two parts;

- Changes to the structure and application of loads are analyzed without any time dependency.

- If any duration has been specified, time-dependent material effects will be also analyzed. During this time, both the structure and applied loads do not change. But, internal stress distribution is updated.

In a stage of the analysis, loads specified on added objects in a group will only be applied to objects that are being added in that stage. In addition time-dependence of aging, creep and shrinkage can be exhibited in time intervals.

During this study, some exploratory analyses are carried out for static staged analysis. The first results reveal less values of deformations than the one phase static analysis. It can be explained as, in the one phase analysis all the loading is applied to the whole structure, all element are affected by a large loading, on the other hand in the staged analysis only the elements added in that stage is affected by the loading created by the corresponding elements.

To reach the aimed displacement, a more comprehensive analysis can be carried out. For this purpose, the FE model can be divided into groups appropriate with the presumption of the construction phases of the structure. The material properties should be modified until a close response to the real displacements is obtained. Moreover the time-dependent material effects can be considered. SAP2000 offers built in time-dependent material properties for concrete. They can be modified to resemble the brick-masonry behaviour.

6.2. Time History Analysis

A linear time history analysis will be appropriate to be performed. Because the records obtained from the real earthquakes at the accelerometers existing on Hagia Sophia are available, the reliability o of the FE model can be testified by time history analysis. The analysis can be performed primarily for the unstrengthened model and then the strengthened models. For two model, the staged construction analysis can be followed by time history analysis that the structural stiffness calculated after the staged analysis can be used as the initial condition for the dynamic analyses. By this way, a more accurate response can be captured to asses the earthquake response of the structure.

REFERENCES

ACI, 2002, *Guide for the Design and Construction of Externally Bonded FRP Systems for Strengthening Concrete Structures (440.2R-02),* American Concrete Institute, Farmington Hills, Michigan.

ACI, 2006, *Report on Fiber-Reinforced Polymer (FRP) Reinforcement for Concrete Structures (440.XR to replace 440R),* American Concrete Institute, Farmington Hills, Michigan.

Çakmak, A.Ş., A. Markopoulos and C. L. Mullen, 1995, "Interdisciplinary Study of Dynamic Behaviour and Earthquake Response of Hagia Sophia", *Solid Dynamics and Earthquake Engineering,* Vol. 14, No. 2, pp. 125-133.

Davidson, R. A., 1993, *The Mother of All Churches: A Static and Dynamic Structural Analysis of Hagia Sophia,* Senior Thesis, Princeton University.

Durukal, E., 1992, *A Study on Structural Identification and Seismic Vulnerability Assessment of Aya Sofya,* M.S. Thesis, Boğaziçi University.

Durukal E., S. Camilla and M. Erdik, 2003, "Dynamic Response of Two Historical Monuments in Istanbul Deduced from the Recordings of Kocaeli and Duzce Earthquakes", *Bulletin of Seismological Society of America,* Vol. 93, No. 2, pp. 694-712, April.

Erdik, M., E. Durukal and H. Keypour, 2003, "Techniques and Materials for the Earthquake Protection of Monuments", *Proceedings: Innovative Technologies and Materials for the Conservation of Monuments,* EU 5th Framework Programme, Advanced Study Course, Athens, 8-20 December 2003.

Hill, K. E., 1991, *Hagia Sophia: Static Analysis of a Finite Element Model,* Senior Thesis, Princeton University.

INRC, 2004, *Guide for the Design and Construction of Externally Bonded FRP Systems for Strengthening Existing Structures,* Italian National Research Council, Rome, http://www.daps.unina.it/

Kachlakev, D., T. Miller, S. Yim, K. Chansawat and T. Potisuk, 2001, *Finite Element Modelling of Reinforced Concrete Structures Strengthened with FRP Laminates – Final Report (FHWA-OR-RD-01-xx),* California Polytechnic State University and Oregon State University.

Keypour, H., 2001, *Comprehensive Nonlinear Dynamic Analysis of Ayasofya,* Ph.D. Dissertation, Boğaziçi University.

R.A. Livingston, P.E. Stutzman, R. Mark, and M. Erdik, 1992, "Preliminary Analysis of the Masonry of the Hagia Sophia Basilica, Istanbul," *Materials Issues in Art and Archaeology III: Materials Research Society Symposium 267*, ed. P.B. Vandiver, et al., Materials Research Society, Pittsburgh, Pa., pp. 721-36.

Natsis, M. N., 1994, *The Enigma of Hagia Sophia: A Dynamic Structural Analysis of Justinian's Great Church,* Senior Thesis, Princeton University.

Mainstone., R. J., 1988, *Hagia Sophia: Architecture, Structure and Liturgy of Justinian's Great Church,* Thames & Hudson, New York.

SAP2000, 2007, *Integrated Structural Analysis and Design Software*, Computer and Structures Inc., Berkeley, California.

Şahin, M., 2002, *Dynamic Response of Hagia Sophia Considering Cracks,* Ph.D. Dissertation, Mimar Sinan University.

Şener, I. N., 2004, *An Innovative Methodology and Structural Analysis for Relocation of Historical Masonry Monuments: A Case Study in Hasankeyf,* M.S. Thesis, Middle East Technical University.

Van Nice, N. L., 1986, *St Sophia in Istanbul: An Architectural Survey.*

Wikipedia, http://en.wikipedia.org/wiki/Hagia_Sophia.

Yüzügüllü, Ö., E. Durukal and K. Beyen, 1997, "Assessment of Mortar and brick Properties of Hagia Sophia by Non-Destructive Testing Techniques", *4th International Symposium on the Conservation of Monuments in the Mediterranean,* PACT, Rhodes, 6-11 May 1997, Vol. 2, pp. 221-229.

APPENDIX A: PAST EARTHQUAKE DAMAGES

• 23 February 532	Construction starts
• 27 December 537	Inauguration
• 553-558	Weakening and consequent collapse of the east main arch and adjacent parts of main and east semi domes
• 9 January 869	Partial damage
• 25 October 989	Collapse of the west main arch and adjacent parts of main and west semi domes.
• 19 May 1346	Collapse of the east main arch and adjacent parts of main and east semi domes.
• 10 Sept. 1509	Partial damage
• 10 May 1556	Partial damage
• 2 Sept. 1754	Partial damage
• 22 May 1766	Partial damage
• 10 July 1894	Light damage (Erdik *et al*., 2003).

APPENDIX B: THE MECHANICAL PROPERTIES OF SOME COMMERCIAL FRPS

Table B.1. Mechanical properties of some commercial FRPs (ACI 440.2R-02)

FRP system	Fiber type	Weight, g/m^2 (lb/ft^2)	Design thickness, mm (in.)	Tensile strength, MPa (ksi)	Tensile elastic modulus, GPa (psi)
Fyfe Co. LLC (2005)					
Tyfo SEH51 sheet	Glass	915 (0.19)	1.3 (0.052)	575 (83.4)	26.1 (3785)
Tyfo SCH41 sheet	Carbon	644 (0.14)	1.0 (0.04)	985 (143)	95.8 (13,900)
Sika Corp. (2005)					
Hex 100G sheet	Glass	915 (0.19)	0.36 (0.014)	2300 (334)	72 (10,400)
Hex 103C sheet	Carbon	610 (0.13)	0.11 (0.004)	3800 (550)	235 (34,000)
CarboDur S plate	Carbon	2100 (0.44)	1.2-1.4 (0.048-0.055)	2800 (406)	165 (23,900)
CarboDur M plate	Carbon	2240 (0.44)	1.2 (0.048)	2400 (348)	210 (30,500)
CarboDur H plate	Carbon	2240 (0.44)	1.2 (0.048)	1300 (189)	300 (43,500)
BASF (2006)					
MBrace EG 900 sheet	Glass	900 (0.19)	0.37 (0.015)	1,517 (220)	72.4 (10,500)
MBrace AK 60 sheet	Aramid	600 (0.12)	0.28 (0.011)	2000 (290)	120 (17,400)
MBrace CF 130	Carbon	300 (0.062)	0.17 (0.007)	3800 (550)	227 (33,000)
MBrace CF 160	Carbon	600 (0.124)	0.33 (0.013)	3800 (550)	227 (33,000)
S&P 100/1.4	Carbon	--	1.4 (0.055)	2700 (390)	159 (23,000)
Hughes Brothers (2005)					
Aslan 400 plate	Carbon	--	1.4 (0.055)	2400 (350)	131 (19,000)
Aslan 500 tape	Carbon	--	2.0 (0.079)	2068 (300)	124 (18,000)
Aslan 500 tape	Carbon	--	4.5 (0.177)	1965 (285)	124 (18,000)